TECHNICAL REPORT STANDARD PAGE

1. Report No.	2. Government Accession No.	3. Recipient's Catalog No.
FHWA/LA91/247		

4. Title and Subtitle	5. Report Date
Detection of Fly Ash In Portland Cement Fly Ash-Concrete	December, 1991
	6. Performing Organization Code
7. Author(s) H. C. Eaton, R. E. Ferrell, Jr., U . Dalvi, A. W. Drew and R. E. Ferrell	8. Performing Organization Report No.
9. Performing Organization Name and Address Louisiana State University Baton Rouge, Louisiana 70803	10. Work Unit No.
	11. Contract or Grant No. 87-1C
12. Sponsoring Agency Name and Address Louisiana Transportation Research Center 410 Gourrier Avenue Baton Rouge, Louisiana 70808	13. Type of Report and Period Covered Final Report June 1987 - December 1991
	14. Sponsoring Agency Code FHWA - LDOTD

15. Supplementary Notes

In cooperation with the U. S. Department of Transportation, Federal Highway Administration

16. Abstract

The chemical composition, phases present, and textural characteristics of a suite of 113 fly ashes were studied. The fly ashes came from Gifford-Hill & Co., Inc. power plants in Cason, TX; Gentry, AR; Westlake, LA; Boyce, LA; Choteau, OK and Oologah, OK. Two ordinary Portland cement (OPC) concrete samples, with 7:3 aggregate to cement weight ratio, and 51 samples with Portland cement partially replaced by fly ash (producing a 70:25.5:4.5 weight ratio) were also studied. The water to pozzolan ratio was 0.4 for both groups.

X-ray diffractometry was used to identify the mineralogy and the glass structure of the fly ashes. Special data reduction techniques were developed to establish the mineralogy of individual ashes and the typical specimen. Quartz, anhydrite, melilite, lime, tricalcium aluminate, dicalcium silicate, merwinite, periclase, ferrite spinel, hematite, and possibly brownmillerite were found. The average structure of the glassy component was studied by examining the maximum of the broad hump in the background. The hump was found to be remarkably constant in its location at approximately 32.0°2Θ.

Minor but significant mineralogical differences, such as the amount of ettringite, were observed between the concrete samples with OPC and OPC and fly ash. The glassy hump in the Portland cement concrete was relatively symmetric and positioned at 33.0°2Θ, whereas the hump for the Portland cement-fly ash concrete was asymmetric with a maximum at 30.0°2Θ. The average structure of the nearly amorphous C-S-H in Portland cement-fly ash concrete is thus different from that in pure Portland cement concrete. The differences in minor mineralogy and the nature of C-S-H between Portland cement and Portland cement-fly ash can be exploited to develop an analytical method for the detection of fly ash in concrete.

Chemical analysis and evaluation of the results by discriminant function and factor analysis revealed little variation in the composition of the ashes from a given power plant sampled. The oxides of Ca and Al were used to formulate a quantitative technique that estimates fly ash at the 4.5 weight percent level in concrete with a total analytical error ± 0.1 weight percent when the sources of fly ash and other concrete components are known. If the mean fly ash composition of all samples is used as a reference, the maximum error of estimation increases to ± 1.0 weight percent.

17. Key Words	18. Distribution Statement
Cement, fly ash, concrete	No restrictions. This document is available to the public through the National Technical Information Service, Springfield, Virginia 22161

19. Security Classif. (of this report)	20. Security Classif. (of this page)	21. No. of Pages	22. Price
Unclassified	Unclassified	120	

Form DOT F 1700.7 (8-69)

DETECTION OF FLY ASH IN PORTLAND CEMENT FLY ASH CONCRETE

FINAL REPORT

by

H. C. EATON, PH.D.
R. E. FERRELL, JR., PH.D.
U. DALVI, M.S.
A. W. DREW, M.S.
R. E. FERRELL, B.S.
LOUISIANA STATE UNIVERSITY
BATON ROUGE, LA 70803

RESEARCH REPORT NO. 247

RESEARCH PROJECT NO. 87-1C

CONDUCTED FOR

LOUISIANA DEPARTMENT OF TRANSPORTATION AND DEVELOPMENT

LOUISIANA TRANSPORTATION RESEARCH CENTER

in Cooperation with

U.S. DEPARTMENT OF TRANSPORTATION

FEDERAL HIGHWAY ADMINISTRATION

DECEMBER 1991

ACKNOWLEDGMENTS

The authors wish to thank Gifford-Hill, Inc. Dallas Texas, for providing fly ash samples and the Louisiana Transportation Research Center for providing financial support for this study.

ABSTRACT

The chemical composition, phases present, and textural characteristics of a suite of 113 fly ashes were studied. The fly ashes came from Gifford-Hill & Co., Inc. power plants in Cason, TX; Gentry, AR; Westlake, LA; Boyce, LA; Choteau, OK and Oologah, OK. Two ordinary Portland cement (OPC) concrete samples, with 7:3 aggregate to cement weight ratio, and 51 samples with Portland cement partially replaced by fly ash (producing a 70:25.5:4.5 weight ratio) were also studied. The water to pozzolan ratio was 0.4 for both groups.

X-ray diffractometry was used to identify the mineralogy and the glass structure of the fly ashes. Special data reduction techniques were developed to establish the mineralogy of individual ashes and the typical specimen. Quartz, anhydrite, melilite, lime, tricalcium aluminate, dicalcium silicate, merwinite, periclase, ferrite spinel, hematite, and possibly brownmillerite were found. The average structure of the glassy component was studied by examining the maximum of the broad hump in the background. The hump was found to be remarkably constant in its location at approximately 32.0°2Θ.

Minor but significant mineralogical differences, such as the amount of ettringite, were observed between the concrete samples with OPC and OPC and fly ash. The glassy hump in the Portland cement concrete was relatively symmetric and positioned at 33.0°2Θ, whereas the hump for the Portland cement-fly ash concrete was asymmetric with a maximum at 30.0°2Θ. The average structure of the nearly amorphous C-S-H in Portland cement-fly ash concrete is thus different from that in pure Portland cement concrete. The differences in minor mineralogy and the nature of C-S-H between Portland cement and Portland cement-fly ash can be exploited to develop an analytical method for the detection of fly ash in concrete.

The texture of the fly ashes and concrete samples with fly ashes were studied by scanning electron and optical microscopy. The iron-rich fly ash spheres could be easily detected by image analysis in the electron probe microanalyzer.

Chemical analysis and evaluation of the results by discriminant function and factor analysis revealed little variation in the composition of the ashes from a given power plant sampled. The oxides of Ca and Al were used to formulate a quantitative technique that estimates fly ash at the 4.5 weight percent level in concrete with a total analytical error $\pm$ 0.1 weight percent when the sources of fly ash and other concrete components are known. If the mean fly ash composition of all samples is used as a reference, the maximum error of estimation increases to $\pm$ 1.0 weight percent.

The quantitative analysis of fly ash in concrete can be accomplished by chemical analysis methods using a total digestion procedure for the determination of weight percent CaO/weight percent Al_2O_3 in concrete. It is based on a simple relationship which can be expressed as:

$$Ak + C(K-x) + Fx = \text{weight percent CaO/weight percent } Al_2O_3 \text{ in concrete}$$

where A= weight percent CaO/weight percent Al_2O_3 in concrete, C= weight percent CaO/weight percent Al_2O_3 in cement, F= weight percent CaO/weight percent Al_2O_3 in fly ash, k = weight fraction of aggregate in concrete, K = (1-k) = weight fraction of non-aggregate material in concrete, and x = weight fraction of fly ash in concrete.

IMPLEMENTATION STATEMENT

This study of methods to quantify fly ash in concrete has produced a method that should be implemented on a routine basis. The method is of potential value in monitoring the quantity of fly ash in plastic and hardened concrete. It may be used to determine if the concrete contains the quantity of fly ash specified for a construction project. The method may also be used to estimate the quantity of fly ash in hardened concrete if estimates of the original chemical composition of the concrete constituents can be obtained. The use of the ratio of Ca and Al oxides provides a simple chemical tracer for fly ash. For application to plastic concrete, the following procedure is recommended:

1. Collect a representative sample of the aggregate, the cement, the fly ash, and the plastic concrete. Sampling frequency will vary, but at least once a week is minimal.

2. Dry and grind all materials to a powder with particles smaller than 20μm.

3. Cone and split the samples several times to obtain a representative portion weighing about 0.5 g.

4. Use Inductively Coupled Plasma Spectroscopy (ICP) and total digestion method (or equivalent) to determine quantities of CaO and Al_2O_3 in a precisely weighed subsample of each of the materials.

5. Determine quantity of aggregate in the plastic concrete directly, or consult specifications.

6. Use the analytical values and the equation below to calculate the quantity of fly ash in the plastic concrete.

7. Repeat the entire procedure at least twice and report the mean and standard deviation of the results.

For hardened concrete, one must rely on archived samples of the aggregate, the cement, and the fly ash (or estimates based on values from the specifications for a particular project) to determine the CaO and Al_2O_3 ratio of the starting materials. The concrete sample may be processed as indicated above. The accuracy of this approach is variable, depending on how well the compositions of the starting materials can be determined. The variability in the amount of aggregate added to a mixture is approximately one percent and the bulk composition of aggregate is not expected to vary greatly.

The equation for the calculation of fly ash in concrete is:

x = (weight percent CaO / weight percent Al_2O_3 in concrete) - (AK + K) (F - C)

where A = weight percent CaO/weight percent Al_2O_3 in aggregate, C = weight percent CaO/weight percent Al_2O_3 in cement, F = weight percent CaO/weight percent Al_2O_3 in fly ash, k = weight fraction of aggregate in concrete, K = (1-k) = weight fraction of non-aggregate material in concrete, and x = weight fraction of fly ash in concrete. The implementation of this program will benefit many on-going studies of the effects of fly ash on the strength and durability of concretes with fly ash substituting for cement. It will require new directives for sampling in order to be successful.

This study also arrived at an x-ray analytical method to quantify the amount of fly ash in OPC-fly ash concrete. The implementation of these methods requires establishment of a database of the various constituents used in concrete production. The specific steps are listed below:

Build a database consisting of chemical composition, phases present, and other relevant properties of fly ashes, hydrated Ordinary Portland Cement (OPC) and OPC-fly ash concrete. The data should be obtained under identical conditions.

Tabulate the mineralogy and the location of the maximum of the glassy hump for the two types of concrete:

For plastic concrete - Detect ash in concrete from the position of the amorphous hump. The glassy hump in Portland cement concrete occurs at 33.0°2Θ whereas in Portland cement-fly ash concrete the hump is closer to 30.0°2Θ. Collect a representative sample of the aggregate, the cement, the fly ash, and the plastic concrete. Sampling frequency will vary, but at least once a week is minimal. Dry and grind all materials to a powder with particles smaller than 20 μm. Cone and split the samples several times to obtain a representative portion weighing about 0.5 gm. Determine the concentration of CaO and Al_2O_3 by an analytical method, preferably inductively coupled plasma spectrometry. Determine the quantity of aggregate in the plastic concrete directly, or consult specifications. Repeat the entire procedure at least twice and report the mean and standard deviation of results.

For hardened concrete - Obtain chemical composition of the constituents from archived samples, (or estimates based on values from the specifications). Use the CaO and Al_2O_3 concentrations to calculate the fly ash content of an OPC-fly ash concrete:

$Ak + C(K-x) + Fx$ = weight percent CaO/weight percent Al_2O_3 in concrete

where A = weight percent CaO/weight percent Al_2O_3 in concrete, C = weight percent CaO/weight percent Al_2O_3 in cement, F = weight percent CaO/weight percent Al_2O_3 in fly ash, k = weight fraction of aggregate in concrete, K = (1-k) = weight fraction of non-aggregate material in concrete, and x = weight fraction of fly ash in concrete.

TABLE OF CONTENTS

TABLE OF CONTENTS (continued)

LIST OF TABLES

LIST OF TABLES

LIST OF FIGURES

LIST OF FIGURES
(continued)

LIST OF FIGURES
(continued)

LIST OF FIGURES
(continued)

I. INTRODUCTION

Fly ash is a waste product of electricity generation from coal-dired furnaces. The mineral impurities in the coal often fuse at the high temperatures in the furnace to produce fly ash. More than 50 million tons of ash is produced in the United States by electrical utilities. About 80 percent of the fly ash is disposed of in landfills or storage ponds and about 20 percent is reused (1) mainly as a partial replacement for cement in concrete mixtures, civil engineering applications and grouting. LaDOTD has approved partial substitution of Ordinary Portland Cement (OPC) by fly ash in concrete.

The American Society for Testing and Materials (ASTM) has issued a standard specification for using fly ash in Portland cement concrete, ASTM: C 618. This specification has two classifications of fly ash. Class F and Class C, based on total silica, alumina and iron. From the compositional standpoint, two ashes differ from each other mainly in calcium content: Class F fly ash usually contains less than 5 percent analytical CaO, whereas C fly ash usually contains 15 percent to 35 percent of analytical CaO by weight. Class F ashes possess pozzolanic properties, and Class C fly ashes may be hydraulic (2). Because of the wide variability both in coals and in the operation of boilers and collection of ash, fly ashes differ from each other in important physical and chemical characteristics. Moreover, considerable variability may be present within a single sample of fly ash.

The use of fly ash in concrete mixes affects all properties of concrete (3). It has a major influence on the properties of concrete: strength development, finishability, permeability to water and aggressive solutions, durability, and long-term stability. If any Portland cement is partially substituted by fly ash, its presence should be known to predict the properties of the resultant concrete. Fly ash, a by-product of coal-fired power plants, has found increasing use by the construction industry as a partial substitute for Portland cement.

Although concrete containing fly ash often has higher long-term strength (4-6), the substitution of fly ash for cement alters the normal cement hydration process. Plain and fly ash-bearing concretes display distinct differences in microscopic texture (7), the kind and amount of hydration products (8,9), and the density and permeability of the final product. Two major categories of fly ash are commonly recognized. Class F, or low-calcium, fly ash relies primarily on the pozzolanic reation between lime and fly ash for strength development. During early curing, this fly ash contributes to the strength of the mix solely through its presence as an inert filler (7). Class C, or high-calcium fly ashes exhibit cementitious properties, producing hydration products by direct reaction of ash compounds and water. Chemical reation is initiated much more quickly, and strength development is largely

independent of cement content. Larger amounts of this fly ash can be substituted for cement before deleterious effects are observed.

The preceding observations suggests that the amount and kind of fly ash used in concrete will greatly affect the physical and structural properties of the final product. Concretes having variable ash to cement ratios have been used successfully by the construction industry (10), but replacement most commonly ranges from 10 to 50 weight percent fly ash for cement. The amount and type of fly ash used depends on the desired properties of the final concrete such as workability, response to compaction, and rate of heat production during hydration.

The increased demand for variable quantities and types of fly ash for different projects illustrates the need for a simple, effective means of quantifying the fly ash component of concretes. Approaches considered by previous researchers include the separation of characteristic denser constituents of fly ash from the concrete mix by use of heavy liquids (11) and measurement of variations in the concentration of distinctive mineral phases (i.e., mullite) attributable to fly ash in the cement mix (12). The high toxicity of heavy liquids and the difficulty of obaining pure, representative samples during the separation are major disadvantages of the former approach. A quantitative technique has yet to be developed.

II. OBJECTIVE

A variety of fly ashes and fly ash-Portland cement concretes were characterized. The objective of the project was to detect and quantify the amount of fly ash in fly ash-Portland cement concrete using x-ray diffraction.

The natural of fly ash is highly variable. Therefore, another objective of the study was to generate a typical, or standard, ash diffractogram. The standard diffractogram could then be used as the basis for comparative investigations of ash composition.

III. SCOPE

Several approaches may be taken to quantify the amount of fly ash in concrete. Both of the major classes of ash can be characterized by a distinctive mineralogy: Class C fly ash contains calcium silicates, periclase, lime, and anhydrite oxides; Class F fly ash contains a large amount of mullite, which is usually absent or rare in Class C fly ash. Quartz and iron oxides are common to both. The presence of Class F fly ash in concrete can be easily verified by testing for the presence of mullite. The problem is more difficult for Class C fly ash because the minerals are present in low amounts and diluted by the large amount of quartz in the aggregate. Also, the close chemical similarity between Class C fly ash and Portland cement makes detection of this type of fly ash by ordinary means difficult. The present study has been limited to the most troublesome mixtures: Class C plus ordinary Portland cement, and Class C plus ordinary Portland cement plus silicate aggregate.

X-ray diffractometry produces a unique pattern for a crystalline substance. Some information about the average molecular structure of amorphous materials can also be obtained by x-ray diffractometry (13,14). Hydrated Portland cement and Portland cement-fly ash mixtures contain several crystalline mineral phases which can be identified by x-ray diffractometry, and can be used for quantifying the amount of fly ash in concrete/fly ash mixtures. For example, the amount of portlandite in Portland cement-fly ash mixtures decrease with age, compared to pure Portland cement (15,16). The nature of the C-S-H in a Portland cement-fly ash sample is also likely to be different (17). A study of C-S-H may help in quantifying the amount of fly ash in mixture.

Another emphasis of the present study is the development of data reduction techniques which can increase the signal to noise ratio, make the study of minor phases easier, and more accurately delineate the background.

The chemical composition of OPC and fly ash may be different. A detailed analysis is necessary to establish compositional limits. Once this is established, the differences may be exploited to fingerprint the constituents of a concrete.

Likewise, textural characteristics of concrete with and without fly ash can be studied, which can suggest some ways of quantifying the amount of fly ash in concrete.

IV. METHOD OF PROCEDURE

The goal of the study was to develop a simple, practical method for measuring the fly ash content of concretes. This process must be preceded by a thorough analysis of the composition (both mineral and chemical) and texture of the fly ash. A comparison of these properties can then be made for fly ash and remaining concrete constituents (i.e. cement and aggregate). In theory,the addition of fly ash to the cement-aggregate mixture could be monitored in two ways. First, if a unique mineralogical or chemical constituent of the fly ash is present in relatively constant amounts, its concentration in the concrete mixture can be used to deduce the amount of fly ash substituted for cement. Like wise, a textural property unique to the fly ash can also be recognized and quantified in the concrete mixture. Second, a given mineral or element may occur in both fly ash and cement, but in appreciably different concentrations. In this case, substitution of fly ash for cement will produce a measurable dilution or concentration of the element in the concrete mix.

The general approach and methodology are similar to those employed by Ferrell et al. (18) in a study of soil stabilization with lime and fly ash. In this study, potential methods will be evaluated with regard to practicality and accuracy. The development of a quantitative method is desirable because it will provide a means for evaluating the manner in which the quantity, and possibly the type, of fly ash used determines the quality of the final product, especially its long-term strength and durability.

A. MATERIALS

Four types of materials were used in the study. Fly ash was collected from several sources. Commercially available cement and a local sand aggregate were used to prepare mixtures of flyash-bearing concrete in the laboratory. Additional samples of concrete containing fly ash were supplied by M. Rasoulian of the Louisiana Transportation Research Center (LTRC).

1. Fly Ash

A total of 85 fly ash samples were obtained from Gifford-Hill & Co., Inc. Samples of the fly ash, sealed in quart-size plastic bags, were collected from power plants in the following six localities: Cason, TX; Gentry, AR; Westlake, LA; Boyce, LA; Choteau, OK; and Oologah, OK. The coal burned in these power plants was from a sub-bituminous source in Wyoming. The fly ashes are Class C types (19). Most samples are tan to grayish tan in

color and very fine-grained. Particles range from clay size up to fine silt size. The samples were supplied at one week intervals between August 20 and November 15, 1987. A complete listing of samples, including plant number, silo or unit number, sample number and the date sampled is provided in Table 1.

2. Cement

A standard Type 1 Portland cement was used to prepare laboratory mixtures of fly ash-bearing concrete. Control samples of the hydrated cement were analyzed via x-ray diffraction (XRD) and ICP for comparison with the results for concrete mixtures prepared with fly ash. The major mineral phases identified in the sample, including portlandite; calcite; ettringite; and various C-S, C-A and C-A-S hydrates; are all characteristic of Type 1 Portland cements. The major peaks for each common phase are labeled in the diffractogram shown in Figure 1. Table 2 lists the chemical composition determined for the cement via ICP analysis. For most of the oxides, the relative standard deviation (standard deviation expressed as percent of the mean) is less than 5 percent of the amount reported.

3. Aggregate

A fine- to medium-grained quartz sand was used as aggregate material in the preparation of laboratory concrete mixtures. According to XRD analyses, this material is essentially pure quartz. ICP analyses reveal an SiO_2 content of over 98 weight percent (Table 2). Al, Ti, and K-oxides each make up less than 1.0 weight percent of the aggregate. This aggregate is not likely to contribute chemical constituents, other than silica, that would interfere with the chemical procedure.

4. Concrete Samples

The first concrete samples examined consisted of two small blocks of hardened concrete prepared under identical conditions. One (concrete A) contained fly ash; the other (concrete B) did not. The samples were examined to determine whether fly ash substitution produces a measurable change in the composition or texture of the concrete. Compositional and textural properties observed in the Gifford-Hill & Co., Inc. fly ash samples were used to evaluate the differences between the two concretes.

A second set of twelve samples was prepared in the LTRC laboratories using one of the Gifford-Hill & Co., Inc. fly ash samples. The chosen fly ash sample was substituted in varying amounts in a concrete mixture of constant composition and water-to-cement ratio. Two concrete samples each were prepared using no fly ash and using 10, 20, 30, 40 and 60 weight

percent substitution of fly ash for cement. Analyses of these samples were performed to assess the feasibility of developing calibration curves to determine the amount of fly ash present in a concrete.

Fifty-three concrete samples were prepared in the laboratories of LSU's Mechanical Engineering department using constant mix proportions and 15 weight percent fly ash for cement substitution. The fly ash represented 4.5 weight percent of the total mixture. Each mixture contained a different sample of Gifford-Hill & Co., Inc. fly ash. These samples were used to test the variability of mixtures and to assess the possible range of compositional and textural properties obtained by varying the kind, rather than the amount, of fly ash substituted into the concrete mix.

B. SOURCES OF FLY ASH AND CEMENT

One hundred thirteen samples of Class C fly ash were received from Gifford-Hill & Co., Inc., Dallas, Texas. The ashes came from plants located in Cason, TX; Gentry, AR; Westlake, LA; Boyce, LA; Chouteau, OK; and Oologah, OK.

C. SAMPLE PREPARATION

Samples were prepared for x-ray diffraction as follows:

(1) All samples were homogenized by quartering and coning. The dry ash was passed through a funnel and separated into approximately four volumetrically equal parts. Each part was numbered. Parts one and three, and two and four, were then passed through the funnel simultaneously to mix. The process was repeated 15 times.

(2) The homogenized samples were ground for 20 minutes in ethanol using an automatic grinder.

(3) Excess ethanol was removed.

(4) The samples were dried in an oven at 120°C.

(5) Dried samples were stored in a desiccator.

A standard, side-loading, aluminum x-ray sample holder was used for XRD. Peaks corresponding to aluminum were easily identifiable during the pattern analysis, and could be used as an internal standard.

Fifty-one concrete mixtures were prepared by combining aggregate (mainly silica), cement and fly ash in a constant weight ratio 70:25.5:45. The water to cement ratio was 0.4.

Two samples were prepared by combining 70 percent aggregate and 30 percent Portland cement. The fly ash and cement contents of the mixture reflected a weight percent substitution of 15 percent fly ash for cement. A water-to-cement ratio of 0.4 was used. Two sample were also prepared under identical conditions using no fly ash. All mixtures were prepared in small paper containers and allowed to set for at least 28 days.

The x-ray instrument parameters used for data collection are listed in Table 17. Identical conditions were used for the concrete samples except that the final scanning range was limited to 50.0°Θ. X-ray data, in the form of intensity (cps) vs. angle (2Θ), were stored on a computer interfaced directly to the diffraction system. Files were transferred to a mini VAX computer and then to an IBM-PC compatible machine using 5 1/4 inch floppy disks.

D. X-RAY DATA PROCESSING AND ANALYSIS

An x-ray diffractometer pattern is a plot of intensity versus 2Θ. The graph contains a series of peaks superimposed on a background. The background is mostly noise, but for samples with a high amorphous content, some information about the average structure of the amorphous material is also present. In order to extract the maximum amount of information from such a pattern, some signal processing is necessary to increase the signal to noise ratio. Signal processing can lead to identification of minor peaks, which are not otherwise detectable, and to better define the background. The details of the procedures adopted for this study are discussed by Dalvi (20). Relevant texts are also mentioned in the bibliography.

A simple procedure was adopted to improve the signal to noise ratio, and obtain a standard pattern for Class C ash: summing a large number of Class C fly ash spectra. Since noise is random, summing results in cancellation of noise through destructive interference; similarly, through constructive interference real peaks are enhanced.

Various digital filters were used to remove the noise and enhance the background. The background was obtained using a least squares, smoothing algorithm and the varying curvature approach (21,22). Peaks were located by the second-derivative method, a common procedure for location of maxima in a graph.

E. QUALITATIVE AND QUANTITATIVE TEXTURAL STUDIES

Three types of fly ash samples were prepared for qualitative and quantitative analysis. Small amounts of several unhydrated samples were loosely placed on glass slides in immersion

oil for examination with an optical microscope. Polished thin sections of unhydrated and hydrated fly ash samples impregnated in a blue-dyed epoxy were also prepared. All sections were prepared by standard methods. Final polishing was performed with a 3.0 μm Al paste. A smaller than normal section thickness of 10 μm permitted a clearer view of the particles. Approximately 4-5 samples were mounted on small aluminum stubs for examination with a JEOL Scanning Electron Microscope. Mounting was accomplished by covering one end of the stub with double-stick tape and dipping it in a small amount of fly ash sample. Loose particles were removed by tapping the edge of the stub against the counter surface. Some SEM samples were gold-coated while others were carbon-coated. The former coating permits clearer imaging of grain surfaces, and the latter permits chemical analysis of individual particles and crystals by energy dispersive x-ray spectrometry (EDX). Several thin sections of the concrete samples were prepared. The procedures followed were identical to those used to prepare fly ash thin sections.

Qualitative studies of fly ash samples included evaluations of particle size, shape and color (optical microscopy) and more detailed studies of amorphous and crystalline particles (optical and SEM morphology). Qualitative studies of concrete thin sections entailed identification of concrete constituents and evaluation of their abundance and physical distribution in samples (optical microscopy).

Microprobe studies were used to obtain detailed analyses of the compositional and associated textural properties of fly ash and concrete constituents in thin sections. Chemical analyses were performed on the individual particles in pure fly ash thin sections. Textural and qualitative compositional analyses were performed on concrete thin sections.

Three Gifford-Hill & Co., Inc. fly ashes were chosen for chemical analysis on the microprobe: Cason Plant-15268, Westlake Plant-108739 and Chouteau Plant-90287. These represented the compositional extremes and an approximate intermediate chemical composition for all fly ash samples analyzed (ICP results). All three sections were thoroughly scanned, and three representative frames from each were selected for chemical analysis. The total number of fly ash particles analyzed ranged from 300 to 850 per sample. Three frames from a thin section of the magnetic fraction of sample Cason Plant-15268 were also analyzed. These contained a total of 376 particles. The particles were analyzed for the concentrations of major element oxides; SiO_2, Al_2O_3, CaO, Na_2O, FeO, MgO, K_2O and TiO_2. Concentrations were reported in units of weight percent.

Textural and qualitative compositional studies were made of concrete samples. Thin sections of all 14 of the samples supplied by the LTRC were examined on a JEOL Superprobe

733. Several frames of concrete samples A and B were photographed. The twelve concrete samples prepared using constant aggregate concrete and water-to-cement ratio and variable (0, 10, 20, 30, 40 and 60 weight percent replacement of cement) fly ash content were thoroughly scanned in the backscattered electron imaging (BEI) mode. BEI images of at least two representative areas of each were acquired at magnifications of 120x. The images were stored in a 512x512 pixel format for later recall on a Tracor Northern 8500 image analysis work station. Compositional differences appear as differences in the brightness, or grey level, of the BEI image. The numerous sizing and shape analyses available via the image analysis software were used to characterize the textural properties of samples.

1. Mineralogical Studies

A variety of air-dried samples were examined with the aid of a Phillips APD 3520 automatic x-ray powder diffractometer with Cu Ka radiation operating at 40 kV and 21 mA. A side-loading powder mount was used to assure good random orientation. The results were primarily used to identify the crystalline components of samples. Rough quantitative estimates (e.g., between samples from different plants) were made solely by comparing relative peak heights for different samples. Quantities of amorphous material were estimated by comparing the intensities of the broad peaks occurring between 20 and 34° 2Θ.

The first large group of XRD samples consisted of the fly ash samples provided by Gifford-Hill & Co., Inc. Eighty-five bulk samples and 28 duplicates were run. A simple coning-and-quartering procedure (repeated 20 times) was used to homogenize samples prior to removing the small sub-samples required for XRD and chemical analyses. Sub-samples were ground to improve peak resolution and intensity. Samples were also dried in an oven for six hours at 90°C to assure that hydrous phases did not develop prior to analysis. Bulk fly ash samples were run from 2 to 70° 2Θ using a step width of 0.04° and a step time of 1 second.

The second major group of samples analyzed consisted of the 53 laboratory concrete mixtures prepared by combining aggregate, cement, and fly ash in the constant weight proportion 70:25.5:4.5 and the 2 control mixtures containing no fly ash. These were also ground to improve peak intensity and reproducibility for crystalline phases. The concrete powders were run from 20° to 50° 2Θ using a step width of 0.04° and a step time of 1 second.

Six additional special sets of samples were also analyzed by X-ray diffraction. The relative proportions of crystalline and amorphous phases were estimated by preparing and running a series of artificially prepared mixtures. Glass and the two major crystalline components of the Gifford-Hill & Co., Inc. fly ashes (quartz and magnetite) were combined in

varying proportions in efforts to reproduce the peak intensities observed for actual fly ash samples. The artificial mixtures were run at settings identical to those used for pure fly ash samples.

Two attempts were made to separate characteristic components of the pure fly ash samples for analysis in hopes that a similar approach could be applied to concrete samples. Separation of the magnetic phases present in most samples was accomplished with the aid of a hand magnet. Separation of the denser phases present in samples was accomplished via heavy liquid (bromoform) separation. The resultant magnetic, non-magnetic, high-density and low-density fractions were analyzed at settings identical to those used for pure fly ash samples.

Four samples of pure Type 1 Portland cement were analyzed to determine an average unhydrated mineral composition for this standard concrete component. The XRD run settings used were identical to those used in the analysis of pure fly ash samples.

The concrete samples prepared by LTRC were also run at the same XRD settings. These included the two concretes (A and B), prepared with and without fly ash under otherwise identical conditions, and the twelve concrete samples prepared using different proportions of a single Gifford-Hill & Co., Inc. fly ash sample.

2. Chemical Studies

All chemical samples were prepared for analysis in an Induction Coupled Plasma Spectrometer (ICP) analysis using a $LiBO_2$ flux, following the standard fusion procedure of Thompson & Walsh (23). Bulk chemical analyses were performed on all samples identified above with the exception of the magnetic and high-density separates removed from some fly ash samples. Analyses were performed on a Perkin-Elmer 6500 ICP. Samples were analyzed for major elements: Si, Al, Fe, Mg, Mn, Ca, Ti, P, Na and K; and trace elements: Ba, Co, Cr, Cu, Ni, S, Sr, V, Zn and Zr. Concentrations were reported in units of ppm. Major elements were converted to weight percent oxide, trace elements were converted to weight percent element, and the total concentrations for all elements in the sample were normalized to 100 weight percent.

V. DISCUSSION OF RESULTS

A. BASIC PHYSICAL PROPERTIES OF FLY ASH

1. Spherical Particles

As coal particles are exposed to progressively higher temperatures for longer residence times, a characteristic continuum of particle morphologies develops (Figure 2) (24). The end product of combustion is the spherical shape which characterizes most fly ash particles. Given sufficient exposure to heat, coal constituents are completely melted or volatilized and, upon cooling, crystallize into spherical droplets of inorganic residue. The majority (> 95 volume percent) of Gifford-Hill & Co., Inc. fly ash particles fall into this morphologic category.

Three types of fly ash particles are common in the Gifford-Hill & Co., Inc. samples: solid spheres, cenospheres (hollow spheres), and plerospheres (spheres containing spheres). Excellent examples of these and a general impression of their size and variability are provided in the optical photomicrographs of Figure 3. In these polished thin-sections it is obvious that most of the particles are translucent solid spheres with diameters typically smaller than 20μm. Figures 3A, 3C, and 3E are particularly representative of the fly ashes investigated in this study.

The variable optical density of spheres is primarily attributable to iron content and the oxidation state of the iron. The opaque spheres (black) in the photomicrographs (Figures 3A and 3C) are extremely iron-rich and consist primarily of either hematite, magnetite, or hercynite. These iron-containing minerals are potentially useful morphological indicator phases and they may represent unique chemical constituents.

Typical plerospheres (P) are illustrated in Figures 3B, 3C, and 3D. They are composed of many smaller spheres enclosed within a larger glassy sphere. Single hollow spheres (G), termed cenospheres, are indicated in Figure 3C. These hollow glassy spheres are less than 10 volume percent of the samples. Ramsden et al. (25) and Roy et al. (26) suggested that cenospheres form during combustion when the coals contain water-bearing clay minerals or gas-producing carbonates. The gases expand the silicate glasses into hollow, thin-walled spheres. Element ratios of the glasses suggest that the coals contained kaolinite and smectite that could provide the required water. The sphere within sphere structure (plerosphere) results from repeated occurrences of this bubbling process (25,27). Compound spheres are most abundant

in the coarsest size fractions of the ashes. All of the hollow glassy spheres are very fragile and may be easily dissolved.

Of the internal precipitates observed, lath- or needle-shaped crystals (X, Figure 3C) of mullite ($3Al_2O_3 \cdot SiO_2$) are most common. These are generally 2-3 μm wide and usually extend across the sphere interiors. They are whitish or clear in color and precipitate parallel to one another or as random intergrowths, criss-crossing sphere interiors. The mechanism most frequently proposed for formation of these crystals is that as the fly ash droplet cools and solidifies, the mullite crystals nucleate on the internal grain surface. Growth proceeds into the interior of the particle, often producing an interlocking network of crystals (24,28).

Additional morphologic detail of fly ash particles is provided in the scanning electron micrographs of Figure 4. A broken plerosphere (Figure 4B) provides a view of the complexity of the interior of some particles. Some particles contain traces of crystal forms within them. Surface precipitates are more abundant and varied though.

Many of the glassy spheres have smaller particles and crystals on their surfaces (Figures 4C and 4D). These crystals may be adhering due to electrostatic effects or may be reaction products formed as the molten glass cooled and reacted with flue gases. Many of the fly ash particles have a rough pebbly appearance (Figure 4C) as a result of the fine-grained powders and crystals on their surface. The fine particles in this photomicrograph do not have a distinctive crystal form like the ones shown in Figure 4D. The prismatic and pyramidal crystals (a) in this figure contain Ca and S and are either anhydride or gypsum. Many other workers have reported alkalis and alkali sulfates similar to these on the surfaces of fly ash particles (28,29). When volatilized in the combustion chamber, Ca, Mg, Na, S, and numerous trace elements are most likely to precipitate on the surfaces of previously formed spheres. Other investigators (24) have observed sulfuric acid condensates on the surfaces of fly ash particles that could promote the formation of the coatings observed in Figures 4C and 4D.

Fe-rich particles separated from the bulk sample with a hand-held magnet often have surface features (Figure 5) that are different from those just described. Two distinct morphologies are displayed by these particles, sections of octahedral (Figures 5A and 5B) and a trellis-like network of intersecting laths (Figure 5C). The most commonly observed octahedral cross section was a series of parallel, equilateral, triangular faces assumed to be the (111) plane of magnetite. The crystals composing the network vary in size and the complexity of interlocking. Both forms are approximately equally abundant in the magnetic fraction, but the network is more abundant in the most dense fractions of the fly ash.

The typical fly ash samples have particle size distributions similar to those depicted for high-Ca fly ashes in Figure 6. As illustrated from the work of previous researchers (19,30)

high-Ca ashes similar to those discussed herein have a larger population of very fine (< 10μm diameter) particles than the low-Ca fly ashes. The maximum diameter of the particles in the Gifford-Hill & Co., Inc. samples is approximately 150μm in diameter while more than 50 percent of the particles have diameters smaller than 20μm (estimate based on visual appraisal of the photomicrographs in Figure 3). Only the uncombusted or residual particles have diameters greater than 100μm.

2. Non-Spherical (Unburned and Partially Fused) Particles

Some of the particles in these fly ashes are coarser, more irregular in shape and more opaque than the typical glassy spheres. For example, Figure 3B contains at least three large irregular particles with curved fractures running through their interiors (Q). These are quartz particles in the coal that have escaped remolding by melting in the combustion chamber because they are highly refractory. Quartz is often the most abundant crystalline phase in the fly ash.

Partially fused particles, such as the one shown in Figure 4A, were occasionally observed in samples. The core of these particles consists of refractory material; typically quartz. The partially melted nature of the particles is evidenced by the presence of molds, spheres and occasional crystalline material on the particle surface.

Coal particles are the most common type of unburnt material in the Gifford-Hill & Co., Inc. fly ashes. These displayed a variety of morphologies and textures. Particles having a high carbon content possess either lacy, vesicular (C, Figure 3D) or platy (Figure 7B) textures. Those containing a mixture of organic and inorganic matter display rounded vesicular textures (Figure 7A & C).

Occasionally, large irregular particles similar to the one shown in Figure 3F are encountered. Their large size and color suggests that they are external contaminants of the fly ash coming from the walls of the collection system or from the sample handling equipment, etc.

3. Hydrated Particle Morphologies

The appearance of fly ash changes when it hydrates after mixing with water or during prolonged exposure to the air (Figure 7). Many of the finest particles dissolve and create a continuous cementitious matrix. Unburned coal particles remain (C, Figures 7A, 7B, and 7C). Their irregular and vesicular nature is particularly evident in these photomicrographs, but their occurrence is not predictable. Many spherical forms remain. A large plerosphere is evident in Figure 7C and many other solid spheres are present in all of the photos. Two cenospheres are apparent in the upper right-rand corner of Figure 7B. The dark solid, Fe-rich spheres (F, Figures 7B and 7D) are the most distinctive textural features that may be used as a tracer, but

their original abundance is difficult to determine. In general, the common silicate spheres cannot be used for quantifying fly ash abundances in concrete because many dissolve and recrystallize during reaction with water.

4. Physical and Textural Properties of Concrete

The fracture surfaces of two concrete samples: A (without fly ash) and B (with fly ash) were thoroughly scanned. The kind and magnitude of hydration products observed in both samples are quite similar (Figures 8 and 9). Clusters of C-S-H Type I fibers (J) are apparent in Figure 8A. C-S-H Type II material is best illustrated in Figure 8D at the (X) location. Type III material displays a nondescript equant grain morphology (K, Figure 8A). Ettringite rods and needles are easily observed in Figures 9A and 9B. Massive platy (hexagonal) crystals such as those observed in Figure 8D are portlandite or a Ca-Al hydrate. Large ($>50\mu$m) spherical voids (A) produced by entrained air are typified by those occurring in Figures 8B, 8C and 8D.

The fly ash-free concrete did not contain any spherical particles, although some of the clusters of cementitious crystals assumed a subspherical shape similar to the aggregates depicted in Figures 9A and 9B. Clearly identifiable, smooth or pebbly surfaced fly ash particles were also not visible in the samples prepared with fly ash. However, several regions containing abundant spherical clusters of particles were noted in concrete 'B' (with fly ash) (Figures 9C and 9D). The particles are thoroughly coated with an extensive layer of hydration products assumed to be C-S-H or a C-A-S hydrate with sulfur. The basic shape and size (generally $<5\mu$m) suggests that they are, in fact, fly ash with a thin film of C-S-H Type I, similar to those observed by Diamond (9). Some of the particles have reacted extensively, and in some instances the glassy spheres appear to have almost completely dissolved. The fly ash particles appear to act as nucleation points for cement hydration and with progressive curing, the reaction products gradually merge (X, Figure 9C) to form an interlocking crystal.

Several consistent differences can be noted between the spherical forms in the fly ash-bearing concrete (Figures 9C and 9D) and the subspherical forms in the fly ash-free concrete (Figures 9A and 9B). The particle sizes are similar, but the particles in Figure 9A and 9B are clearly much less spherical and appear flattened. The hydration products coating these grains also lack the homogeneous fibrous texture typical of the C-S-H Type I seen in Figures 9C and 9D.

Differences in the texture of concrete samples with and without fly ash were also evaluated through backscattered electron image analysis of selected thin sections on a JEOL Superprobe 733. A total of four concrete thin sections were scanned, and backscattered

electron images (Figure 10) of representative areas on each thin section were acquired at constant magnification. The concrete samples examined included concrete A with no fly ash (Figure 10A), concrete B with fly ash (Figure 10B), and 2 samples (1416 and 1425) from the series of six concretes discussed earlier. Sample 1416 (Figure 10C) contains no fly ash, while sample 1425 (Figure 10D) contains 60 percent substitution of fly ash for cement by weight.

The primary textural difference observed was in the relative abundance of spherical particles. Plain concrete samples contain no spherical particles. The "framework" or non-matrix components of these samples include only irregular pieces of aggregate and unhydrated cement clinker. Spherical particles were readily visible in fly ash-bearing concretes.

A second textural difference observed between fly ash-bearing and flyash-free samples was the size and abundance of void spaces. The fly ash-containing specimen shows smaller and more numerous void spaces.

5. Mineral Composition and Fly Ash

Eight crystalline phases were identified in the bulk Gifford-Hill & Co., Inc. fly ashes. Table 3 lists them and gives the nominal compositions of each phase. Quartz is the dominant crystalline phase in all samples (peak intensity >100 counts per second). Additional minerals present in significant quantities (peak intensity between 50 and 200 counts per second), in order of decreasing abundance, include anhydride, lime, periclase and hematite. Minor crystalline phases present (relative peak intensity normally <50 counts per second) include an Fe-rich spinel (probably either magnetite or hercynite), melilite and merwinite. The major peaks for each of these phases are identified in the diffractogram of Gifford-Hill & Co., Inc. fly ash Cason Plant-15268 shown in Figure 11.

Quartz is the only mineral inherited directly from the parent coal material. The detrital origin of this phase is indicated by the coarse, fractured and broken appearance of most grains. Unfused quartz is commonly observed in fly ash samples (25,28,31). Its presence is expected because of its refractory nature and the normally short residence time of the coal in combustion chambers.

Calcium-rich phases originally present in the coal (e.g. calcite) often decompose to lime (CaO) upon intense heating. Some of this material may later recombine with the sulfur commonly present in the combustion chamber. These reactions account for the presence of crystalline-free lime and anhydride in the Gifford-Hill & Co., Inc. fly ash samples. The nature of the process explains why free lime and anhydride typically precipitate on sphere surfaces. The lime can also recombine with CO_2, but the absence of calcite in most samples suggest that this reaction is rare. Calcium is sometimes added to the sample via flue-gas desulfurization

(FGD): a process in which wet limestone is sprayed into the coal-burning plant's hot exhaust gases for the purpose of scavenging and preventing emission of the sulfur dioxide present (32). FGD may explain the abundance of CaO in the Gifford-Hill & Co., Inc. samples and the consistent variations of CaO content observed among samples from different plants.

Merwinite and melilite are both Ca-Al-Mg silicates. Both minerals are most likely to form by direct crystallization from the melt or devitritification of the glass cooled from these melts (33). The chemical composition of Merwinite for a given ash is generally constant (34). Melilite is a solid solution mineral with a composition between akermanite ($Ca_2MgAlSi_2O7$), gehlenite ($Ca_2Al_2Si_2O7$), and Na-melilite ($NaCaAlSi_2O7$). Gehlenite was more abundant than the other two end members in most samples, suggesting that either the Gifford-Hill & Co., Inc. fly ashes are relatively depleted in Mg and Na or that these elements have preferentially precipitated out in other phases.

Oxidation of the Mg in coal can readily account for the presence of periclase in samples. Oxidation of the iron present in pyrite explains the presence of such phases as hematite and magnetite. Reaction of iron with the readily available Mg and Al may also produce a variety of iron-rich spinel phases, as illustrated by the compositions plotted in Figure 12. Most particles have a magnetite composition, but some contain enough Al and Mg to be classified as spinels. Both magnetite (Fe_3O4) and hercynite ($FeAl_2O4$) were commonly identified in samples via peak matching routines. The precise composition of this phase was not determined, however, because differences in the position and intensities of major peaks for members for the magnetite-spinel (Fe_3O_4 - $MgAl_2O_4$) series are so small.

XRD results for the magnetic and high-density fractions of selected samples suggest that both fractions consist primarily of hematite and an Fe-spinel (Figures 13 and 14). XRD analyses of the high- (>2.85) and low-density (<2.85) fractions also revealed substantial differences in the glass content of these two fractions. (The broad peak around 32°C 2Θ in bulk patterns is larger in diffractograms of the low-density fraction and barely detectable in diffractograms of the high-density fraction (Figure 13).) The light fraction therefore consists primarily of glass, while the high-density and magnetic fractions contain higher concentrations of crystalline material.

The relative abundance of crystalline and amorphous material in the Gifford-Hill & Co., Inc. fly ashes is difficult to estimate from bulk x-ray diffractograms alone. Several artificial samples were prepared by combining various quantities of pure glass and two of the major mineral components of the Gifford-Hill & Co., Inc. fly ashes: quartz and magnetite. Four such samples were mixed, ground and run on the XRD in a manner identical to that used to analyze fly ash samples. The crystalline peak intensities for the sample containing 92 weight

percent glass came closest to reproducing peak intensities observed for the bulk fly ash samples, but the results were so variable that the approach was abandoned.

Two main variations in mineral composition were observed among fly ash samples. First, the greatest variations occur between samples from different localities (relative peak intensities are generally consistent for samples from a given plant). Second, the primary variations noted among plants are in the intensity rather than the number or kind of crystalline peaks present. Peak intensities are greatest for samples from Cason Plant and Gentry Plant, indicating that these samples contain the greatest amount of crystalline material. Samples from the Westlake Plant and the Boyce Plant display the lowest peak intensities, while samples from Chouteau Plant and Oologah Plant display intermediate intensities. Variations in the amount of crystalline material present are presumably due to differences in the intensity (i.e. exposure time, temperature) of the coal-burning process. Thus, mineralogical determinations will not be reliable indicators of fly ash quantities.

Free lime is the chief crystalline phase which shows large variations in concentration in samples from different plants. The concentration of crystalline lime is vastly different between the Boyce Plant and the Cason Plant in relation to the concentrations of the remaining crystalline phases. As the CaO content of the bulk sample increases, the position of the amorphous glass hump maxima also shifts upwards from 32 to 33° 2Θ. This change reflects increased incorporation of CaO into the glass structure (35). The shape of the amorphous hump also changes with increasing CaO content: from a nearly symmetrical hump to one which is sharply skewed toward higher 2Θ angles. As these changes occur, the intensity of the crystalline free lime peaks also increases, suggesting that there is a limit to the amount of CaO that can be accommodated by the glass phase.

Efforts to apply quantitative XRD methods to the present samples proved unsuccessful. Of the eight crystalline phases identified in Gifford-Hill & Co., Inc.'s fly ash samples, hematite, magnetite, merwinite and members of the high-temperature solid solution series do not occur in plain concrete samples. However, because of their low concentrations in pure fly ash samples, the major peaks for these minerals are rarely visible in the XRD traces of concrete mixtures. If these minerals are to be used to quantify the fly ash component of a concrete mix, the concrete must first be fractionated in a manner which will isolate and concentrate them.

The above results are not surprising. Previous studies recommending the use of characteristic mineral phases to deduce the amount of fly ash in the concrete mix have dealt primarily with Class F fly ashes (e.g. (12)). This type of fly ash is more likely to contain significant quantities of distinctive crystalline phases, such as mullite ($3\ Al_2O_3 \cdot 2\ SiO_2$). Class

C fly ash commonly contains less crystalline material and phases such as C_3A, CS, CaO and C_4A_3S which also occur in Portland cements (19,26). It is therefore less likely to contain large quantities of phases, such as magnetite and melilite, which are not found in Portland cements.

Assuming fractionation of the concrete is an option, the two iron oxide phases might prove useful in quantifying the fly ash component of samples for three reasons. First, they can be separated from the remainder of the concrete sample more readily than other diagnostic phases (e.g., by density or magnetic separation procedures). Second, they are chemically more resistant to the pozzolanic reactions affecting concrete mixtures than the Ca-Al silicate phases present. Iron is less likely to be incorporated into hydration products, and a good portion of the magnetic and high density fractions is crystalline rather than amorphous. Third, X-ray diffractograms and chemical analyses both suggest that the concentration of these phases in samples is nearly constant. The most intense hematite peak in diffraction profiles is about 10 percent of maximum peak intensity for most samples, while the concentration of FeO in samples only ranges from 5 to 7 weight percent. However, separations are extremely difficult because of the fine sizes of the fly ash and other particles in the concrete.

B. CHEMICAL COMPOSITION

1. ICP Results for Fly Ash

The 96 samples of Gifford-Hill & Co., Inc. Class C fly ash from the six coal-fired power plants (Table 1) were analyzed by ICP Spectroscopy. The range, mean and standard deviation of element concentrations obtained for the samples are presented in Table 4. Tables 5 - 10 provide the analogous results for samples by individual plant. Although the mean values are only slightly different, there are differences which permit the recognition of the fly ash from different plants. The standard deviation of the chemical constituents accounting for more than 1.0 weight percent of the sample is usually less than 10 percent of the mean. Chemical variability is even smaller when only the samples from a single power plant are considered.

The bulk chemistry of samples mirrors the variety and relative abundance of crystalline phases identified via XRD. Silicon, calcium and aluminum are the predominant elemental constituents, reflecting the abundance of phases such as quartz, free lime, melilite and merwinite. Other elements present in quantities exceeding 1 weight percent, in order of decreasing abundance, included Fe, Mg and Na. The quantities of Fe and Mg present (generally up to 7 weight percent each) are comparable to the peak height percentages observed for crystalline oxide phases composed of these elements in X-ray diffractograms. The small quantities of Na present in samples (generally <3 weight percent), together with the high glass

content of samples suggest that Si, Al and Ca may comprise a large portion of the glassy phase. Al is probably more abundant in the glass than the other two, since a major crystalline phase composed primarily of Al was not detected in samples.

Additional efforts to characterize the melt from which the Gifford-Hill & Co., Inc. fly ashes formed were accomplished by plotting the results of 34 selected chemical analyses on an oxide weight percent CaO-Al_2O_3-SiO_2 ternary diagram (Figure 15). The data plots entirely in the Gehlenite ($2CaO$-Al_2O_3-SiO_2) and Anorthite (CaO-Al_2O_3-SiO_2) compositional fields. The analyses form a linear trend which points from the CaO apex towards a point on the SiO_2-Al_2O_3 approximately midway between the locations where kaolinite and montmorillonite would plot. Such a constant SiO_2/Al_2O_3 ratio suggests that the concentrations of these elements in samples are determined largely by the clay minerals associated with the coal deposits.

2. Discriminant Function and Factor Analysis

Discriminant function and factor analyses were performed to further aid in the interpretation of chemical results. Factor analyses proved useful in identifying differences and trends in the chemical composition of samples, particularly between different plants. Discriminant function analyses demonstrated how well chemical composition can be used to predict the plant (locality) from which the sample originated.

The results of factor analysis document significant differences in the chemical composition of fly ash samples obtained from different plants. A total of four factors were derived having eigenvalues greater than 1 (Table 11). Together these factors account for 82 percent of the variation in chemical composition observed among samples from different plants.

The first factor accounts for the greatest fraction of variance: approximately 41 percent. It explains the variations in two major groups of elements: those primarily associated with silica-rich phases (Al_2O_3 and possible K_2O and V) and those associated with calcium-bearing phases (Sr, MnO, MgO, and Ba). The strong inverse relationship between the abundance of silica- and calcium-rich phases documented by factor 1 provides the most decisive means of identifying the source (plant number) of a fly ash sample. Two possible explanations exist for these variations:

(i) variations in the mineral content of the coal supplied to the plant,

and

(ii) differences in the manner in which the raw material is processed and burned.

Both of the above can account for day-to day variations in the chemistry of samples obtained from the same plant, but they are much smaller in magnitude than the between-plant variation. Chemical composition is a good indicator of the source of the fly ash.

Much of the Ca in samples occurs in either the glassy amorphous state (indicated by the high 2Θ position of the amorphous hump in X-ray diffractograms) (35) or as crystalline free lime (CaO). Only minor quantities of chemically more complex Ca-rich crystalline phases (e.g., melilite, gehlenite) were observed. The chemical state of Ca in samples suggests that much of it was supplied in relatively simple mineralogical form (i.e. calcite as opposed to clay minerals and other silicates).

Carbonate minerals often occur in appreciable quantities in coal deposits (e.g. carbonate-rich coal balls, or localized precipitates in cracks and fissures). Some calcium enrichment is probably attributable to FGD as mentioned earlier (32). The relatively simple chemical state of much of the Ca in samples and the consistent relationship between Ca content and source (plant) also support the latter hypothesis. Si is likely to vary inversely with Ca content, since both elements are major components of the samples.

The second factor accounts for about 26 percent of the variation in sample chemistry by plant. Elements having a significant fraction of variation explained by this factor include: major and trace elements associated with iron oxide-rich phases (FeO, TiO_2, V, Cr, and Zr), trace elements associated with sulfide-bearing phases (Cu, Co), trace elements associated with calcium-rich phases (Sr and Ba), and the major element most commonly associated with the glassy portion of fly ash spheres: Na. The abundance of elements from the first three groups (trace elements and elements associated with the less abundant mineral phases) vary inversely with the abundance of sodium.

These results are most easily explained by separating fly ash constituents into two major categories: crystalline and non-crystalline. The concentrations of iron-, sulfide- and calcium-bearing phases are not likely to vary directly with one another in coal samples. However, all three phases will vary inversely with the amorphous, or glass, content of fly ash samples. The covariance can also be accounted for by assuming that the trace elements of interest are concentrated primarily in the glassy phase of particles. If this is the case, certain processes (e.g. higher temperatures or extended combustion times) could lead to the enrichment of trace elements in the glassy phase. Na would then, necessarily, be depleted.

Factors 3 and 4 account for significantly smaller fractions of the total observed variance (8.63 percent and 6.83 percent respectively). Factor 3 documents a high covariance between major elements Na and Fe, and an inverse relationship between the concentrations of these two elements and trace elements (Cu, Ni) associated with sulfide-bearing phases. Factor 4 explains

a significant fraction of the variation in concentration of elements Na and Ni and suggests that in some instances these two elements vary directly. The low Na content of samples is apparently controlled by more than one mineral.

According to the results of discriminant function analyses (Table 12), the chemical composition of a fly ash sample can be used to determine the location (plant number) from which it was derived. Samples from Westlake, Boyce, Chouteau, and Oologah Plants were correctly classified 100 percent of the time. Samples from the Cason Plant were correctly classified over 95 percent of the time. Samples from the Gentry Plant were correctly classified over 87 percent of the time. Misclassified samples from the latter two plants were always classified as coming from the other of the two plants. The similarities in the chemical composition of samples from plants 78 and 81 are apparent in Tables 5 and 6.

C. MICROPROBE RESULTS

The analytical results for individual particles obtained via microprobe studies show similar, though less well-defined trends in major element chemistry. The chemical analyses for several particles from Gifford-Hill & Co., Inc. sample Chouteau Plant-90287 are plotted on a CaO-SiO_2-Al_2O_3 ternary diagram in Figure 16. The reported compositions cover a much broader portion of the diagram than did the results for 34 ICP analyses. However, a very diffuse linear trend extending from the CaO apex towards the regions where kaolinite and montmorillonite plot on the SiO_2-Al_2O_3 join is still visible.

The classification scheme of Roy et al. (29) (Figure 17) was used to further characterize the samples based on the results of microprobe and ICP analyses. The ICP results for 34 samples are very consistent, falling almost entirely within the 'calsialic' field boundary. Microprobe results for Gifford-Hill & Co., Inc. sample Chouteau Plant-90287 (and also for samples Cason Plant-15268 and Westlake Plant-108739) plot along most of the right side (in the ferrocalsialic, calsialic and calcic fields) and in the bottom left corner ('ferric' field) of the triangle (Figure 18).

Microprobe analyses also permitted more detailed characterization of the magnetic fraction of fly ash samples. The results of chemical analyses of 376 particles from the magnetic fraction of sample Cason Plant-15268 are plotted on an FeO-Al_2O_3-MgO ternary diagram in Figure 12. Most analyses lie close to the FeO apex of the diagram. However, a diffuse trend extending from the spinel composition on the Al_2O_3-MgO join through the Hercynite, ferrian Spinel and Magnesioferrite fields is also visible. The number of analyses is

greatest between the FeO and Hercynite points on the diagram, suggesting that the spinel phase in the samples contains more aluminum than magnesium.

1. ICP Results for Concrete

The concrete mixtures used to assess differences in the chemistry of plain and fly ash-bearing concretes included the 6 pairs of concrete samples prepared using variable (0, 10, 20, 30, 40 and 60 weight percent substitution for cement) fly ash content, and the 55 laboratory concrete mixtures prepared using 15 weight percent substitution of fly ash for cement (including two control mixtures prepared without fly ash). The fly ash used to prepare the samples was the same as that analyzed and discussed in the preceding section. Additional mixture components included a standard Type 1 Portland cement and a fine-grained quartz sand (aggregate). The chemical composition (range, mean and standard deviation) of these components was presented earlier (Table 2).

The chemical composition of the fly ash used (Table 4) differs substantially from that of the cement and aggregate. These differences are equally apparent in the results of chemical analyses for the two sets of plain and fly ash-bearing concrete samples analyzed. For example, the aluminum content of the Gifford-Hill & Co., Inc. fly ashes is much greater than that of the cement or aggregate. The aluminum content of the total mixture should increase as the fly ash content increases. This trend is clearly illustrated in Figure 19, which plots weight percent Al_2O_3(A) and weight percent CaO(B) versus weight percent fly ash for the C series samples. The best-fit linear regression for Al_2O_3 is positive with an R-squared equal to 0.967. For CaO, the relationship has a negative slop with an R-squared of 0.9. Over the wide range of compositions illustrated, either oxide will predict the abundance of fly ash at the 95 percent confidence level within plus or minus 10 percent. A similar relation can be observed for the change in the Al composition of samples with 0, 4.5, and 100 weight percent fly ash (Figure 20). Correlation coefficients for the other chemical constituents reveal results similar to those shown above (Table 13). The abundances of a variety of elements vary with the quantity of fly ash in the concrete samples. Given the readily detectable effects of one fly ash addition on sample chemistry, all that remains is to determine how accurately these effects can be measured when the fly ash comes from multiple sources. Accuracy is essential if chemical analyses are to be used to discern small differences in the amount of fly ash substituted for cement.

There is a good correlation between the chemical composition of the Gifford-Hill & Co., Inc. fly ash sample and its source (plant number) (Table 12). However, these differences will be much more difficult to discern in concrete samples, because:

(i) fly ash composes a relatively minor fraction of the concrete (only 4.5 weight percent of the present samples),

and

(ii) differences in the chemical compositions of cement, aggregate and fly ash components are much greater than the chemical variation observed between fly ash samples from different plants.

2. Factor Analysis and Discriminant Function

Factor analysis was performed on the analyses of concrete samples containing 4.5 weight percent fly ash. Attempts to group concretes on the basis of fly ash source yielded four factors having eigenvalues greater than 1 (Table 14). Together, these factors account for 64.3 percent of the observed variation in concrete chemistry. This analysis essentially demonstrates the reliability of the quantitative approach. Although the factors are different, the source of the fly ash can be identified most of the time.

The first factor accounts for 19.21 percent of the variance and explains much of the observed variation in concentration for four major trace elements: Cr, Cu, V and Co. All are essentially unique to the fly ash component of the concrete mix. V and Cr are commonly associated with oxide phases, while Cu and Co are generally associated with sulfide-bearing phases.

The second factor accounts for 19.01 percent of the variance. It explains much of the variation of major elements: Fe, Al, Mg and Ti. All four elements are present in both fly ash and cement components. Concentrations are generally higher and more variable in the fly ash. A higher proportion of the variation explained by Factor 2 is probably attributable to the fly ash component of the mix.

Interestingly, both Factor 1 and Factor 2 account for roughly the same amount of variance. Factor 1 explains variations in the trace element chemistry of fly ash. Factor 2 accounts for variations in the major element chemistry of the same. A natural distinction thus appears to exist between the type of chemical variation associated with trace and major element components of fly ash samples. This is similar to the distinction observed for factor analysis of pure fly ash samples (i.e. Factor 1 and Factor 2).

The third Factor accounts for 15.90 percent of the variation explained by factor analysis. It accounts primarily for a strong inverse relationship between the Si and Ca content of samples. A good portion of the variation in K content is also accounted for. The inverse relationship between Si and Ca is analogous to the situation noted for pure fly ash samples. Much of the variation accounted for by factor 3 is thus probably also attributable to the fly ash used.

The fourth Factor accounts for 10.24 percent of the variation. It explains a large fraction of the variation observed for trace elements Sr and Ba. These elements are generally associated with the calcium-rich phases which occur in both fly ash and cement components. Although Ca is much more abundant in cements, Ba and Sr are much more concentrated in fly ash samples (Tables 5 - 10). The detected variations are more likely associated with the fly ash component of concrete samples.

The results of discriminant function analysis of concrete samples illustrate the difficulty of distinguishing the source of the fly ash used in concrete mixtures (Table 15). Samples from only one plant (Cason Plant), were classified correctly 100 percent of the time. Of the two samples containing fly ash from plant Gentry Plant, neither was classified correctly. Samples from remaining plants were classified correctly between 60 and 89 percent of the time. Samples were most frequently misclassified as belonging to Cason Plant. In summary, the accuracy of chemical analyses is such that they can be used to correctly identify the source of the fly ash much more than 50 percent of the time. The frequency with which chemical composition can be used to correctly identify the source (plant) of the fly ash used in a concrete sample is a good indicator of the accuracy of chemical method.

D. PREDICTIVE METHODS

Accurate prediction of weight percent fly ash in the concrete mix from chemical composition requires a prior knowledge of the chemistry of the fly ash and other concrete components (cement and aggregate), as well as their chemical variability. The nominal bulk composition of aggregate is not expected to vary greatly and the weight fraction of aggregate added in a mix varies approximately one percent (36). Then the total concentration of a given element in the concrete sample can be predicted using the following general equation:

$$Az + Cy + Fx = (\text{Tot Weight percent Oxide}) \quad (1)$$

where A = weight percent oxide in aggregate, C = weight percent oxide in cement, F = weight percent oxide in fly ash, z = weight fraction of aggregate in concrete, y = weight fraction of cement in concrete, and x = weight fraction of fly ash in concrete.

If chemical analyses are available for each of the three components of concrete mixtures and the weight fraction of each component in the mix is known, the total concentration of an element in the concrete sample (total weight percent oxide) is easily calculated. Similarly, if the concentration of the element in the concrete sample is known, Equation (1) can be used to

solve for any of the other variables, such as the weight fraction of fly ash substituted for cement. In the latter example, there are actually two unknowns: weight fraction of fly ash in the concrete (x), and weight fraction of cement in the concrete (y). In order to solve for both variables, a second equation is necessary. The obvious choice is derived through realization that the weight fraction of all components present in the concrete sample must sum to 1:

$$z + y + x = 1 \tag{2}$$

Assuming that the weight fraction of aggregate (z) is known, equation (i) can be related as:

$$Az + C\{(1-z)-x\} + Fx = (\text{Tot Weight percent Oxide}) \tag{3}$$

where only one variable remains. Finally, fly ash is usually added to concrete mixtures on a cement replacement basis. That is, a given weight of Portland cement is replaced with an equal weight of fly ash. The amount of aggregate in the sample is unaffected by the substitution and remains constant. Equation (1) can thus be simplified further by substituting the following two constant values:

k = weight fraction of aggregate in concrete
K = (1-k) = weight fraction of non-aggregate material in concrete.

The final equation thus reads:

$$Ak + C(K-x) + Fx = (\text{Tot Weight percent Oxide}) \tag{4}$$

One major obstacle still remains to using the above relationship to accurately predict the concentration of fly ash in a concrete sample. That is the error associated with obtaining values for each of the variables in Equation (4). Variations in the measurement of the weight fraction of aggregate in the sample are likely to be small and they are unlikely to contribute significant error. However, values for variables A, C and F are obtained from chemical analyses of separate samples of each component. There is no guarantee that the chemical composition of the sample chosen for analysis will be identical to its actual counterpart in concrete samples. The reliability of each of these three values is thus directly related to the homogeneity of the component. The greater its homogeneity, the greater the chance that the value entered into Equation (4) will reflect the true concentration of the element in the concrete

sample. The results of chemical analyses for aggregate and Portland cement samples (Table 2) indicate that these two components are relatively homogenous. Fly ash, on the other hand, can be quite heterogeneous (Tables 5 - 10). Evaluation of this latter component presents the greatest obstacle to accurate prediction of weight percent fly ash for a concrete sample.

The uncertainties associated with each of the values substituted into equation (ib) will contribute to the inaccuracy of the final result. Figure 21 schematically depicts the greatest amount of departure of predicted weight percent fly ash values from actual weight percent fly ash, assuming the chemical variables A, C and F are the only one contributing to the error.

Case (1) uses the minimum element concentration of each component. The equation defining this line thus represents the lowest possible estimate of fly ash content. Case (2) uses maximum observed element concentrations to graphically depict the other extreme. Attempts to predict the weight percent fly ash in a concrete sample will be in error when one of these two equations is assumed to represent the concentration of a given element in the sample when, in actuality, the other equation defines the true concentration. Assume, for instance, that the concentration of an element e in each component of a concrete sample is accurately defined in case (1), and that the sample contains 4.5 weight percent fly ash. If the observed concentration of element e in the sample is H, use of Equation (1) will result in prediction of the correct value for weight percent fly ash. Use of Equation (2) to predict weight percent fly ash will yield a value which is much too high.

The geometry of the situation depicted in Figure 21 suggests that attempts to predict weight percent fly ash in a sample are more likely to overestimate than to underestimate the true value. The shaded triangular areas A and B define the range of possible values for weight percent element, and the corresponding predicted values for weight percent fly ash. Both triangles share one leg, which is, therefore, the same length. However, the hypotenuse of B will always be greater than the hypotenuse of A, since the slope of Equation (2) is always less than the slope of Equation (1). The chance of overestimating weight percent fly ash is thus greater than the chance of underestimation.

As discussed above, the chemical heterogeneity of fly ash poses the greatest obstacle to obtaining accurate results. Additional uncertainties arise because of undetermined variations in the chemical composition of the element and the aggregate. Assuming that the results of the chemical analyses for fly ash samples (Tables 4 - 10) are representative of the variation in the fly as produced by plants in the Gulf Coast region, the maximum and minimum reported values can be used to assess the error associated with fly ash variability from all plants (Table 4). The actual concrete samples prepared contain 4.5 weight percent fly ash. The maximum amount by which predicted and actual weight percent fly can differ is thus calculated for the

case in which a fly ash having the chemical variability of the Gifford-Hill & Co., Inc. fly ash samples is used to prepare a concrete sample which contains 4.5 weight percent fly ash. Average compositional values for the aggregate and cement components (Table 2) are used in order to simplify the illustration. Equation (4) reduces to:

$$0.7A_{avg} + 0.255C_{avg} + 0.045F = \text{(Tot Weight percent Oxide)} \quad (5)$$

The minimum possible value for weight percent fly ash potentially determined from the results of chemical analyses for Gifford-Hill & Co., Inc. fly ash samples is calculated in two steps:

1. Assume F = the maximum concentration of the element observed in fly ash samples, and solve for total weight percent oxide.

2. Assume F = the minimum concentration of the element observed in fly ash samples, total weight percent oxide = the value obtained in step '1', and weight percent fly ash is unknown. Solve for weight percent fly ash.

The maximum value potentially calculated for weight percent fly ash is determined by reversing the values for F used in steps 1 and 2.

Figure 22 graphically depicts the results for samples from all plants. The maximum estimated value was 15 weight percent fly ash and the minimum was below zero. The quantity of fly ash predicted varied with the chemical constituent used in the calculation. SiO_2 and others were very poor predictors, while Al_2O_3 and CaO were reasonably good. CaO and Al_2O_3 allowed the fly ash content to be estimated somewhere between 3-7 weight percent. The differences associated with different elements and oxides are due to a variety of factors related to their abundance in the cement, the aggregate, and the fly ash as well as the chemical analysis method. The range in the estimates illustrated in Figure 22 is an extreme one that would have less than one chance in 100 to occurring. In practice the estimates should be much closer to the value of five weight percent which can be calculated with the analytical mean and standard deviations reported above.

Figure 23 depicts the spread in the maximum and minimum fly ash estimates for individual plants. CaO and Al_2O_3 are obviously the best predictors. The range of fly ash estimates is clearly reduced by considering samples from only one plant. This finding is in agreement with the results of factor analyses, which demonstrate clear differences in the

chemical composition of samples with plant. If one knows the chemical composition of the fly ash used in a concrete, then the reliability of the chemical method is improved.

Some elements and oxides consistently produced smaller error ranges. Several of these (Ca, Al, Fe and Ba) were chosen to determine whether the error range could be further reduced by substituting a ratio of the concentrations of two elements for F in Equation (5). While all ratios reduced the error range to some extent, the results for Ca/Al are outstanding (Table 16). Despite the large variation in Ca and Al content of samples, calculations suggest that weight percent fly ash can be predicted to within less than +/- 0.1 weight percent for samples containing 4.5 weight percent fly ash by using this ratio. This corresponds to an error of less than 2.2 percent. In summary, chemical analyses provide a very accurate means of determining the fly ash content of a concrete sample. However, the quality of the result is strongly contingent on the following two conditions:

(i) Errors attributable to small variations in the concentration of individual elements or oxides can be minimized by using the ratio of the concentration of the two in the concrete sample (e.g. CaO/Al_2O_3) rather than the concentration of a single constituent to predict weight percent fly ash.

(ii) The approximate composition of the fly ash (also cement and aggregate) added to the concrete must be known. Large errors in estimation of the chemical composition of the ash, such as may exist between Class C and Class F fly ashes, are likely to produce unacceptable results. On the other hand, compositional variations as large as those observed for the Gifford-Hill & Co., Inc. fly ashes do not affect prediction results appreciably.

E. USE OF IMAGE ANALYSIS TECHNIQUES

Fe-rich fly ash particles are easily identified in backscattered electron images of concrete samples because they possess:

(i) a uniquely spherical shape,

and

(ii) a much higher density (formula weight) than do most other concrete constituents.

If the Fe-rich fly ash particles can be isolated and identified, then quantification of this component should be relatively straight forward. The key to developing a successful quantification procedure is to devise a means of accurately and rapidly measuring the fly ash

component that does not depend on a physical or chemical separation. This goal is readily accomplished with the aid of polished thin sections of concrete and the software available on the Tractor-Northern Image Analysis Work Station. Backscattered electron images similar to those presented in Figure 10 can be used to create a binary image of the Fe-rich particles. However, the distinction between fly ash and non-fly ash components is not complete in this image, since it also includes the small, dense fragments of unhydrated clinker which commonly occur in concretes. The presence of these particles necessitates use of a shape factor and other image treatments to obtain complete discrimination of the fly ash component.

Prior to shape analysis the image is filtered to remove particles consisting of fewer than 4 or 5 pixels. The combined erosion dilation filtering process eliminates the small features which would produce unreliable results. Shape analysis classifies particles according to the following equations:

$$\text{Shape} = \frac{\text{Perimeter}^2}{4\ \pi\ \text{Area}} \tag{6}$$

For spherical particles this relationship reduces to:

$$\frac{(\pi D)^2}{4\pi(\pi r^2)} = 1 \tag{7}$$

The more spherical the particle, the more closely the shape factor approximates 1.

The image analysis technique has some promise, but does require knowledge of the quantity of Fe-rich fly ash components originally present. As reported by Ferrell and Drew (37) the method involves five steps:

(i) A backscattered image of the sample is acquired and stored. Compositional differences are recorded as differences in the brightness, or grey level, of the image.

(ii) Compositional, or grey level, differences provide the means for creating a binary image which distinguishes fly ash particles from the rest of the sample.

(iii) The resultant binary image is filtered to eliminate the smallest particles and pieces of particles from the analysis.

(iv) Shape factor analysis distinguishes spherical fly ash particles from irregular shaped grains of unhydrated cement clinker.

(v) The volume percent of nearly spherical particles is calculated and adjusted to compare the percentage of spherical particles in the matrix of fly ash-containing specimens to the percent in a control specimen with no fly ash.

Additional research on the fly ash component of concrete is suggested by the information gained from air-void and cement matrix binary images. Increased fly ash substitution has little effect on the total air-void content of samples. However, it has a marked effect on the size and distribution of pore spaces. More research is required to evaluate the suitability of image analysis procedures for the quantitative analysis of fly ash bearing concretes.

F. X-RAY DIFFRACTOGRAM ANALYSIS

The patterns were summed for individual power plants and are shown in Figures 24 through 29. All six sum patterns were summed to yield a single Master Sum Fly Ash Pattern (MSFP). The MSFP can be regarded as the representative, or standard, pattern for Class C fly ash samples as is shown in Figure 30.

X-ray diffractograms of 56 concrete mixtures with some of the ashes used in the present study were also obtained and examined after digital pattern enhancement. Sum patterns for concrete mixtures with ash corresponding to individual power plants are given in Figures 31 through 36, and a Master Sum Pattern for concrete mixtures is given in Figure 37.

The crystalline phases identified, and their nominal chemical compositions, are given in Table 18. D-spacings corresponding to these crystalline phases are given in Table 19. Relative intensities of these crystalline phases are reported with respect to the highest intensity peak of quartz identified at d = 0.334nm. Individual peaks identified in this sum pattern are also given in Table 19.

Peaks corresponding to d = 0.306 nm, 0.298 nm, 0.189 nm, 0.186 nm and 0.152 nm, could not be identified using the PDF files or other references. The peak at d=0.152 nm can be identified as mullite, but stronger mullite peaks are absent; therefore, its presence cannot be strongly argued. Similarly, peaks corresponding to d=0.161 nm can possibly be identified as ferrite spinel (38). Peaks corresponding to d=0.23 nm can be identified as quartz plus mullite.

Quantitative x-ray diffractometry has shown that 70 to 90 percent of the fly ash by weight is glassy (11). Consequently, fly ash XRD patterns have a distinct broad hump due to

x-ray scattering from the glassy phase. A careful examination of a sum file of the fly ashes used in this study revealed a broad hump with a maximum intensity at 32°2Θ, along with sharp crystalline peaks, in accordance with the findings of Diamond and Lopez-Flores (35,39). Most of the peaks that are present in the master sum pattern for fly ash are present in the sum patterns for the six individual power plants as seen in Figures 24 through 30.

Characteristics of each plant with reference to crystalline phases, identified and unidentified peaks, are illustrated in Tables 20 and 21. Table 20 gives crystalline phases identified in the diffractogram of each plant, and Table 21 gives unidentified peaks for each plant. The positions of the maxima of the glass humps are given in Table 22.

In the sum pattern for fly ash samples from the Cason Plant, crystalline phases observed were quartz, gehlenite, anhydrite, ilmenite, melilite, hematite, ferrite spinel, and possibly mullite. Identification of mullite was based on peaks at d=0.170 nm and d=0.152 nm, and was probable. The sum pattern for the Oologah power plant contains one unusual peak at d=0.279 nm that is not present in any other sum pattern. However, the peak at d=0.164 nm in the Master Sum Pattern is not present in this pattern. Most of the peaks identified in the Master Sum Pattern are present in the Boyce sum pattern. The relative intensity of the lime peak with respect to the strongest quartz peak is low compared to the sum patterns of other plants (including the Master Sum Pattern), except the Westlake sum pattern (Figure 28). A characteristic of the Gentry sum pattern is distinct gehlenite peaks. The Westlake sum pattern was observed to have all the peaks seen in the Master Sum Pattern, but lime peaks were observed to be relatively weak compared to other sum patterns. The Chouteau sum pattern was observed to be very similar to the Master Sum Pattern.

The Master Concrete Sum Pattern (MCSP) in Figure 37 for concrete mixtures revealed a number of distinct crystalline phases: quartz, ettringite, portlandite, calcite, anhydrite, and unhydrated calcium silicates. Aluminum peaks were also observed, but were due to the specimen holder. Names of these phases and their d-spacings are given in Table 23. When the XRD pattern was replotted by assigning an arbitrarily low value to the intensity of the 0.334 nm quartz peak, a broad amorphous hump was observed, indicating that it was suppressed due to the magnitude of the intensity of the quartz peak. Another advent of editing the quartz peak was that more crystalline peaks that were not visible in the original pattern were observed. Among these were ettringite peaks identified at d = 0.960, 0.557, 0.467, 0.373, 0.324, 0.296, 0.256, and 0.215 nm; an additional dicalcium silicate peak was also observed at 0.296 nm and a gypsum, dicalcium silicate, or calcium aluminum hydrate (C_2AH_{13}) was observed at 0.288 nm. Sum patterns of the concrete mixtures containing fly ash from individual power plants are given in Figure 31 through 36. The phases identified in each pattern are listed in Table 24,

and the position of the amorphous maximum is given in Table 22. Sum patterns with edited quartz peak at d=0.334 nm are given in Figures 38 through 43. In the edited sum patterns, ettringite peaks not observed in the individual patterns are often found; for example, ettringite peaks at d = 0.467, 0.373, 0.324, 0.256, and 0.215 nm are not found in the individual patterns. Similarly, peaks corresponding to different polymorphs of dicalcium silicate, at d=0.296 and 0.288 nm, are only found in the edited sum patterns.

Fly ashes are assembled of (mostly) spherical particles produced by combustion and melting of mineral impurities in ground coal. Because of the wide variability, both in coals and in the operation of boilers and collection of ash, specific fly ash samples differ in commposition and mineralogy. Each particle is heated and undergoes changes independent of the neighboring particle while passing chaotically through the burning zone of the power plant boiler. Particle composition reflects both the inorganic and organic portions of the particular coal fragment from which the particle originates with whatever changes have occurred due to selective vaporization of components and perhaps subsequent surface deposition (40). Moreover, the chemical composition and other characteristics of different fly ash particles in a given ash may vary considerably. Another complicating feature is that individual fly ash particles vary in the content of included crystalline components (viz. quartz, iron oxide, calcium bearing compounds, and others). Therefore, it becomes an obvious choice to study a standard XRD pattern from a large data set, hence our generation of sum files. Thus, a list of component minerals is obtained from the XRD patterns which includes the minerals likely to be found in a typical sample of Class C fly ash, but which may not always be present in a specific ash.

The Master Sum Pattern for fly ash (MSPF) given in Figure 46 represents 113 high calcium Class C fly ash samples. The MSPF is a standard diffractogram of fly ash derived from high calcium sub-bituminous coal. The pattern reveals more information, in terms of the number of crystalline peaks observed, than other individual diffractograms of fly ash. The sum pattern consists of peaks corresponding to the crystalline phases melilite, dicalcium silicate, tricalcium silicate, ilmenite, quartz, anhydrite, hematite, periclase, ferrite spinel, lime, merwinite,and possibly mullite. This higher calcium concentration in Class C fly ash results in the formation of lime, tricalcium aluminate and other calcium silicates such melilite, dicalcium silicate, and merwinite. Periclase, crystalline MgO, results from the oxidation of organic Mg from the lower rank coals, or from the decomposition of dolomite. At d=0.269 nm in the master sum pattern, a very strong peak of tricalcium aluminate ($Ca^3O^2O^6$) and merwinite $Ca^3Mg(SiO^4)^2$ appears. A detailed study has revealed that tricalcium aluminate is a dominant phase, and its peak overlaps with that of merwinite. The merwinite peak is distinctly visible in some diffractograms of individual fly ash samples from Cason, TX. Melilite, $(Ca,Na)^2(Mg,F-$

e,Al)(Si,Al)^{2}O^{7}, is a solid solution series between gehlenite ($CA^{2}Al^{2}SiO^{7}$) and akermanite ($Ca^{2}MgSi^{2}O^{7}$), although pure end members are very rare. Ilmenite, $FeTiO^{4}$, forms as a result of combustion of iron and titanium present in the coal. Hematite is present in all ashes and forms as the final combustion product of pyrite during and after combustion. Individual hematite peaks are not visible because the strongest peaks overlap with those of ferrite spinel. Ferrite spinel, (Mg,Fe)(Fe,Al)^{2}O^{4}, along with hematite, results from the oxidation of pyrite in coal.

A very careful study of the sum pattern of the ash reveals a very weak peak at 12.2$_{o}$2Θ, which might be considered a peak from brownmillerite ($Ca^{4}Al^{2}Fe^{2}O^{10}$) (38). Brownmillerite is not observed in the individual patterns where this is hidden in the background; it is identified only after data reduction techniques have enhanced the peak. Brownmillerite has been found in Class C fly ash, but only occasionally.

The nature of the glass present in the ash is of primary importance since the glass is a predominant phase constituting 60 percent to 90 percent of the total weight. In recent years, the importance of the glass phase in cememt reactions, and for strength gain in concrete, has been realized (15,35). Because of the extreme variability in the composition of fly ash particles, the glass present within different particles is likely to vary considerably in composition. This has been established by ESCA studies (39). Glasses from different fly ash samples are also likely to be different in composition. However, Diamond (35) observed that beyond 20 percent analytical CaO content, the position of the glass maximum is independent of composition. In the present study, where all the fly ash samples have a CaO ranging from 19.91 to 36.02 percent, the sum diffractogram gives a broad asymmetric hump for the glass phase with the maximum intensity at 32.0$_{o}$2Θ. The value obtained thus corroborates Diamond's data, but is more definitive as it is derived from a larger data set with lower noise. When sum patterns from individual plants are considered, very little variation is seen from one plant to another. The mineralogical variations from different plants does not appear to affect the composition of the glassy phase.

The XRD patterns of amorphous materials generally reflect their average structure. For example, pure silica glass produces a maximum around 24°Θ, corresponding to the most intense peak of cristobalite, the form the glass should acquire under equilibrium conditions (13,14). The broad hump in Class C fly ash represents some average structure of the glass, which is not highly variable.

Figure 44 gives XRD a pattern of concrete without fly ash. Crystalline phases observed in this sum pattern were quartz, portlandite, calcite, and unhydrated clinker phases tri- and di-calcium silicates. Phase identification is summarized in Table 25. Quartz peaks are from

the sand present in the admixture. - Clacite is the carbonation product of lime, portlandite or calcium silicate hydrate (C-S-H). The maximum of the amorphous hump is observed at approximately 33.3°2Θ. .This amorphous peak corresponds to calcium silicate hydrate (C-S-H), the hydration product of tri-calcium and di-calcium silicates. C-S-H is a highly non-stoichiometric and very poorly crystalline compound. In pure cement paste the C-S-H can constitute about 70 percent by weight, but unambiguous sharp x-ray peaks for C-S-H have not been observed. Some workers have suggested that peaks at 0.303 and 0.182 nm in a pure paste pattern are due to C-S-H but strong peaks of calcite and portlandite also have the same or very similar d-spacings. Thus, examination of the amorphous hump may be an effective way of studying the C-S-H.

The Master Sum Pattern of Concrete with fly ash given in Figure 37 is the typical concrete mixture pattern, and represents 53 individual diffractograms of concrete mixtures containing fly ash from various plants. From the figure, it is observed that the pattern is similar to the sum concrete pattern without fly ash, except for the position of the amorphous peak. The crystalline phases observed are almost the same as in the XRD pattern of concrete without fly ash. However, the pattern of concrete with fly ash contains a greater number of peaks (9) of ettringite than the one without fly ash (5); the ettringite peaks at d=0.465, 0.396, 0.376, 0.359, and 0.216 nm are only found in the pattern of concrete with fly ash. A few new peaks are also found, e.g., at d=0.507 nm, which are not present in the pattern without fly ash. The maximum of the amorphous hump is observed at approximately 2Θ=30.5°. Its maximum intensity relative to the quartz peak at d-0.334 nm is less than that of pure ash glass. The hump in the XRD patterns of these samples is always asymmetric, similar to those of the pure fly ash glasses, but unlike those of Portland cement concrete. The position of the hump is also very different when the Portland cement-fly ash concretes from individual plants are considered, which are given in Table 22. When the Portland cement-fly ash concretes are compared to their raw fly ashes, the position of the hump is sometimes identical, but at other times has changed. The chance is likely to be due to several factors, such as: the degree of reaction of the fly ash; and the resultant C-S-H, which has a different average structure than the glass. The position of the hump for concretes with fly ashes from individual plants is quite different from the master sum pattern. The asymmetric nature of the hump is partly responsible for this. The master sum pattern also contains a larger data set and lower noise.

In order to assess the presence of fly ash in concrete, the average patterns of both concretes with and without fly ash were studied (Figure 45 and 46). Even though most of the crystalline peaks were common to both patterns, the noticeable difference was in the position of their amorphous maxima. In comparison with the glass hump in pure ash, the amorphous

hump in concrete is more symmetric. The amorphous maximum for concrete without ash was located at approximately 33.3°2Θ, and that for concrete with fly ash at 30.5°2Θ. A study of the position of the hump is advantageous because it excludes all the crystalline components and focuses on the amorphous material, which constitutes the bulk of the sample. The position of the hump is also unaffected by the amount of sand added to the sample. A shift in the position of the hump reveals that an addition of fly ash to a concrete mixture considerably affects the structure of the C-S-H formed, and is not a mere mechanical mixture. The mechanical mixture would have yielded an amorphous peak position between that for the glass hump of pure fly ash and the amorphous peak of C-S-H of concrete without fly ash. The average structure of the C-S-H in concrete with fly ash is different from that without fly ash.

VI. CONCLUSIONS

1. X-ray diffractometry can be used to identify the presence of fly ash in a concrete without any knowledge of the type of fly ash used. The method is based on the presence of some minor peaks and the position of the amorphous hump.

2. Data smoothing techniques, namely a summing algorithm and a cubic least-squares method, have been found to be superior compared to studying individual spectra in the analysis of powder diffractograms.

3. The background stripping algorithms facilitated locating maxima of the amorphous hump in powder diffractograms of pure fly ash and concrete with and without fly ash.

4. The Master Sum Pattern of Class C fly ashes is a standard XRD pattern of that type of fly ash. The minerals present in the pattern are those typically expected from a Class C fly ash. The sum pattern also contains crystalline phases indicative of the bulk chemistry of Class C fly ashes, namely anhydrite, ferrite spinel, hematite, ilmentite, lime, melilite, merwinite, periclase, quartz, and tri-calcium aluminate, and possibly brownmilerite.

5. The tentative presence of the brownmillerite phase is established by special data reduction techniques which otherwise would not have been possible with the study of individual diffractograms.

6. Powder diffractograms of concretes with and without fly ash have practically identical crystalline phase assembly. They, however, differ in the position of the amorphous hump due to the C-S-H present, and the number of peaks observed for ettringite.

7. The structure of C-S-H formed in concrete with fly ash is significantly different than that formed in concrete with pure Portland cement.

VII. RECOMMENDATIONS

The quantitative analysis of fly ash in concrete can be accomplished by chemical analysis methods using a total digestion procedure for the determination of weight percent CaO/weight percent Al_2O_3 in concrete. It is based on a simple relationship which can be expressed as:

$$Ak + C(K-x) + Fx = \text{weight percent CaO/weight percent } Al_2O_3 \text{ in concrete}$$

where A = weight percent CaO/weight percent Al_2O_3 in aggregate, C = weight percent CaO/weight percent Al_2O_3 in cement, F = weight percent CaO/weight percent Al_2O_3 in fly ash, k = weight fraction of aggregate in concrete, K = (1-k) = weight fraction of non-aggregate material in concrete, and x = weight fraction of fly ash in concrete.

This analysis cannot be done without knowing the values of CaO and Al_2O_3 in the aggregate, the cement, and the fly ash as well as the weight fraction of aggregate in the concrete. For many situations, these requirements restrict the applicability of this method. When the information is available, the total analytical error in the determination of a sample with 4.5 weight percent fly ash is +/- 0.1 weight percent. Errors due to sampling were not evaluated directly in this study and may decrease the precision and accuracy of the determination.

For application to plastic concrete, the following procedure is recommended:

(1) Collect a representative sample of the aggregate, the cement, the fly ash, and the plastic concrete.

(2) Dry and grind all materials to a powder with particles smaller than 20μm.

(3) Cone and split the samples several times to obtain a representative portion weighing about 0.5g.

(4) Use ICP and total digestion method (or equivalent) to determine quantities of CaO and Al_2O_3 in a precisely weighed subsample of each of the materials.

(5) Determine quantity of aggregate in the plastic concrete directly, or consult specifications.

(6) Use the analytical values and the equation above to calculate the quantity to fit ash in the plastic concrete.

(7) Repeat the entire procedure at least twice and report the mean and standard deviation of the results.

For hardened concrete, one must rely on archived samples of the aggregate, the cement, and the fly ash (or estimates based on values from the specifications for a particular project) to determine the CaO to Al_2O_3 ratio of the starting materials. The concrete sample may be processed as indicated above. The accuracy of this approach is variable, depending on how well the compositions of the starting materials can be determined.

The following procedure is recommended for exploiting the conclusions:

(1) Build a data base consisting of XRD patterns of Portland cement and Portland cement-fly ash concrete examined under identical instrumental conditions.

(2) Tabulate the mineralogy of the maximum of the amorphous hump between the two types of concrete.

(3) Quantify the mineralogical differences between the two types of concrete by using an internal standard such as synthetic corundum (Al_2O_3). Two separate runs may be necessary for this step: one to establish the qualitative presence of fly ash and another for quantitative determination.

(4) Determine the position of the hump from the background.

(5) The amorphous hump for Portland on this procedure should be near 33.0°2Θ.

(6) A computer program based on this procedure should be developed. The program could completely automate the process.

VIII. REFERENCES

[1]Diamond, S., Cement and Concrete Research, Vol 14, 1984, pp. 455-462.

[2]Dunstan, E.R., "Fly Ash and Fly Ash Concrete," REC-ERC-82-1, Bureau of Reclamation, U. S. Department of the Interior, Denver, Colo., Engineering and Research Center, May 1984.

[3]Dunstan, E.R., Berry, E. E. and Malhotra, Vol. M., American Concrete Institute, Vol.77, March/April 1980, pp. 59-73.

[4]Kovacs, R., Effects of the Hydration Products on the Properties of Fly Ash Cements, Cement & Concrete Research, Vol. 5, 1975, pp. 73-82.

[5]Bamforth, P. B., In situ Measturement of the Effect of Partial Cement Replacement Using Either Fly Ash or Ground Granulated Blast-furnace Slag on the Performance of Mass Concrete, Proc. Instn. CiVol. Engrs., Vol. 69, 1980, pp. 778-8000.

[6]Berry, E. and Vol. M. Malhotra, Ash for Use in Concrete - A Critical Review, ACI Journal, 1980, pp. 59-73.

[7]Montgomery, D. G., D. C. Hughes and R. I. T. Williams, Fly Ash In Concrete - A Microstructure Study, Cement & Concrete Research, Vol. 11, 1981, pp. 591-603.

[8]Grutzeck, M. W., D. M. Roy and B. E. Scheetz, Microstructure of High-lime Fly Ash Cementicious Mixtures, Cement & Concrete Research, Vol. 11, 1981, pp. 291 - 294.

[9]Diamond, S., The Occurrence of Duplex Films On Fly Ash Surfaces, Cement & Concrete Research, Vol. 10, 1980, pp. 297-300.

[10]Swamy, R. N., Utilization of Fly Ash: A Challenge to Concrete Technology - 1, Indian Concr. J., 59, 1985, pp. 119-122.

[11]Sethi, K. L. and Kumar, Determination of Pozzolana Content in Portland Pozzolana Cement, Indian Concr. J., 59, 1985, pp. 325-327.

[12]Dron, R., Les Pozzolanes, et.al., Pozzolanicite, Revue des Materiaux de Construction, n. 692, 1975, pp. 27-30.

[13]Klug, H. and Alexander, L. E., X-ray Diffraction Procedures for Polycrystalline and Amorphous Materials, John Wiley and Sons, New York, 1974, p. 966.

[14]Warren, B. E., Journal of Applied Physics, Vol. 8, 1937, pp. 645-654.

[15]Roy, D. M., Luke, K. and Diamond, S., Materials Research Society Symp. Proc., Vol. 43, 1985, pp. 3-20.

[16]Marsh, B. K. and Day, R. L., Cement and Concrete Research, Vol. 18, 1988, pp. 301-310.

VIII. REFERENCES (continued)

[17]Helmuth, R., Fly Ash in Cement and Concrete, Portland Cement Association, Skoakie, Illinois, 1987.

[18]Ferrell, R. E., Jr.; A. Arman and G. Baykal, Effects of Combined Lime and Fly Ash Stabilization on the Elastic Moduli of Montmorillonitic Soils (Final Report), Louisiana Transportation Research Center Research Report FHWA/LA - 88-209, 1988, pp. 181.

[19]Mehta, P. K., Mineral Admixtures, in Concrete Admixtures Handbook: Properties, Science and Technology, Noyes Publications, Park Ridge, N. J., 1984, pp. 626.

[20]Dalvi, U. R., "Characterization of Fly Ash and Fly Ash-Cement Concrete," Master's Thesis, Louisiana State University, May 1989.

[21]Cullity, B. D., Elements of X-ray Diffraction, Addison-Wesley Co., Inc., Reading, Mass., 1978.

[22]Sonneveld, E. J. and Visser, J. W., Journal of Applied Crystallography, Vol. 8, 1975, pp. 1-7.

[23]Thompson, M. and Walsh, J. N., A Handbook of Inductively Coupled Plasma Spectrometry, Chapman & Hall, New York, N. Y., 1983, pp. 273.

[24]Fisher, G. L., Prentice, B. A., Silberman, D., Ondov, J. M., Biermann, A. H., Ragaini, R. C., and McFarland, A. R., Physical and Morphological Studies of Size- Classified Coal Fly Ash, Environmental Science and Technology, Vol. 12, 1978, pp. 447-451.

[25]Ramsden, A. R. and Shibaoka, M., Characterization and Analysis of Individual Fly Ash Particles From Coal-Fired Power Stations by a Combination of Optical Microscopy, Electron Microscopy and Quantitative Electron Microprobe Analysis, Atmospheric Environment, Vol, 16, 1981, pp. 2191-2206.

[26]Roy, D. M., Characterization of Fly Ash and its Reactions in Concrete, in Fly Ash and Coal Conversion By-products: Characterization, Utilization and Disposal I. MRS Symposium Proceedings, Vol. 43, 1985, pp. 3-20.

[27]Fisher, G. L., Chang, D. P. Y., and Brummer, M. Fly Ash Collected from Electrostatic Precipitators: Microcrystalline Structures and the Mystery of the Spheres, Science, Vol. 192, 1976, pp. 553-555.

[28]Hulett, L. D., Weinberger, A. J., Ferguson, N. M., Northcutt, K. J., and Lyon W.S., Trace-Element and Phase Relations in Fly Ash (Final Report), Electric Power Research Institute, EA-1822, Research Project 1061, 1981, pp. 63.

[29]Roy, W. R., Thiery, R. G., Schuller, R. M., and Suloway, J. J., Coal Fly Ash: A Review of the Literature and Proposed Classification System with Emphasis on Environmental Impacts, Illinois State Geological Survey. Environmental Geology Notes, Vol. 96, 1981, pp. 69.

[30]Page, A. L., Elseewi, A. A., and Straughan, I. R., Physical and Chemical Properties of Fly Ash from Coal-fired Power Plants with Reference to Environmental Impacts, Residue Reviews, 1979, pp. 83-120.

[31]McCarthy, G. J., Swanson, K. D., Keller, L. P., and Blatter, W. C., Mineralogy of Western Fly Ash, Cement & Concrete Research, Vol. 14, 1984, pp. 471-478.

[32]Mohnen, Vol. A, The Challenge of Acid Rain, Scientific American, Vol. 259, 1988, pp. 30-38.

[33]McCarthy, G. J., Keller, L. P., Stevenson, R. J., Galbreath, K. C., and Steinwand, A. L., Characterization of a Lignite Ash from the METC Gassifier. I. Mineralogy, in Fly Ash and Coal Conversion By-products: Characterization, Utilization and Disposal I. MRS Symposium Proceedings, Vol. 43, 1985, pp. 165-176.

[34]Stevenson, R. J., and Larsen, R. A., Characterization of a Lignite Ash from the METC Gassifier. II. Scanning Electron Microscopy, in Fly Ash and Coal Conversion By-products: Characterization, Utilization and Disposal I. MRS Symposium Proceedings, Vol. 43, 1985, pp. 177-186.

[35]Diamond, S., Cement and Concrete Research, Vol. 13, 1983, pp. 459-464.

[36]Rasoulian, Masood, LTRC, Private Communication.

[37]Ferrell, R. E., Jr., and Drew, A. W., (in press) Quantification of Fly Ash in Concrete By Image Analysis Techniques A Preliminary Investigation, In Fly Ash and Coal Conversion By-products: Characterization, Utilization and Disposal Vol. MRS Symposium Proceedings.

[38]McCarthy, G. J. and Johansen, D. M., Powder Diffraction, Vol. 3, 1988, pp. 156-161.

[39]Diamond, S. and Lopez-Flores, F., Effects of Fly Ash Incorporation in Cement and Concrete, Symposium Proceedings, N, Materials Research Society Annual Meeting, No Vol., 1981, pp. 34-45.

[40]Raask, E., Mineral Impurities in Coal Combustion, Hemisphere, New York, 1987.

IX. BIBLIOGRAPHY

Eckersley, M. C., "Structural Ordering In Calcium Silicate Glass", Nature, vol. 135, Oct. 1988, pp. 525-527.

Ernst, R. R., "Sensitivity Enhancement In Magnetic Resonance", Adv. In Magnetic Resonance, Waugh, ed., 1964.

Goehner, R. P., "Background Subtract Subroutine For Spectral Data", Analytical Chemistry, Vol. 50, No. 8, 1978, pp. 1223-1225.

Hilderband, F. B., "Introduction To Numerical Analysis", McGraw-Hill, New York, 1956.

Ibers, J. A., "Mathematical Basis Of Least Squares Refinement", Lecture Transcript, Dept. Of Chemistry, Northwestern University, Evanston, Illinois.

Parrish, W. and Enzo S., "A Method Of Background Subtraction For the Analysis Of Broadened Profiles", Adv. in X-ray Analysis, Vol. 23, 1979, pp. 37-44.

Parrish, W. et al., "Experimental Study Of precise Peak Determination in X-ray Powder Diffraction", Adv. in X-ray Analysis, Vol. 23, 1979, pp. 53-60.

Pyrros, N. P. and Hubbard C. R., "Powder Pattern: A System Of Programs For Processing and Interpreting Powder Diffraction Data", Adv. in X-ray Analysis, Vol. 23, 1979.

Savitzky, A. and Golay, M. J. E., "Smoothing and Differentiation Of Data by Simplified Least Squares Procedures", Analytical Chemistry, Vol 36, No. 8, July 1964, pages 1627 to 1639.

Schreiner, W. N. and Jenkins, R., "Profile Fitting For Quantitative Analysis in X-ray Powder Diffraction", Adv. in X-ray Analysis, Vol. 23, 1979, pp. 141-147.

Schreiner, W. N. and Jenkins, R., "A Second Derivative Algorithm For Identification Of Peaks In Powder Diffraction Patterns", Adv. in X-ray Analysis, Vol. 23, 1979, pp. 287 -293.

Warren, B. E. et al, "Fourier Analysis Of X-Ray Patterns Of Vitreous SiO_2 and B_2O_3", Journal Of American Ceramic Society, vol. 19, 1936, pp. 202-206.

Whitaker, S. and Pigford, R. L., "An Approach to Numerical Differentiation Of Experimental Data", Industrial and Engineering Chemistry, Vol. 52, No. 2,Feb. 1960, pp. 185-187.

Wilson, P. A. and Edwards T. H., "Sampling and Smoothing Of Spectra", Applied Spectros copy Reviews, Brame, Jr., E. G., ed., 12(1), 1-81, 1976.

Whittaker, E. T., and Robinson, G., "The Calculus of Observation", 1924.

Yin, C.D. et al., "Structure analysis Of $MgSiO_3$ Glass", Journal of Non-Crystalline Solids, Vol. 55, 1983, pp. 131-141.

TABLES

TABLE 1.

LIST OF FLY ASH SAMPLES SUPPLIED BY GIFFORD-HILL, INC.

SAMPLE NUMBER	LOCATION	PLANT #	SILO/UNIT #	SAMPLE DATE
45	Westlake, LA	82	Unit 6	25-Aug-87
46	Westlake, LA	82	?	1-Sep-87
47	Westlake, LA	82	?	5-Sep-87
48	Westlake, LA	82	Unit 6	15-Sep-87
49	Westlake, LA	82	Unit 6	22-Sep-87
50	Westlake, LA	82	Unit 6	29-Sep-87
51	Westlake, LA	82	Unit 6	6-Oct-87
52	Westlake, LA	82	Unit 6	13-Oct-87
53	Westlake, LA	82	Unit 6	20-Oct-87
54	Westlake, LA	82	Unit 6	21-Oct-87
55	Boyce, LA	84	-	26-Aug-87
56	Boyce, LA	84	Silo 1	8-Sep-87
57	Boyce, LA	84	-	15-Sep-87
58	Boyce, LA	84	-	22-Sep-87
59	Boyce, LA	84	-	28-Sep-87
60	Boyce, LA	84	-	6-Oct-87
61	Boyce, LA	84	-	12-Oct-87
62	Boyce, LA	84	-	20-Oct-87
63	Boyce, LA	84	-	24-Oct-87
64	Boyce, LA	84	-	31-Oct-87
65	Boyce, LA	84	-	10-Nov-87
66	Boyce, LA	84	-	15-Nov-87
67	Chouteau, OK	85	-	27-Aug-87
68	Chouteau, OK	85	-	2-Sep-87
69	Chouteau, OK	85	-	8-Sep-87
70	Chouteau, OK	85	-	10-Sep-87
71	Chouteau, OK	85	-	17-Sep-87
72	Chouteau, OK	85	-	25-Sep-87
73	Chouteau, OK	85	-	5-Oct-87
74	Chouteau, OK	85	-	13-Oct-87
75	Oologah, OK	88	-	2-Sep-87
76	Oologah, OK	88	-	9-Sep-87
77	Oologah, OK	88	-	16-Sep-87
78	Oologah, OK	88	-	23-Sep-87
79	Oologah, OK	88	-	30-Sep-87
80	Oologah, OK	88	-	7-Oct-87
81	Oologah, OK	88	-	14-Oct-87
82	Oologah, OK	88	-	21-Oct-87
83	Oologah, OK	88	-	28-Oct-87
84	Oologah, OK	88	-	4-Nov-87
85	Oologah, OK	88	-	10-Nov-87

TABLE 1 (cont'd)

LIST OF FLY ASH SAMPLES SUPPLIED BY GIFFORD-HILL, INC.

SAMPLE NUMBER	LOCATION	PLANT #	SILO/UNIT #	SAMPLE DATE
1	Cason, TX	78	Silo 2	?
2	Cason, TX	78	Silo 2	?
3	Cason, TX	78	Silo 2	?
4	Cason, TX	78	Silo 1	20-Aug-87
5	Cason, TX	78	Silo 2	20-Aug-87
6	Cason, TX	78	Silo 3	20-Aug-87
7	Cason, TX	78	Silo 1	27-Aug-87
8	Cason, TX	78	Silo 2	27-Aug-87
9	Cason, TX	78	Silo 3	27-Aug-87
10	Cason, TX	78	Silo 1	2-Sep-87
11	Cason, TX	78	Silo 2	2-Sep-87
12	Cason, TX	78	Silo 3	2-Sep-87
13	Cason, TX	78	Silo 1	10-Sep-87
14	Cason, TX	78	Silo 2	10-Sep-87
15	Cason, TX	78	Silo 3	10-Sep-87
16	Cason, TX	78	Silo 1	17-Sep-87
17	Cason, TX	78	Silo 2	17-Sep-87
18	Cason, TX	78	Silo 3	17-Sep-87
19	Cason, TX	78	Silo 1	24-Sep-87
20	Cason, TX	78	Silo 2	24-Sep-87
21	Cason, TX	78	Silo 3	24-Sep-87
22	Cason, TX	78	Silo 2	1-Oct-87
23	Cason, TX	78	Silo 3	1-Oct-87
24	Cason, TX	78	Silo 2	7-Oct-87
25	Cason, TX	78	Silo 3	13-Oct-87
26	Cason, TX	78	Silo 3	22-Oct-87
27	Cason, TX	78	Silo 1	26-Oct-87
28	Cason, TX	78	Silo 1	29-Oct-87
29	Cason, TX	78	Silo 3	29-Oct-87
30	Cason, TX	78	Silo 1	5-Nov-87
31	Cason, TX	78	Silo 3	5-Nov-87
32	Cason, TX	78	Silo 2	6-Nov-87
33	Cason, TX	78	Silo 1	12-Nov-87
34	Cason, TX	78	Silo 2	12-Nov-87
35	Cason, TX	78	Silo 3	12-Nov-87
36	Gentry, AR	81	-	26-Aug-87
37	Gentry, AR	81	-	3-Sep-87
38	Gentry, AR	81	-	10-Sep-87
39	Gentry, AR	81	-	16-Sep-87
40	Gentry, AR	81	-	23-Sep-87
41	Gentry, AR	81	-	30-Sep-87
42	Gentry, AR	81	-	8-Oct-87
43	Gentry, AR	81	-	14-Oct-87
44	Gentry, AR	81	-	21-Oct-87

TABLE 2.

CHEMICAL VARIABILITY OF AGGREGATE AND PORTLAND CEMENT USED IN CONCRETE MIXTURES

	AGGREGATE				PORTLAND CEMENT			
ELEMENT /OXIDE	MIN. WT%	MAX. WT%	MEAN WT%	STD. DEV.	MIN. WT%	MAX. WT%	MEAN WT%	STD. DEV.
SIO2	98.57	98.60	98.59	0.01	20.39	22.12	21.44	0.74
AL2O3	0.67	0.69	0.68	0.01	4.63	5.04	4.83	0.17
FEO	0.08	0.09	0.08	0.01	2.62	2.82	2.74	0.08
MGO	<DL	<DL	<DL	-	2.51	2.76	2.65	0.11
MNO	<DL	<DL	<DL	-	0.06	0.06	0.06	0.00
CAO	0.07	0.07	0.07	0.00	66.07	68.74	67.20	1.12
TIO2	0.10	0.11	0.11	0.01	0.24	0.26	0.25	0.01
P2O5	0.03	0.05	0.04	0.01	0.05	0.07	0.06	0.01
NA2O	0.01	0.05	0.03	0.02	0.09	0.12	0.11	0.01
K2O	0.37	0.38	0.37	0.01	0.57	0.59	0.58	0.01
BA	0.02	0.02	0.02	0.00	0.01	0.01	0.01	0.00
SR	<DL	<DL	<DL	-	0.05	0.05	0.05	0.00

<DL-not detected; STD. DEV.-Standard Deviation

TABLE 3.

MINERALS IDENTIFIED IN FLY ASH AND THEIR CHEMICAL COMPOSITION

Mineral	Symbol	Chemical Composition
Quartz	Q	SiO_2
Lime	L	CaO
Anhydrite	A	$CaSO_4$
Periclase	P	MgO
Hematite	H	Fe_2O_3
Ferrite Spinel (Magnetite)	FSp (M)	$(Mg,Fe)(Fe,Al)_2O_4$
Melilite	Ml	$Ca_2(Mg,Al)(Si,Al)_2O_7$
Merwinite	Mw	Ca3Mg(SiO4)2

TABLE 4.

CHEMICAL VARIABILITY OF FLY ASH FROM ALL GIFFORD HILL PLANTS

ELEMENT /OXIDE	MINIMUM WT%	MAXIMUM WT%	MEAN WT%	STANDARD DEVIATION
SIO2	28.56	43.92	35.20	3.65
AL2O3	16.95	22.92	18.95	1.27
FEO	4.84	7.43	6.05	0.53
MGO	3.77	7.17	5.63	0.82
MNO	0.03	0.09	0.05	0.02
CAO	19.91	36.02	28.30	4.14
TIO2	0.83	1.97	1.26	0.23
P2O5	0.27	1.24	0.78	0.22
NA2O	1.57	3.23	2.27	0.35
K2O	0.08	0.85	0.42	0.21
BA	0.35	0.71	0.48	0.09
SR	0.18	0.48	0.32	0.09

TABLE 5.

CHEMICAL VARIABILITY OF FLY ASH FROM GIFFORD HILL PLANT NO. 78

ELEMENT /OXIDE	MINIMUM WT%	MAXIMUM WT%	MEAN WT%	STANDARD DEVIATION
SIO2	29.68	33.66	31.90	0.89
AL2O3	17.12	19.60	18.13	0.59
FEO	5.60	7.03	6.25	0.39
MGO	5.51	6.95	6.26	0.36
MNO	0.05	0.07	0.06	0.01
CAO	29.09	35.01	31.91	1.26
TIO2	1.02	1.85	1.21	0.19
P2O5	0.27	0.95	0.73	0.16
NA2O	1.57	2.57	2.11	0.23
K2O	0.08	0.35	0.23	0.07
BA	0.39	0.71	0.54	0.09
SR	0.27	0.48	0.40	0.06

TABLE 6.

CHEMICAL VARIABILITY OF FLY ASH FROM GIFFORD HILL PLANT NO. 81

ELEMENT /OXIDE	MINIMUM WT%	MAXIMUM WT%	MEAN WT%	STANDARD DEVIATION
SIO2	28.56	34.08	32.19	1.73
AL2O3	16.95	19.33	18.04	0.88
FEO	4.84	6.08	5.57	0.45
MGO	5.41	7.17	6.62	0.63
MNO	0.05	0.09	0.07	0.01
CAO	28.59	36.02	31.69	2.25
TIO2	1.22	1.97	1.56	0.22
P2O5	0.31	0.98	0.56	0.23
NA2O	1.84	2.75	2.32	0.28
K2O	0.21	0.31	0.26	0.04
BA	0.43	0.54	0.47	0.04
SR	0.29	0.35	0.31	0.02

TABLE 7.

CHEMICAL VARIABILITY OF FLY ASH FROM GIFFORD HILL PLANT NO. 82

ELEMENT /OXIDE	MINIMUM WT%	MAXIMUM WT%	MEAN WT%	STANDARD DEVIATION
SIO2	36.53	41.05	39.54	1.37
AL2O3	19.12	20.94	20.17	0.47
FEO	5.46	6.58	5.89	0.34
MGO	4.36	5.60	4.88	0.33
MNO	0.03	0.04	0.04	0.01
CAO	22.31	25.21	23.34	0.96
TIO2	1.07	1.70	1.26	0.20
P2O5	0.80	1.23	0.90	0.13
NA2O	1.96	2.63	2.32	0.19
K2O	0.57	0.72	0.66	0.05
BA	0.38	0.52	0.42	0.04
SR	0.20	0.26	0.21	0.02

TABLE 8.

CHEMICAL VARIABILITY OF FLY ASH FROM GIFFORD HILL PLANT NO. 84

ELEMENT /OXIDE	MINIMUM WT%	MAXIMUM WT%	MEAN WT%	STANDARD DEVIATION
SIO2	36.69	40.11	38.53	1.02
AL2O3	17.83	21.46	19.45	0.95
FEO	5.88	7.43	6.44	0.43
MGO	4.43	5.11	4.80	0.22
MNO	0.03	0.04	0.03	0.00
CAO	22.65	25.71	24.19	1.06
TIO2	1.06	1.66	1.27	0.23
P2O5	0.32	1.24	0.85	0.24
NA2O	2.52	3.23	2.85	0.22
K2O	0.55	0.70	0.62	0.05
BA	0.35	0.55	0.40	0.05
SR	0.18	0.29	0.21	0.03

TABLE 9.

CHEMICAL VARIABILITY OF FLY ASH FROM GIFFORD HILL PLANT NO. 85

ELEMENT /OXIDE	MINIMUM WT%	MAXIMUM WT%	MEAN WT%	STANDARD DEVIATION
SIO2	35.64	38.57	37.10	1.16
AL2O3	17.73	19.59	18.38	0.63
FEO	5.29	6.04	5.61	0.24
MGO	5.15	5.65	5.37	0.19
MNO	0.04	0.05	0.05	0.01
CAO	25.92	29.74	27.84	1.46
TIO2	1.06	1.68	1.38	0.20
P2O5	0.36	0.88	0.67	0.21
NA2O	1.77	2.28	2.11	0.19
K2O	0.33	0.45	0.38	0.04
BA	0.42	0.51	0.45	0.03
SR	0.27	0.40	0.32	0.05

TABLE 10.

CHEMICAL VARIABILITY OF FLY ASH FROM GIFFORD HILL PLANT NO. 88

ELEMENT /OXIDE	MINIMUM WT%	MAXIMUM WT%	MEAN WT%	STANDARD DEVIATION
SIO2	35.26	43.92	38.69	2.66
AL2O3	18.91	22.92	20.68	1.14
FEO	4.89	6.86	5.62	0.59
MGO	3.77	5.70	4.87	0.60
MNO	0.03	0.08	0.05	0.02
CAO	19.91	28.44	24.25	2.98
TIO2	0.83	1.51	1.18	0.23
P2O5	0.40	1.20	0.94	0.24
NA2O	1.66	2.56	2.08	0.28
K2O	0.50	0.85	0.67	0.11
BA	0.38	0.56	0.45	0.05
SR	0.19	0.41	0.28	0.07

TABLE 11.

FACTOR ANALYSIS RESULTS: DISTINCTION OF GIFFORD HILL FLY ASH SAMPLES BY PLANT NUMBER

CHEMICAL CONSTITUENT	FACTOR 1	FACTOR 2	FACTOR 3	FACTOR 4
SIO2	0.927			
K2O	0.896			
ZN	0.835			
AL2O3	0.805			
V	0.679	0.581		
P2O5	0.600	0.485		
CR	0.567	0.548		
SR	-0.702	0.592		
MNO	-0.732			
MGO	-0.924			
CAO	-0.937			
CU		0.771		
ZR		0.688		
CO		0.659		
BA	-0.480	0.641		
FEO		0.595	-0.517	
TIO2		-0.750		
NI			0.687	0.526
NA2O		-0.460	-0.534	0.494
Eigenvalue	7.421	4.695	1.566	1.239
% Variance Explained	40.88	25.86	8.63	6.82

TABLE 12.

DISCRIMINANT FUNCTION ANALYSIS RESULTS FOR GIFFORD HILL FLY ASH SAMPLES

PLANT	# OF SAMPLES	# (%) OF SAMPLES CORRECTLY CLASSIFIED	OTHER PLANTS CLASSIFIED TO
78	41	39 (95.12)	81
81	8	7 (87.50)	78
82	10	10 (100.00)	- -
84	15	15 (100.00)	- -
85	7	7 (100.00)	- -
88	14	14 (100.00)	- -

TABLE 13.

CORRELATION COEFFICIENTS FOR C-SERIES RESULTS

ELEMENT	R^2
Si	0.822
Al	0.900
Fe	0.871
Ca	0.953
Na	0.940
Ti	0.900
P	0.919
Ba	0.937
Sr	0.838
V	0.750

TABLE 14.

FACTOR ANALYSIS RESULTS: DISTINCTION OF CONCRETE MIXTURES BY THE TYPE (PLANT NO.) OF FLY ASH USED

CHEMICAL CONSTITUENT	FACTOR 1	FACTOR 2	FACTOR 3	FACTOR 4
CR	0.892			
CU	0.848			
V	0.846			
CO	0.732			
FEO		0.942		
AL2O3		0.902		
MGO		0.857		
TIO2		0.736		
CAO			0.934	
K2O			0.589	
SIO2			-0.963	
SR				0.892
BA				0.795
ZN				
MNO				
ZR				
NI				
NA2O			0.417	
P2O5	0.429			
Eigenvalue	3.240	3.207	2.683	1.728
% Variance Explained	19.21	19.01	15.90	10.24

TABLE 15.

DISCRIMINANT FUNCTION ANALYSIS RESULTS FOR CONCRETE SAMPLES CONTAINING 4.5 WEIGHT PERCENT FLY ASH

PLANT	# OF SAMPLES	# (%) OF SAMPLES CORRECTLY CLASSIFIED	OTHER PLANTS CLASSIFIED TO
78	25	25 (100.00)	
81	2	0 (0.00)	78
82	5	4 (80.00)	78
84	9	8 (88.89)	78
85	2	1 (50.00)	88
88	10	6 (60.00)	78

TABLE 16.

VARIATIONS IN PREDICTED WEIGHT PERCENT FLY ASH USING OXIDE RATIOS OF SELECTED ELEMENTS

ELEMENT RATIO	CAO/AL2O3		FEO/AL2O3		BA/AL2O3		(FEO+BA)/AL2O3		(CAO+BA)/AL2O3	
PLANT#	MIN. WT% F.A.	MAX. WT% F.A.	MIN. WT% F.A.	MAX. WT% F.A.	MIN. WT% F.A.	MAX. WT% F.A.	MIN. WT% F.A.	MAX. WT% F.A.	MIN. WT% F.A.	MAX. WT% F.A.
7 8	4.47	4.53	3.91	5.18	2.80	7.24	3.58	5.66	4.46	4.54
8 1	4.44	4.57	4.04	5.02	4.02	5.04	3.94	5.13	4.43	4.58
8 2	4.49	4.51	4.04	5.01	3.56	5.68	3.93	5.16	4.48	4.52
8 4	4.47	4.53	4.19	4.84	3.36	6.03	4.04	5.02	4.48	4.52
8 5	4.48	4.52	4.33	4.67	4.09	4.95	4.28	4.73	4.48	4.52
8 8	4.43	4.57	3.91	5.19	3.66	5.54	3.80	5.33	4.42	4.58

TABLE 17.

INSTRUMENTAL SETTINGS

Tube type	:	Cu
Alpha 1, 2 wavelength	:	1.54060, 1.54439 Angstrom
Intensity ratio	:	0.50000
Tube focus	:	Long fine
Generator	:	40 kV, 21 mA
Take-off angle	:	6.00 deg
Divergence slit	:	Automatic
Receiving slit	:	0.2 mm
Scatter slit	:	None
Monochromator	:	Yes
Detector type	:	Scintillation
High angular limit	:	125.00 deg
Starting angle	:	2.00 deg
Final angle	:	70.00 deg
Step size	:	0.040 deg
Counting time	:	1.00 sec

TABLE 18.

CRYSTALLINE PHASES IDENTIFIED IN FLY ASH SAMPLES

NAME	NOMINAL COMPOSITION
Anhydrite	$CaSO_4$
Dicalcium silicate	Ca_2SiO_4
Ferrite Spinel	$(Mg,Fe)(Fe,Al)_2O_4$ (Probable)
Gehlenite	$2CaO.AlO_3.SiO_2$
Hemetite	Fe_2O_3
Ilmenite	$FeTiO_4$
Lime	CaO
Melilite	$(Ca,Na)_2(Mg,Al,Fe)(Si,Al)_2O_7$
Mullite	$Al_6Si_2O_{13}$ (probable)
Merwinite	$Ca_3Mg(SiO_4)_2$
Periclase	MgO
Quartz	SiO_2
Tri-calcium Aluminate	$Ca_3Al_2O_6$

TABLE 19.

X-RAY DIFFRACTION DATA FOR MASTER FLY ASH SUM PATTERN

2θ deg.	d (nm)	I/I_0	Crystalline Phase
21.0	0.423	28.0	Quartz
23.8	0.371	28.0	Gehlenite
25.5	0.349	50.0	Anhydrite
26.6	0.334	100.0	Quartz
31.5	0.284	50.0	Gehlenite
32.5	0.275	43.8	?
33.3	0.269	72.5	Tricalcium aluminate; Merwinite
35.5	0.253	33.8	Hematite
36.5	0.246	29.7	Quartz
37.5	0.240	50.6	Lime
38.5	0.234	77.8	Aluminum
39.5	0.228	27.2	Quartz
40.8	0.221	31.6	Quartz; Mullite (?)
42.5	0.213	26.6	Quartz; Mullite
42.9	0.210	58.6	Periclase
44.8	0.201	34.1	Aluminum
45.8	0.199	24.7	Quartz
50.3	0.182	35.9	Quartz
52.2	0.175	25.0	Anhydrite; Melilite
54.1	0.170	39.1	Melilite; Hematite
55.0	0.167	22.8	Quartz
57.2	0.161	24.4	Spinel (?)
60.0	0.154	33.8	Quartz
60.8	0.152	25.0	Mullite (?)
62.4	0.149	44.1	Periclase
65.2	0.143	47.5	Aluminum

TABLE 20.

MINERALS OBSERVED IN FLY ASH SAMPLES OF VARIOUS PLANTS

	BOYCE	CASON	CHOUTEAU	GENTRY	OOLOGAH	WESTLAKE
anhydrite	*	*	*	*	*	*
Ferrite Spinel	*	*		*	*	*
Gehlenite	*	*	*	*	*	*
Hemetite	*	*	*	*	*	*
Ilmenite		*	*	*	*	*
Lime	*	*	*	*	*	*
Melilite	*	*	*	*	*	*
Merwinite	*	*	*	*	*	*
Mullite	?	?	?	?	?	?
Periclase	*	*	*	*	*	*
Quartz	*	*	*	*	*	*
Tri-calcium aluminate	*	*	*	*	*	*

TABLE 21.

D-SPACINGS OF UNIDENTIFIED PEAKS

OBSERVED IN FLY ASH SAMPLES OF VARIOUS PLANTS

d (nm)	BOYCE	CASON	CHOUTEAU	GENTRY	OOLOGAH	WESTLAKE
0.404	w	*		*		
0.388	*				*	*
0.318	*			*	*	*
0.308	*			*	w	*
0.298	*	*	*		*	
0.281						*
0.243		*	*	*		
0.230	*	*		*	*	*
0.206			*			

Note : w indicates intensity of the peak is very low or the distinction of the peak from other peaks is not very clear.

TABLE 22.

MAXIMUM OF AMORPHOUS MATERIAL HUMP (2θ)

	Chouteau	Cason	Gentry	Westlake	Boyce	Oologah
Fly ash	32.0	32.0	32.5	32.0	32.0	32.0
	av. = 32.08 ± 0.20					
	from the master sum pattern = 32.0					
Fly ash in concrete	32.0	31.0	32.5	33.0	32.0	32.8
	av. = 32.21 ± 0.72					
	Sum of all fly ash-cement concrete = 30.5					

TABLE 23.

X-RAY DIFFRACTION DATA FOR THE SUM PORTLAND CEMENT-FLY ASH CONCRETE PATTERN

2θ deg	d (nm)	I/I_0	Crystalline Phase
9.16	0.964	1.09	Ettringite
15.84	0.559	0.97	Ettringite
17.48	0.507	0.93	
18.08	0.490	4.37	Portlandite
19.08	0.465	0.93	Ettringite
20.92	0.424	13.04	Quartz
23.00	0.396	1.29	Ettringite
23.64	0.376	1.04	Ettringite
24.4	0.364	1.01	(?)
24.8	0.359	1.03	Ettringite
25.64	0.347	1.3	Ettringite
26.68	0.334	100.0	Quartz
27.52	0.324	2.47	Ettringite
28.72	0.311	2.35	Portlandite
29.48	0.303	2.57	Calcite
30.12	0.296	1.81	C_2S
31.04	0.288	1.82	Gypsum (?); C_2S
32.28	0.277	2.94	C_2S; C_3S
32.64	0.274	2.67	C_2S; C_3S
34.12	0.263	6.48	Portlandite
36.6	0.245	9.04	Quartz
38.44	0.234	4.41	Aluminum
39.48	0.228	9.42	Quartz; Calcite
40.32	0.223	5.33	Quartz
41.36	0.218	1.68	C_2S
41.84	0.216	1.49	Ettringite
42.48	0.213	7.55	Quartz
42.92	0.211	1.61	Periclase
44.64	0.203	1.96	Aluminum
45.8	0.198	6.09	Quartz
47.16	0.193	3.48	Portlandite

TABLE 24.

PHASES IDENTIFIED IN THE XRD PATTERNS OF

PORTLAND CEMENT-FLY ASH CONCRETE

Plant	Quartz	Ettringite	Calcite	Portlandite	C_2S	C_3S	An
Boyce	X	X	X	X	X	X	
Cason	X	X	X	X	X	X	
Chouteau	X	X	X	X	X	X	
Gentry	X	X	X	X	X	X	
Oologah	X	X	X	X	X	X	
Westlake	X	X	X	X	X	X	

X = present

TABLE 25.

X-RAY DIFFRACTION DATA FOR THE SUM PORTLAND CEMENT-FLY ASH CONCRETE PATTERN

2θ deg	d (nm)	I/I_0	Crystalline Phase
9.16	0.964	1.09	Ettringite
15.84	0.559	0.97	Ettringite
17.48	0.507	0.93	
18.08	0.490	4.37	Portlandite
19.08	0.465	0.93	Ettringite
20.92	0.424	13.04	Quartz
23.00	0.396	1.29	Ettringite
23.64	0.376	1.04	Ettringite
24.4	0.364	1.01	(?)
24.8	0.359	1.03	Ettringite
25.64	0.347	1.3	Ettringite
26.68	0.334	100.0	Quartz
27.52	0.324	2.47	Ettringite
28.72	0.311	2.35	Portlandite
29.48	0.303	2.57	Calcite
30.12	0.296	1.81	C_2S
31.04	0.288	1.82	Gypsum (?); C_2S
32.28	0.277	2.94	C_2S; C_3S
32.64	0.274	2.67	C_2S; C_3S
34.12	0.263	6.48	Portlandite
36.6	0.245	9.04	Quartz
38.44	0.234	4.41	Aluminum
39.48	0.228	9.42	Quartz; Calcite
40.32	0.223	5.33	Quartz
41.36	0.218	1.68	C_2S
41.84	0.216	1.49	Ettringite
42.48	0.213	7.55	Quartz
42.92	0.211	1.61	Periclase
44.64	0.203	1.96	Aluminum
45.8	0.198	6.09	Quartz
47.16	0.193	3.48	Portlandite

FIGURES

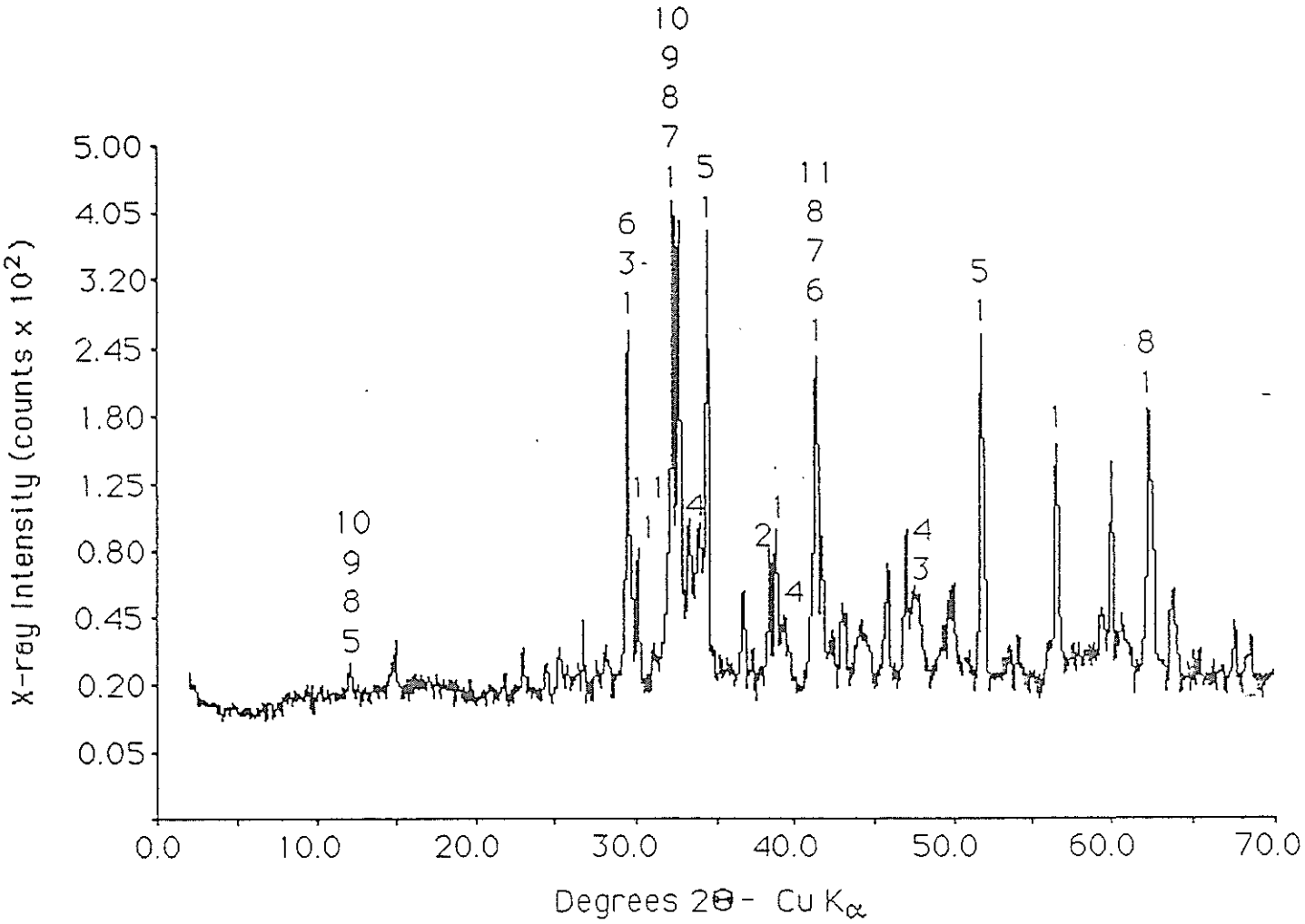

Identification Key:

1 - Alite	7 - C_2S
2 - Al sample holder	8 - CAF
3 - Calcite	9 - CF
4 - C_3A	10 - Brownmillerite
5 - C_2A	11 - Wollastonite
6 - CA	

FIGURE 1. X-ray powder diffraction pattern for Portland Cement used in laboratory concrete mixtures.

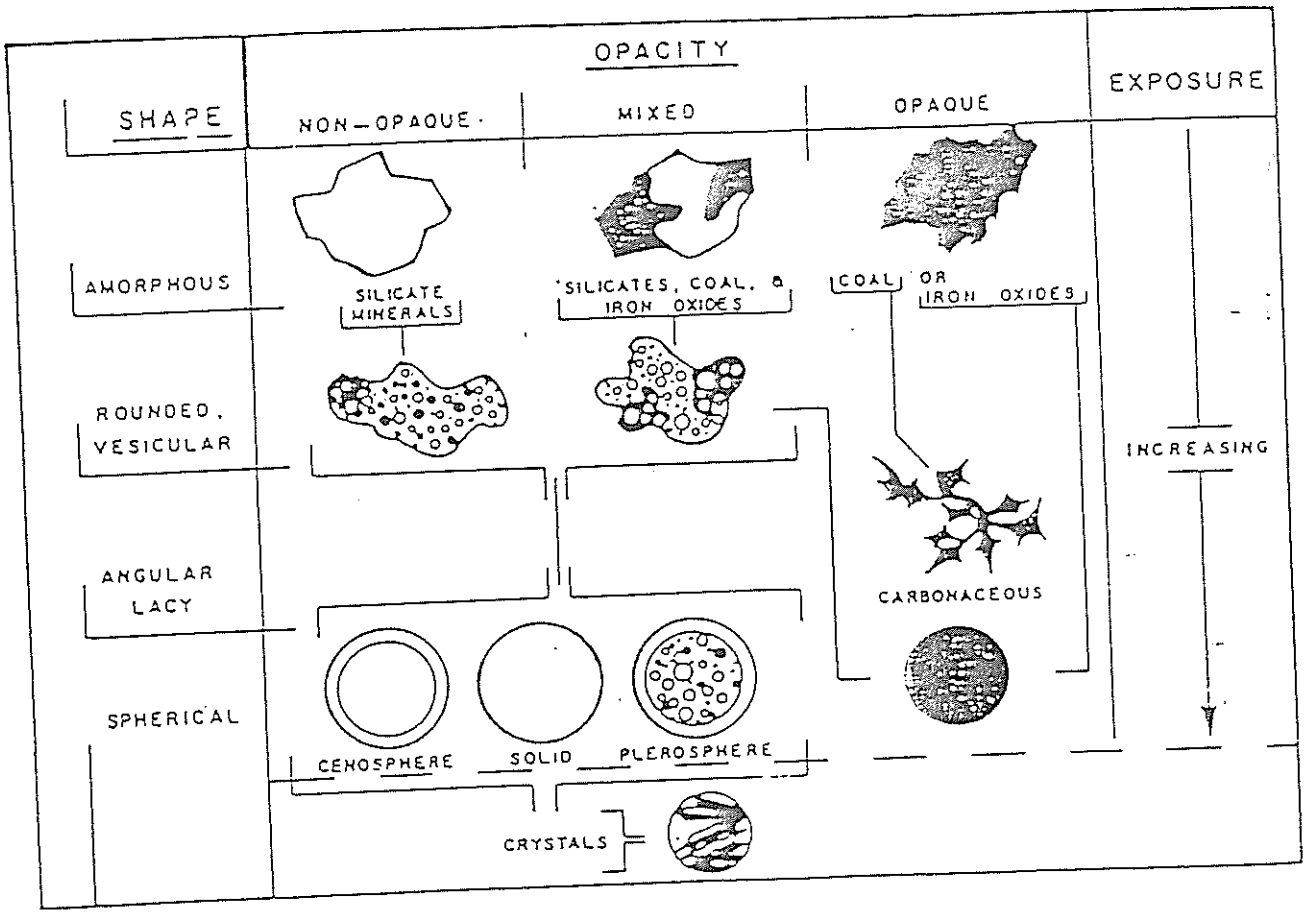

FIGURE 2. Evolution of fly ash particle morphology related to composition and exposure in combustion chamber (24).

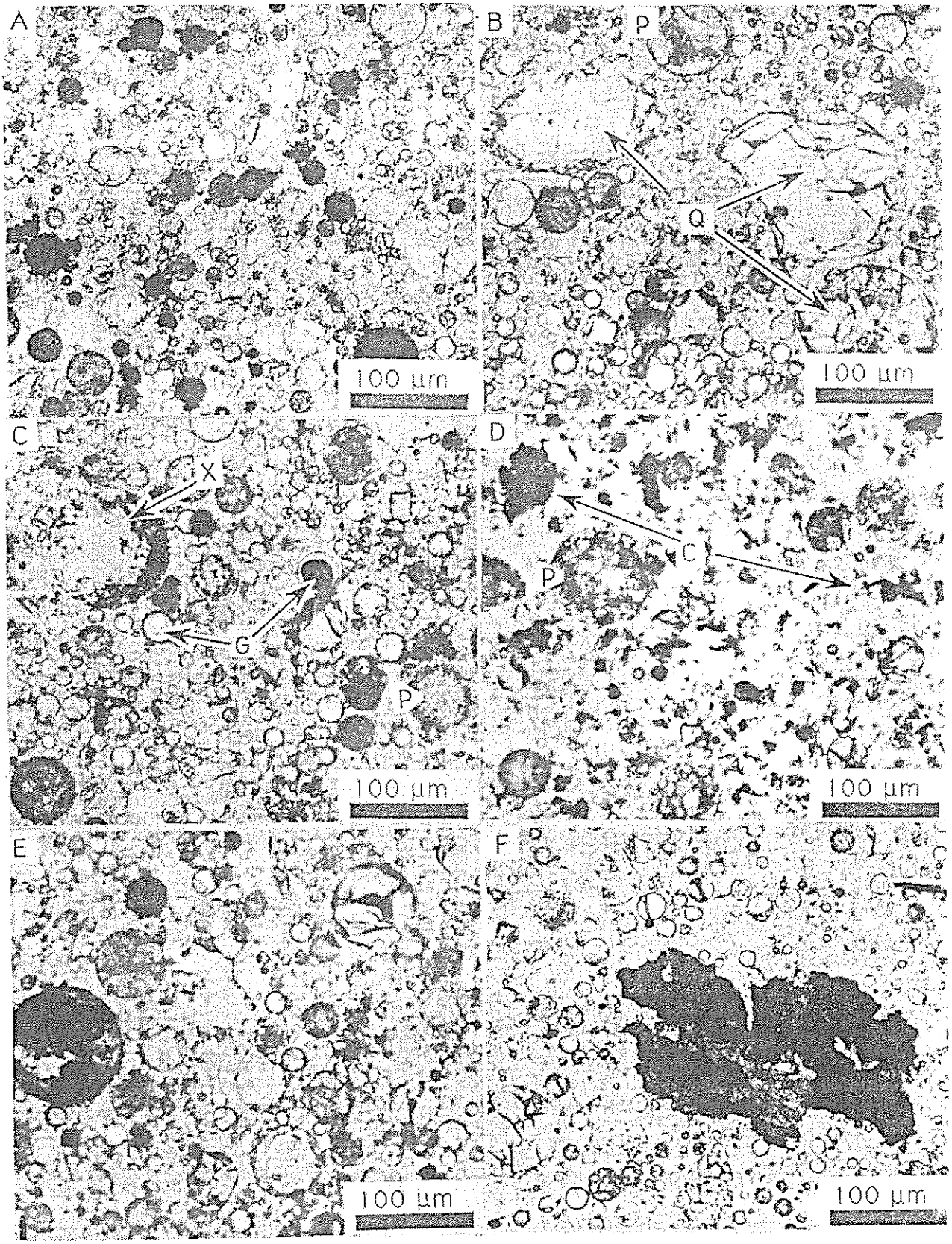

FIGURE 3. Optical photomicrograph of fly ash particles in polished thin sections of Gifford-Hill samples. For explanation of symbols, refer to text.

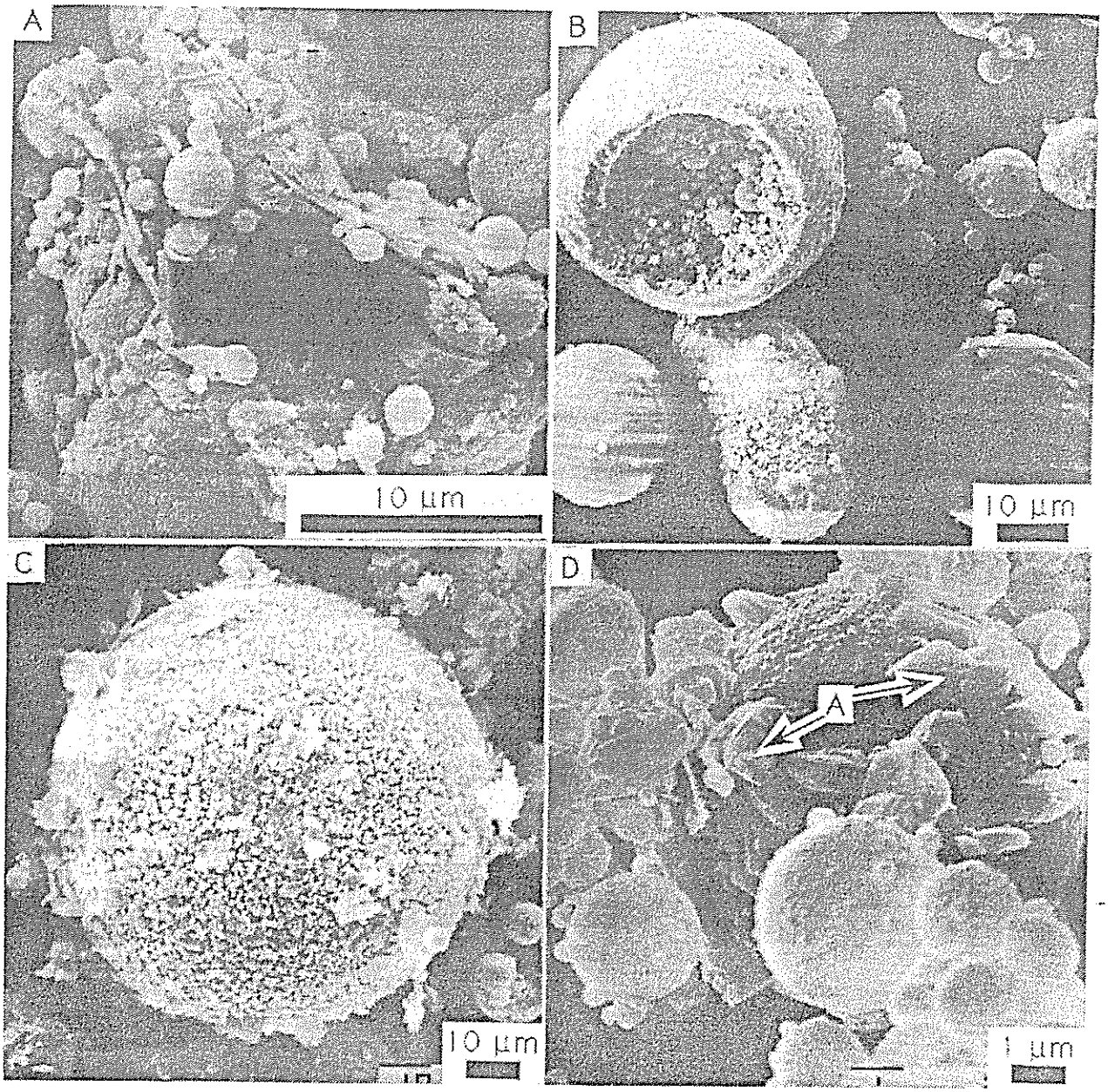

FIGURE 4. Scanning electron photomicrograph of fly ash particles.

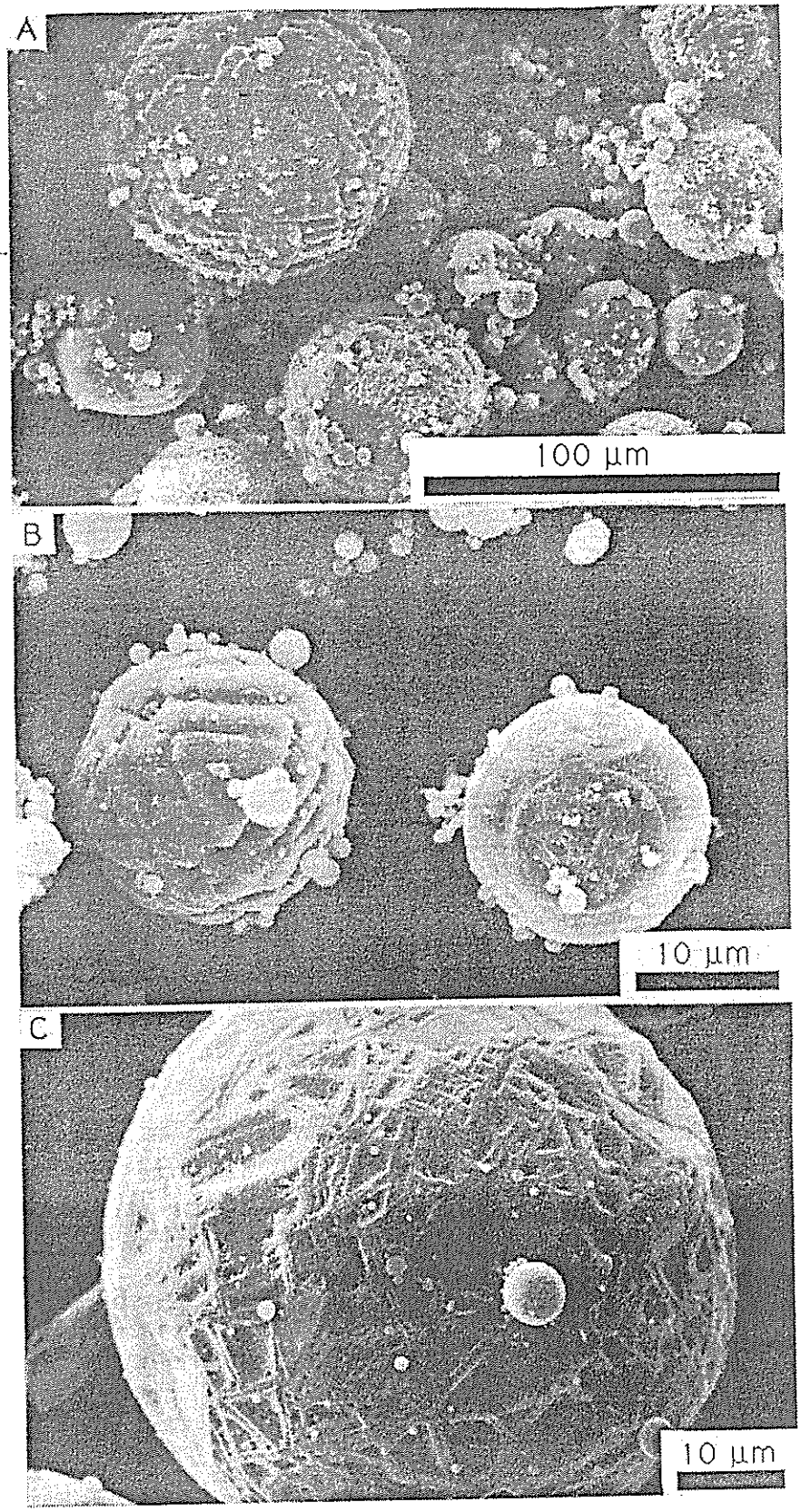

FIGURE 5. Scanning electron photomicrograph of Fe-rich fly ash particles separated with hand-held magnet.

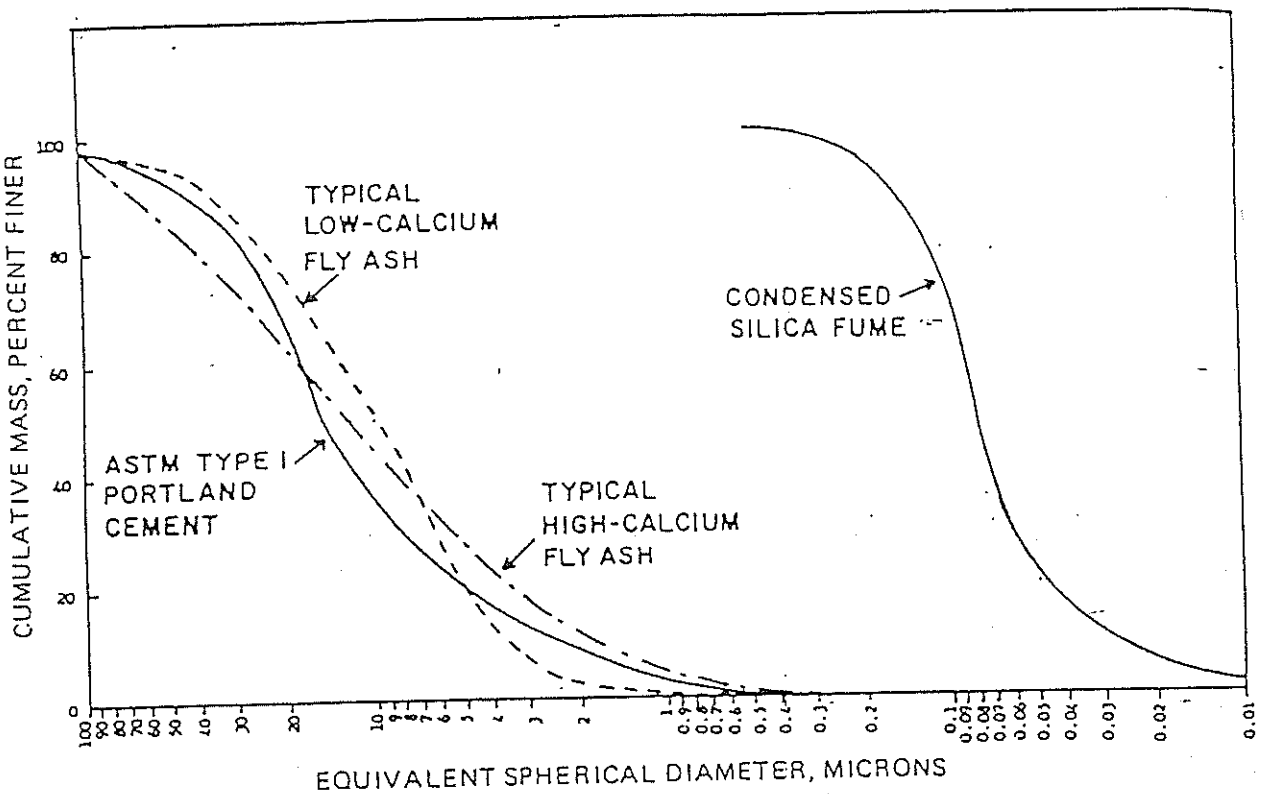

FIGURE 6. Particle size distribution curves for typical low-Ca and high-Ca fly ashes and other materials (19).

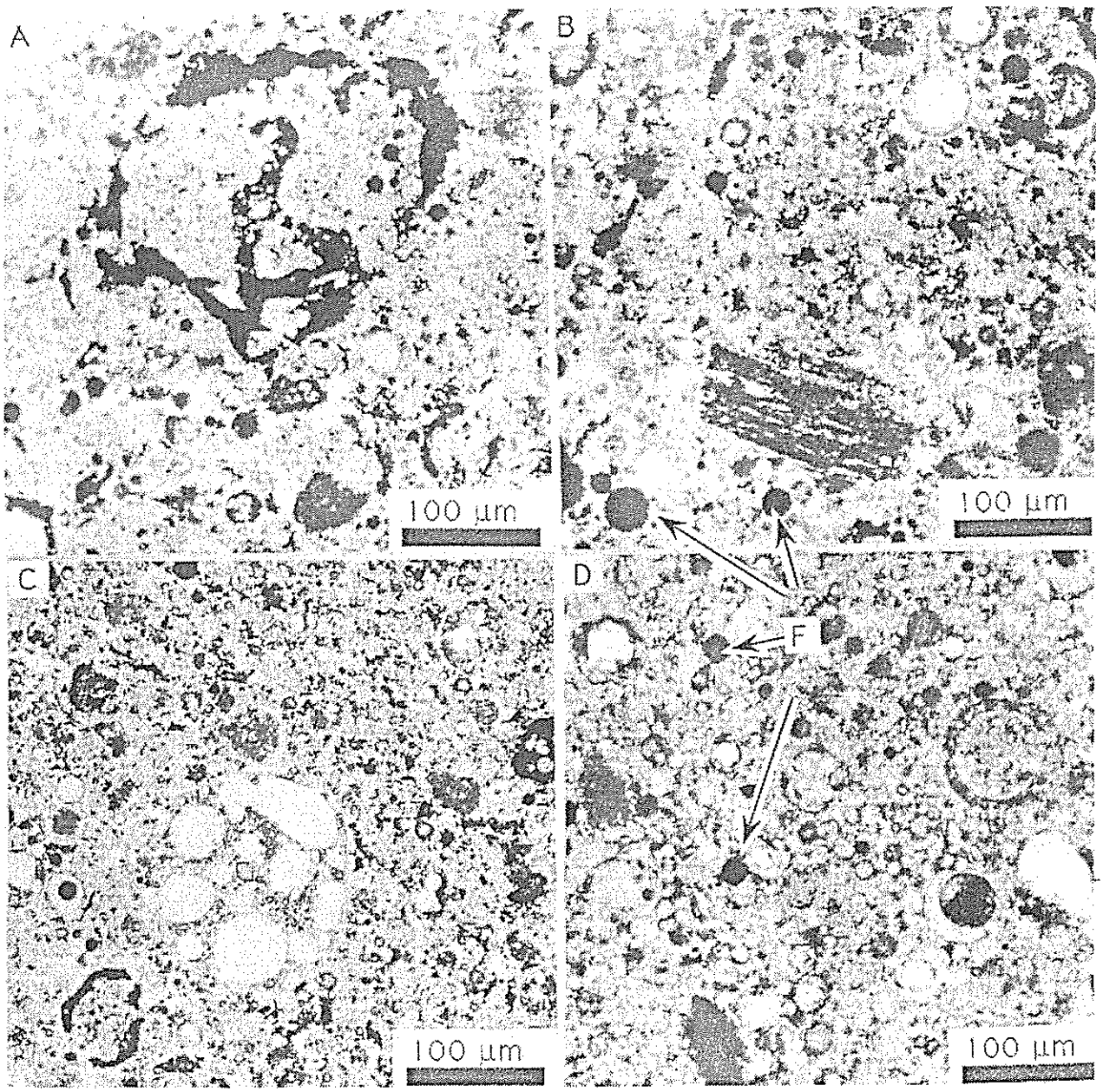

FIGURE 7. Optical photomicrographs of polished thin sections of hydrated fly ash.

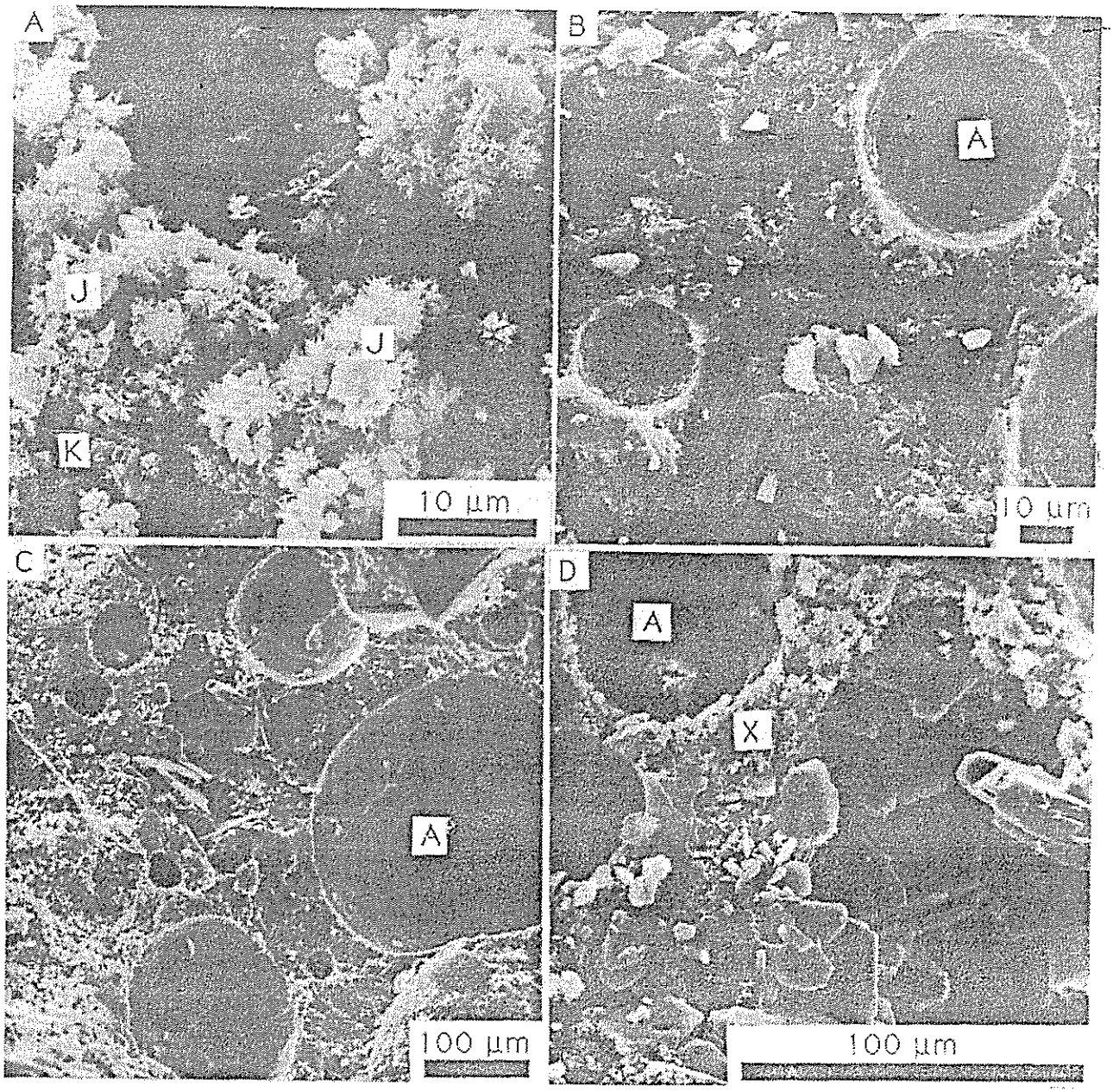

FIGURE 8. Scanning electron photomicrographs of fracture surfaces from a fly ash-free concrete.

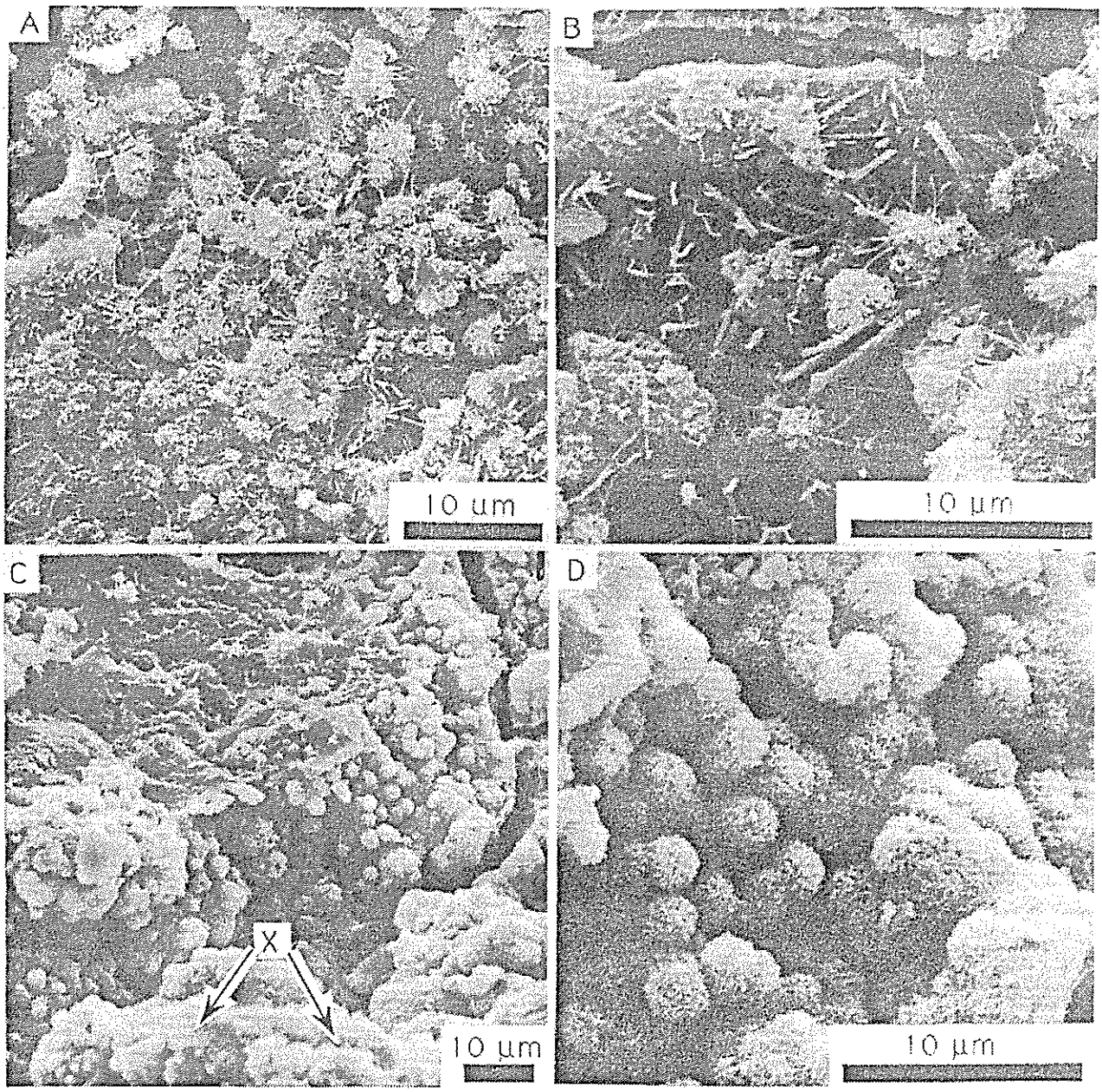

FIGURE 9. Scanning electron photomicrograph of subspherical, spherical and acicular crystals in a fly ash-free concrete (A and B) and a fly ash-containing concrete (C and D).

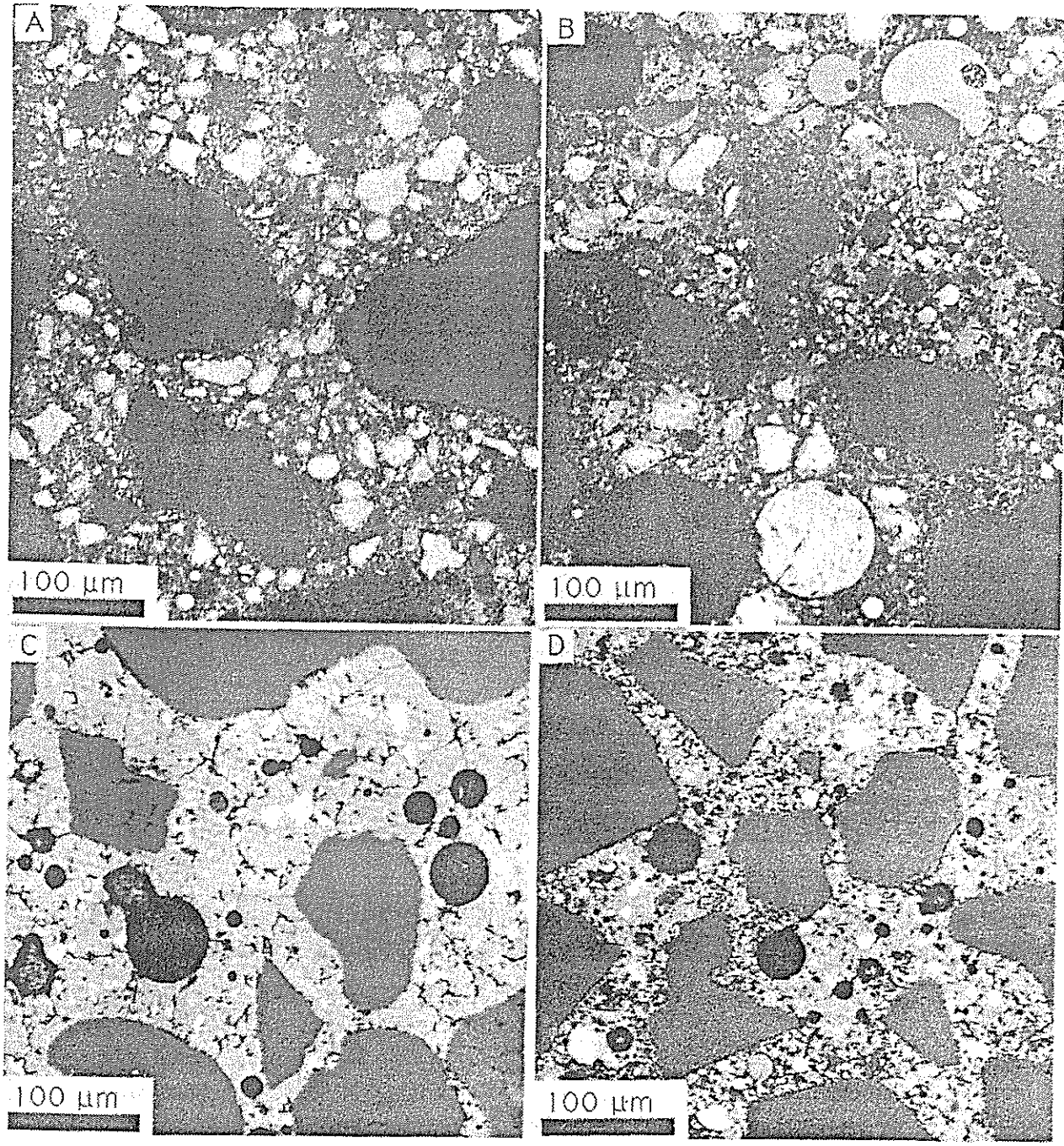

FIGURE 10. Backscattered electron image of polished thin section of fly ash-free concrete (A and C) and concrete with fly ash substituted for Portland Cement (B and D).

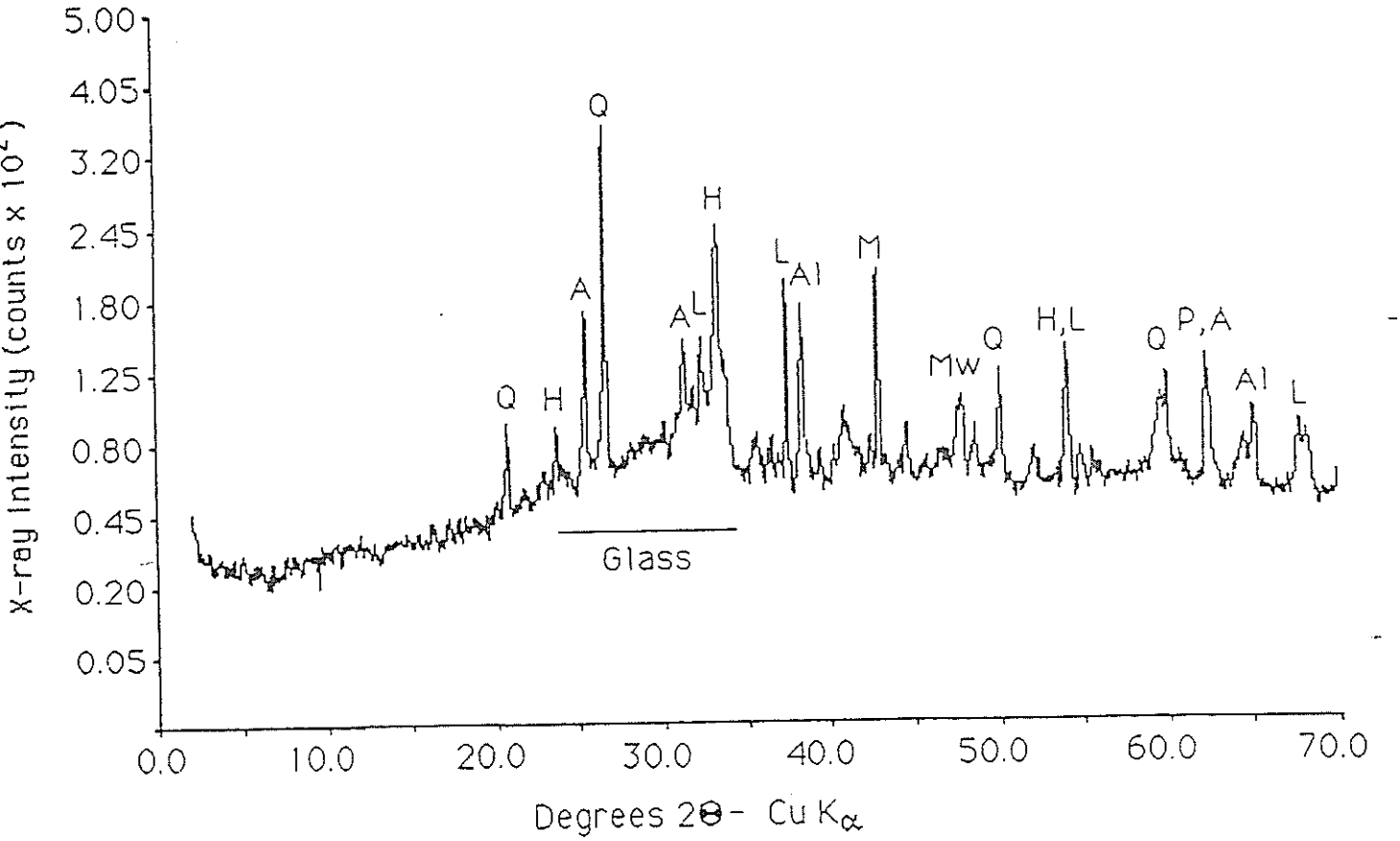

FIGURE 11. X-ray powder diffraction pattern for typical fly ash from plant no. 78.

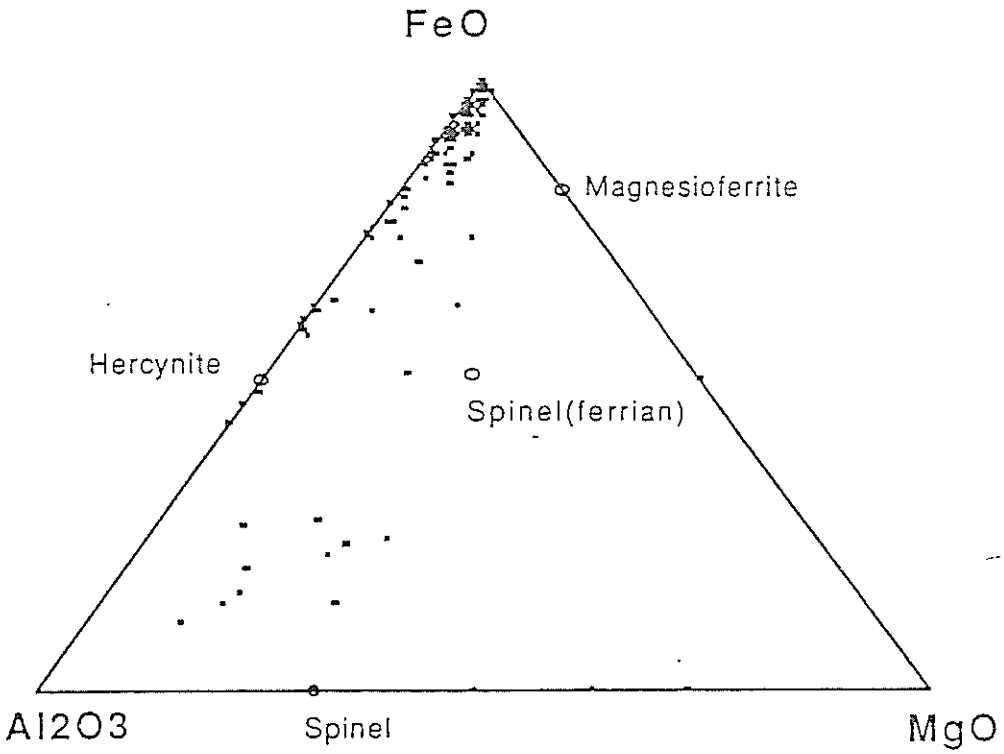

FIGURE 12. Common phases in the FeO-Al2O3-MgO system. Points represent electron microprobe determined compositions of individual particles in the magnetic fraction of a fly ash.

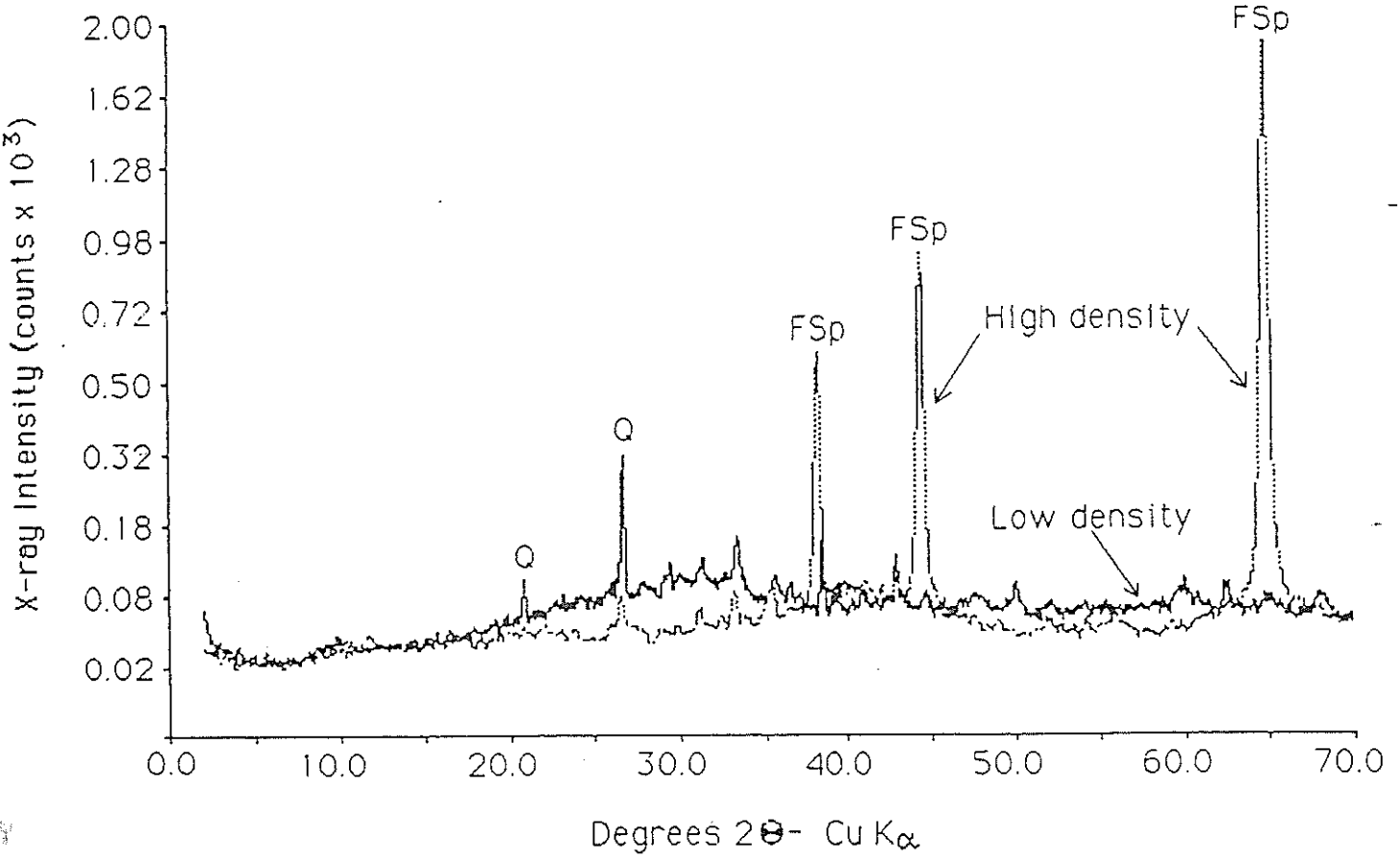

FIGURE 13. X-ray powder diffraction pattern of high and low density fractions of a representative fly ash.

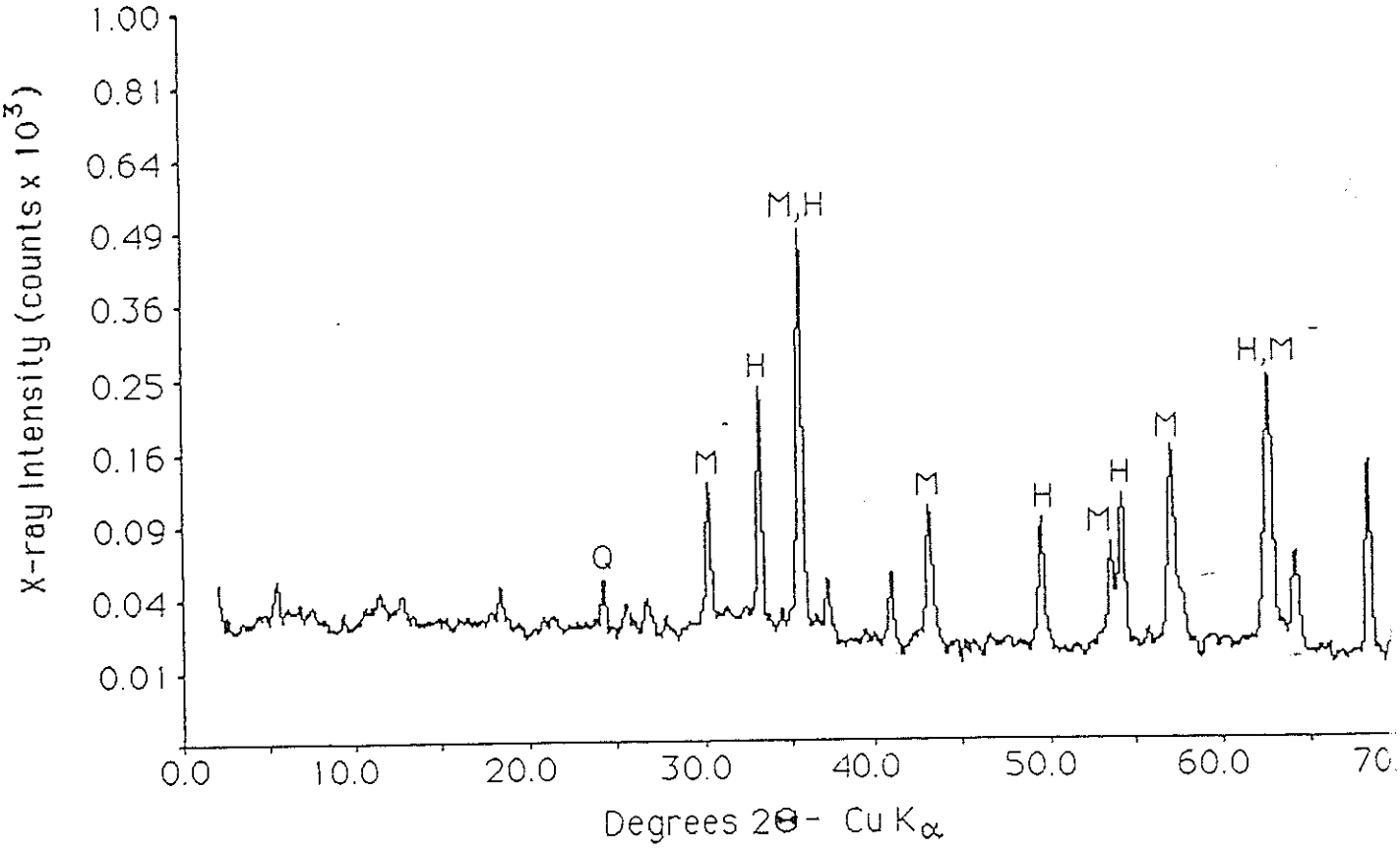

FIGURE 14. X-ray powder diffraction pattern of the magnetic fraction from a typical fly ash.

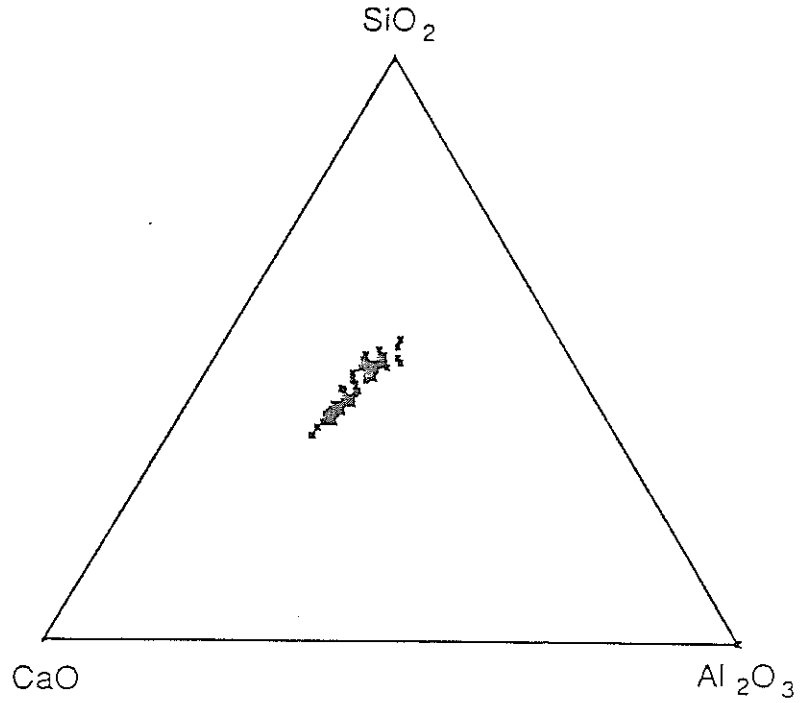

FIGURE 15. Ternary plot (CaO-Al_2O_3-SiO_2) of the compositions of all bulk fly ash samples determined by ICP method.

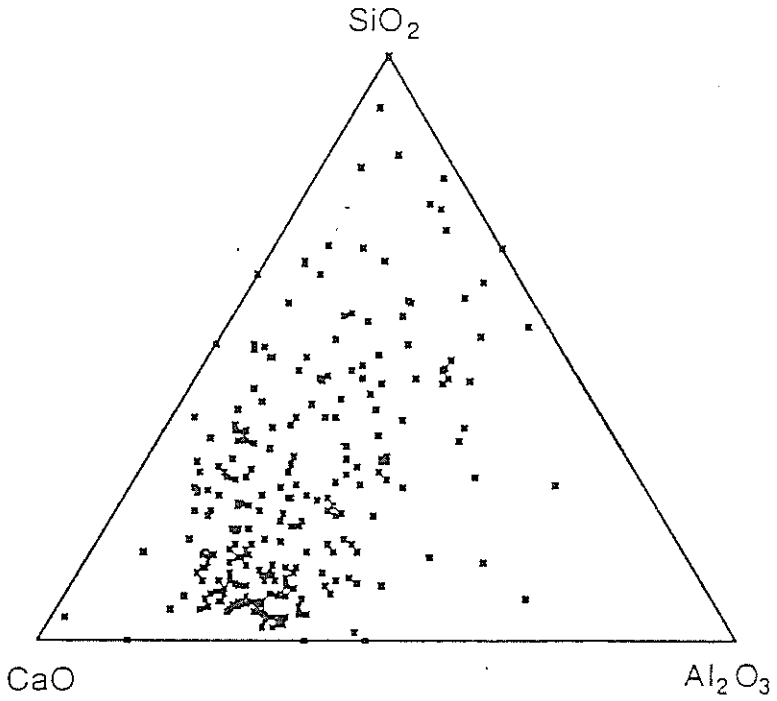

FIGURE 16. Results of microprobe analyses of individual particles in a fly ash sample from plant no. 85.

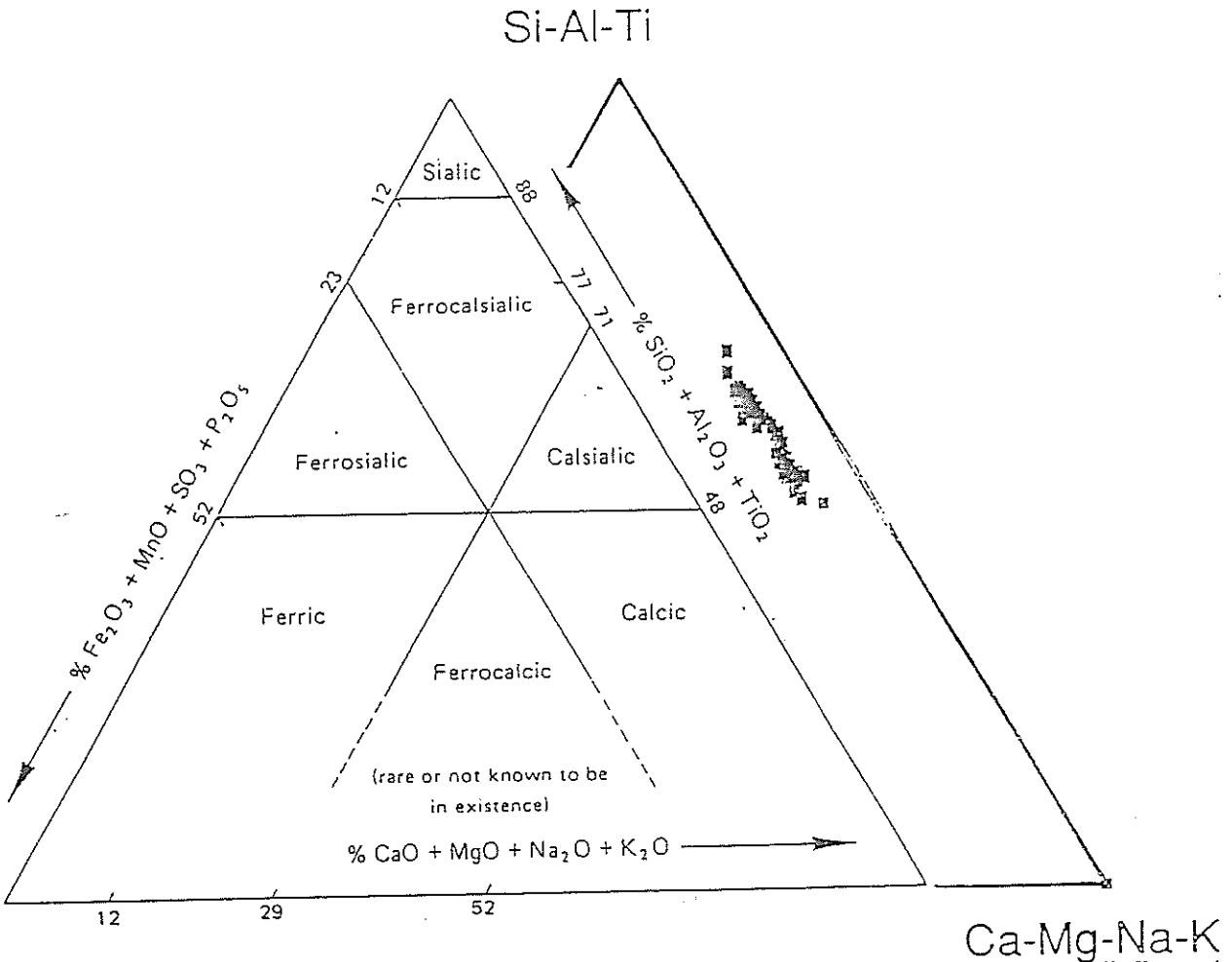

FIGURE 17. Comparison of ICP chemical composition results for all fly ash samples with the classification scheme proposed by Roy et al., 1981 (26).

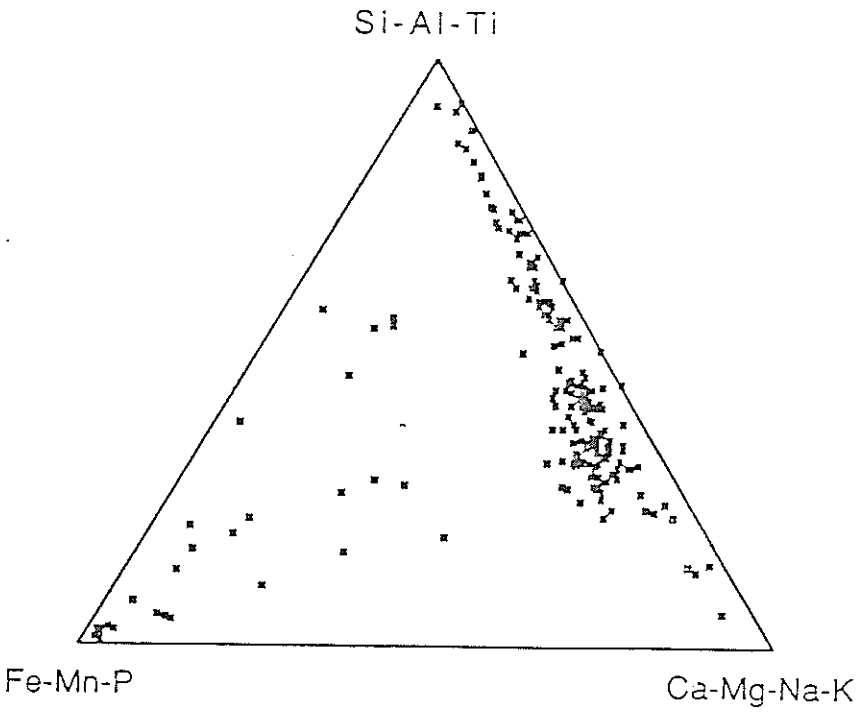

FIGURE 18. Compositional variability determined by electron microprobe analysis of individual particles of fly ash in a sample from plant no. 85.

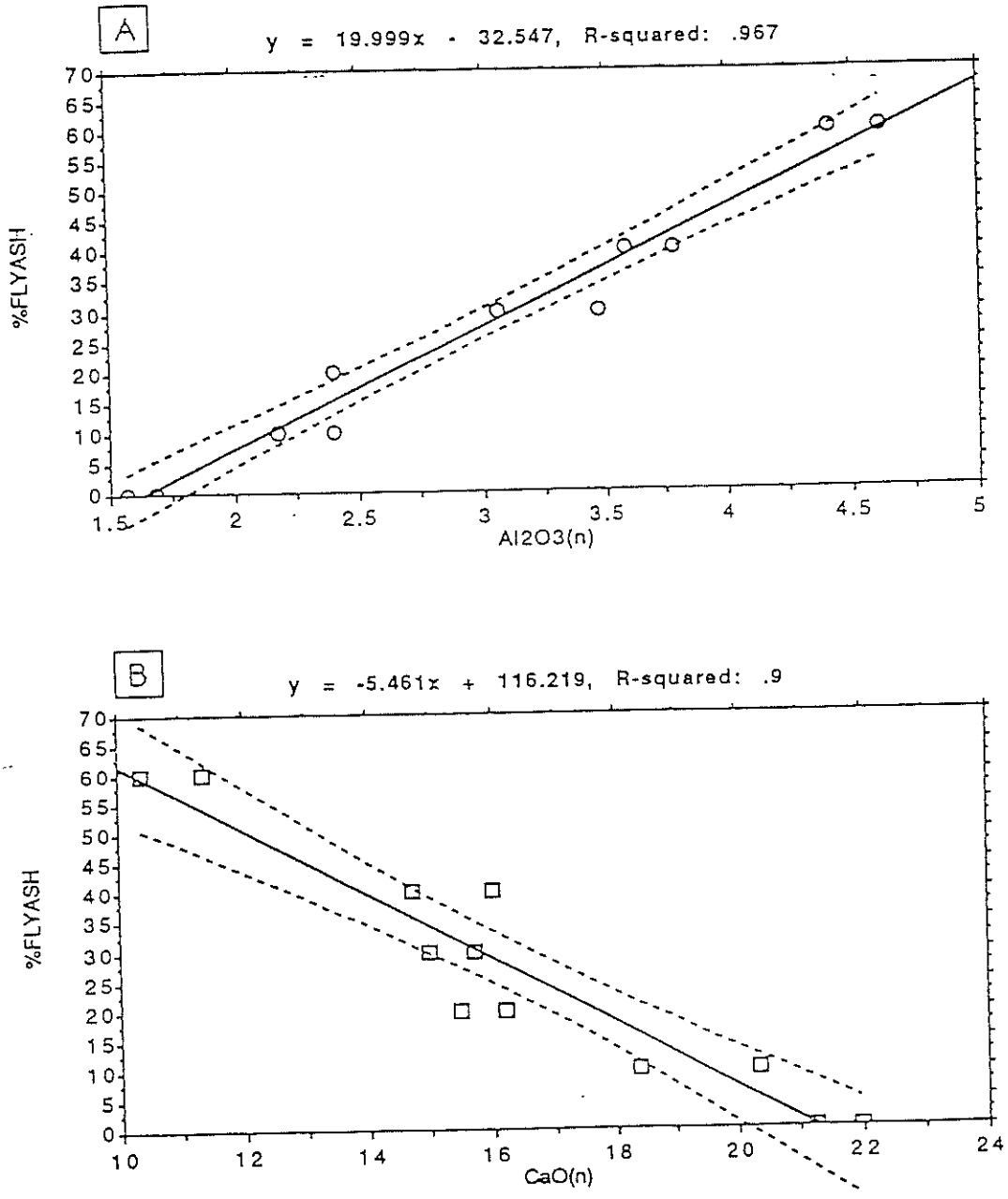

FIGURE 19. Line of linear regression with 95% confidence limits for weight percent fly ash versus Al_2O_3 (a) and CaO (B) in C-series concrete samples.

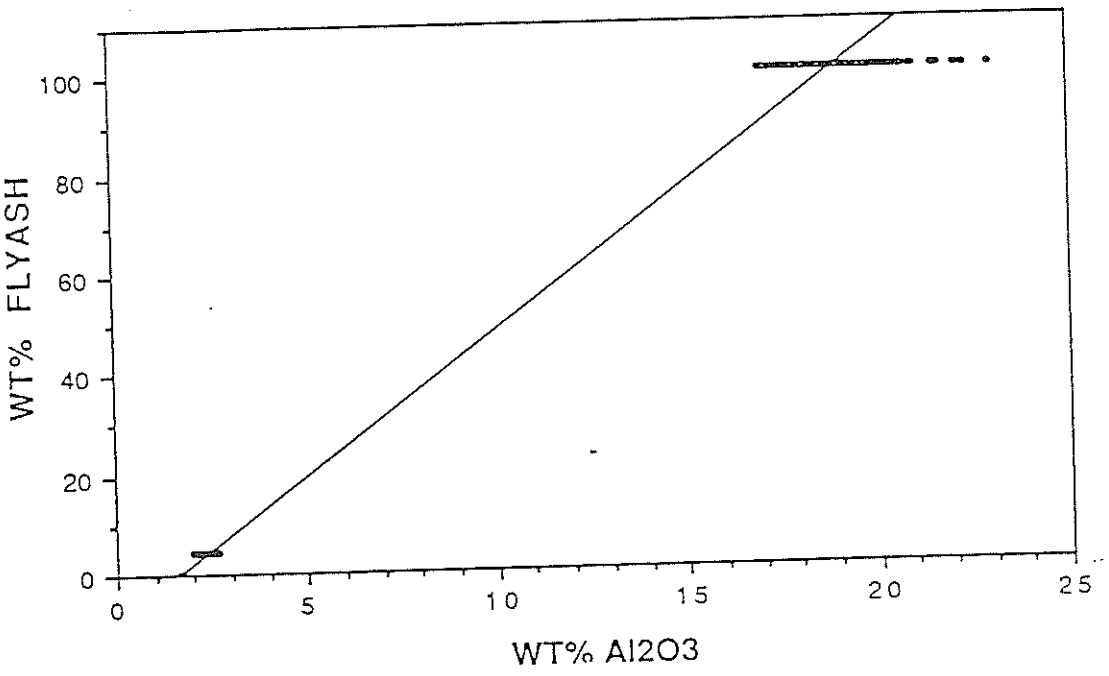

FIGURE 20. Weight percent fly ash versus Al2O3 in laboratory prepared mixtures containing 0, 4.5, and 100 percent fly ash.

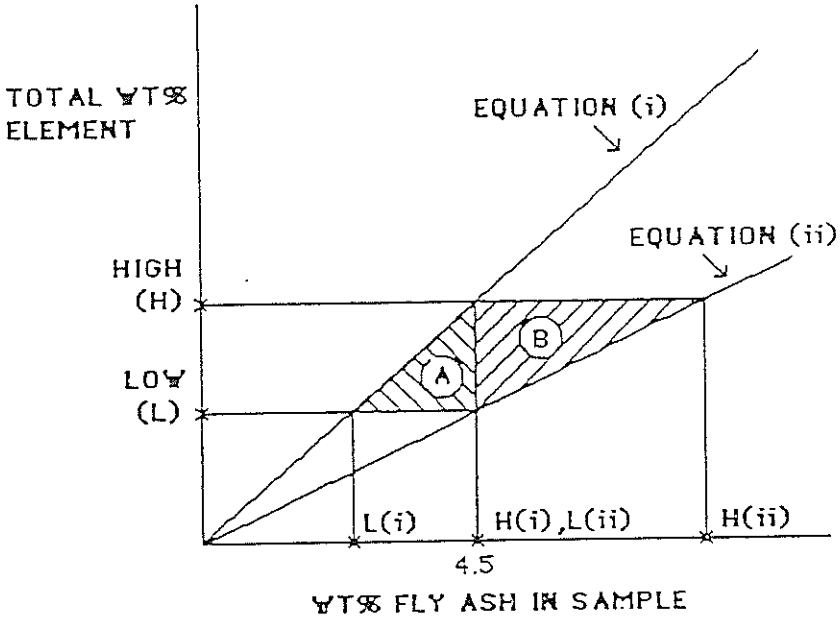

EQUATION (i) :

$$A_{max}\,k + C_{max}\,(K-x) + F_{max}\,x = (\text{Tot Wt\% Oxide})_{max}$$

EQUATION (ii) :

$$A_{min}\,k + C_{min}\,(K-x) + F_{min}\,x = (\text{Tot Wt\% Oxide})_{min}$$

FIGURE 21. Schematic illustration of maximum errors in calculated weight percent fly ash in concrete.

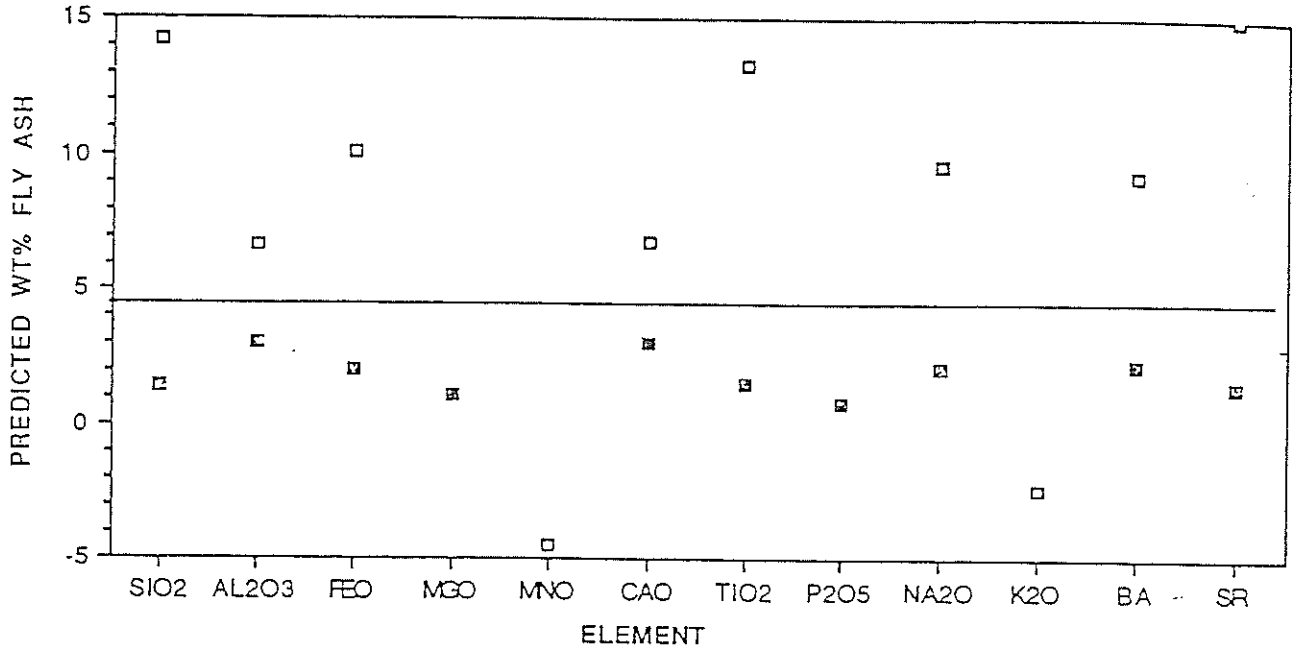

FIGURE 22. Predicted maximum and minimum percentages of fly ash in concrete prepared with 4.5 weight percent fly ash. Estimates for each chemical constituent are based on determination for all analyzed fly ashes. Open squares-maximum; filled squares-minimum.

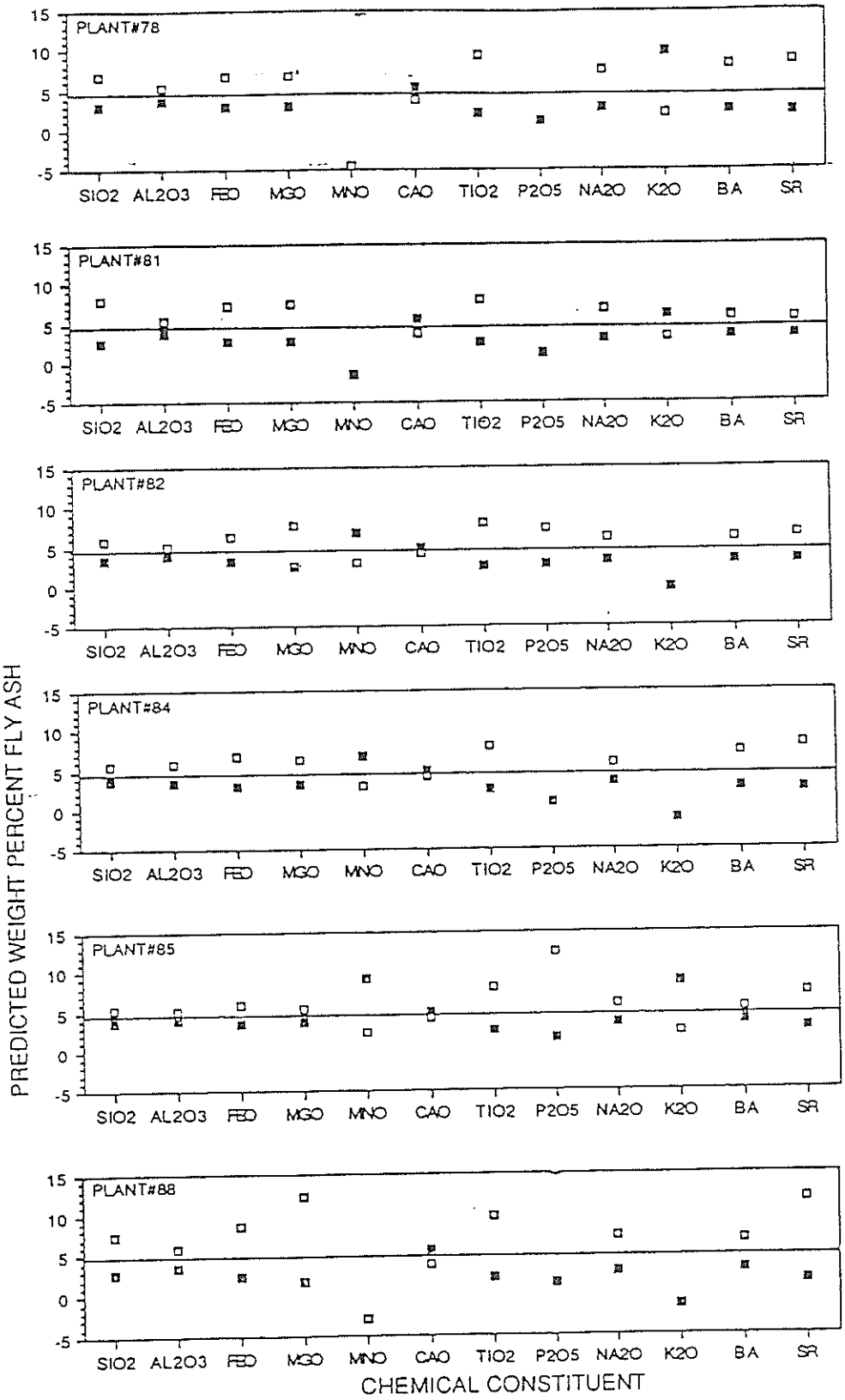

FIGURE 23. Predicted maximum and minimum percentages of fly ash in concrete prepared with 4.5 weight percent fly ash. Estimates for each chemical constituent are based only on samples from the indicated plants. Open square-maximum; filled squares-minimum.

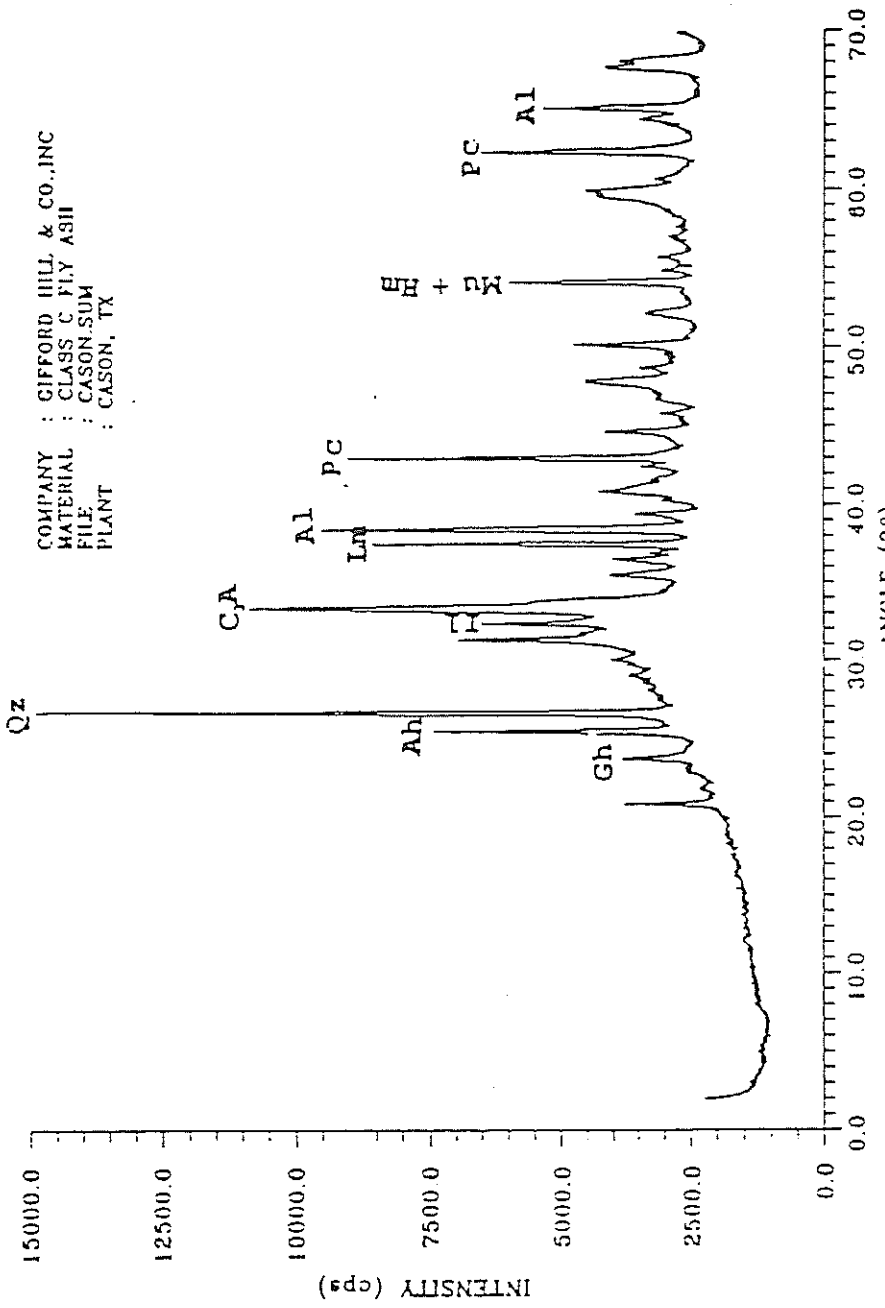

FIGURE 24. Sum pattern of fly ash from Cason plant.

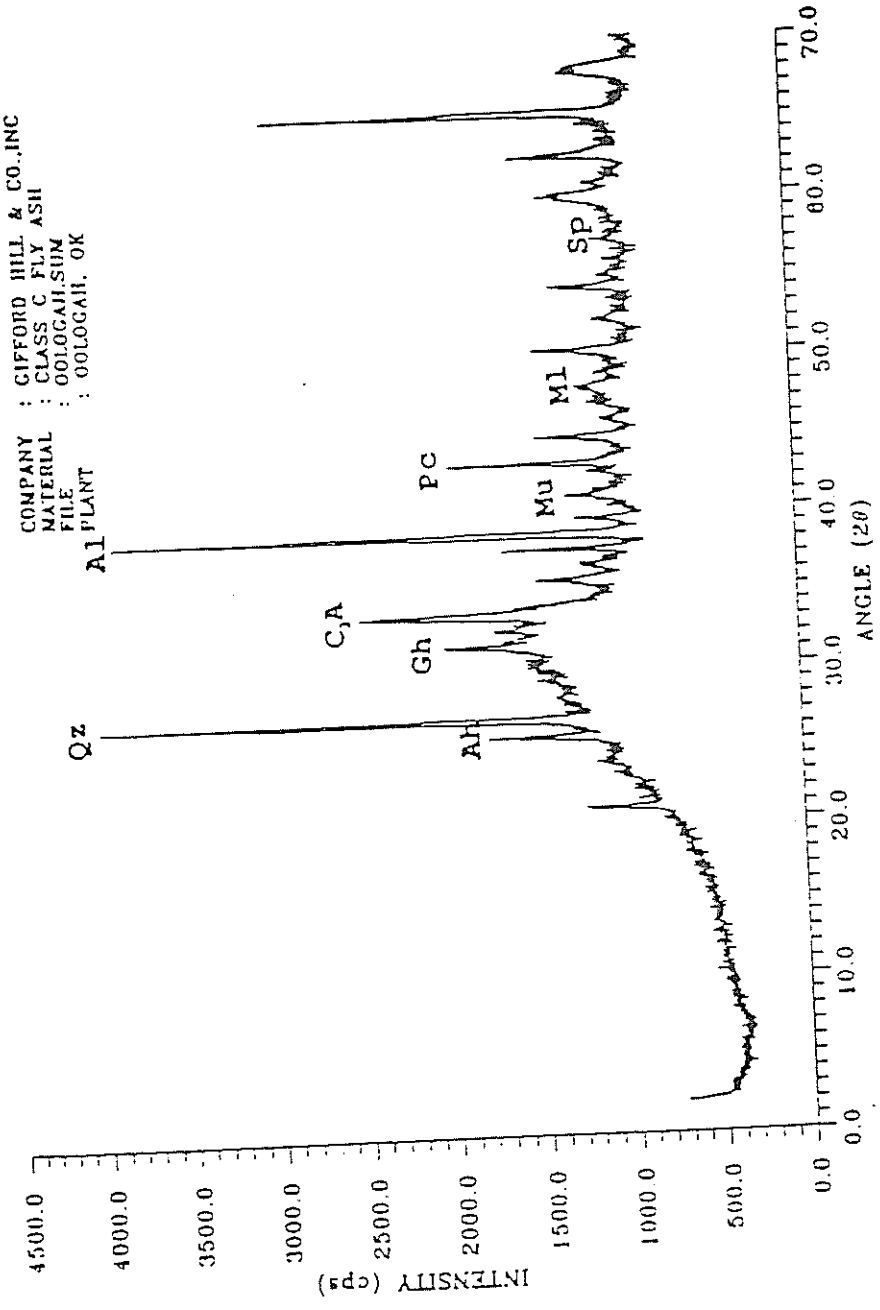

FIGURE 25. Sum pattern of fly ash from Oologah plant.

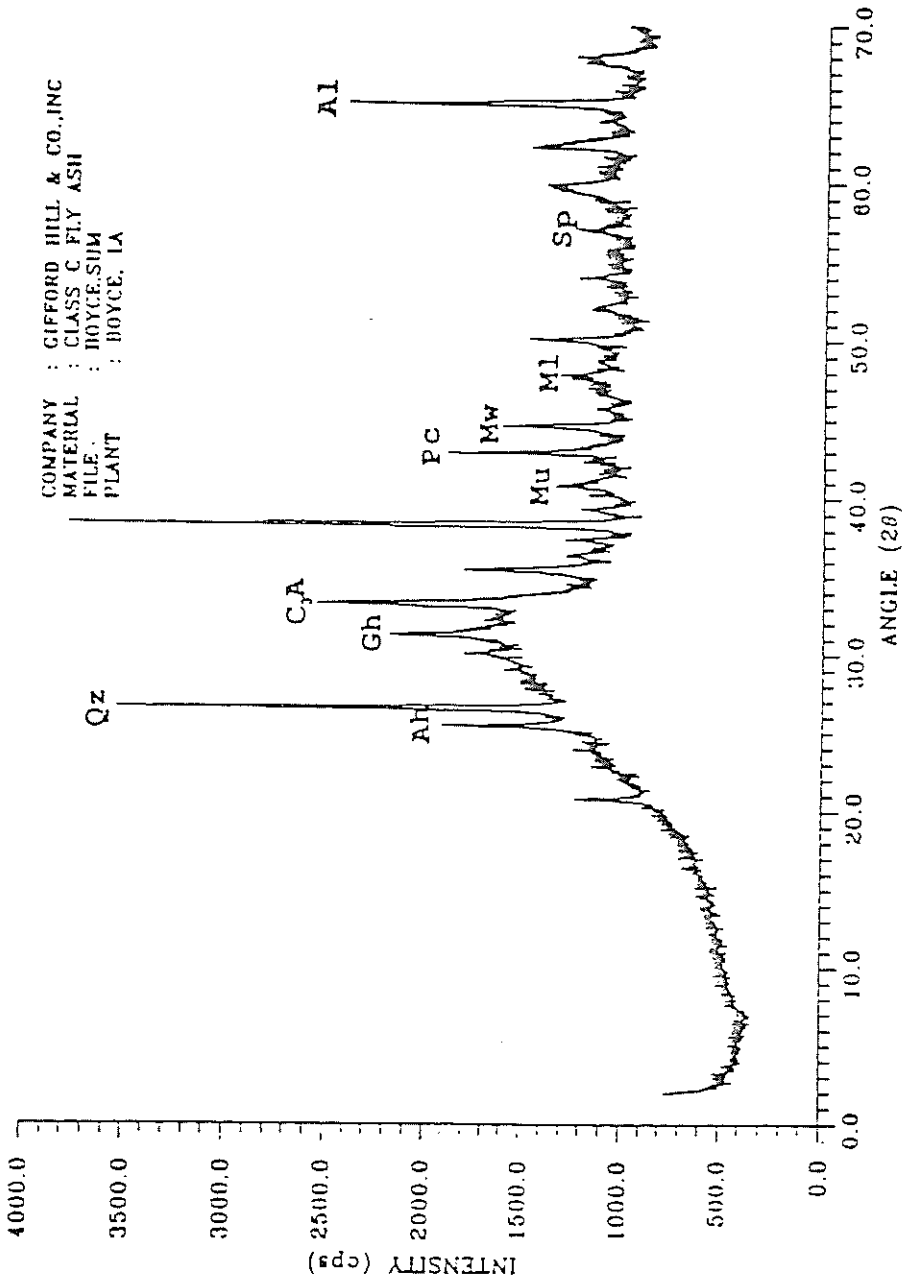

FIGURE 26. Sum pattern of fly ash from Boyce plant.

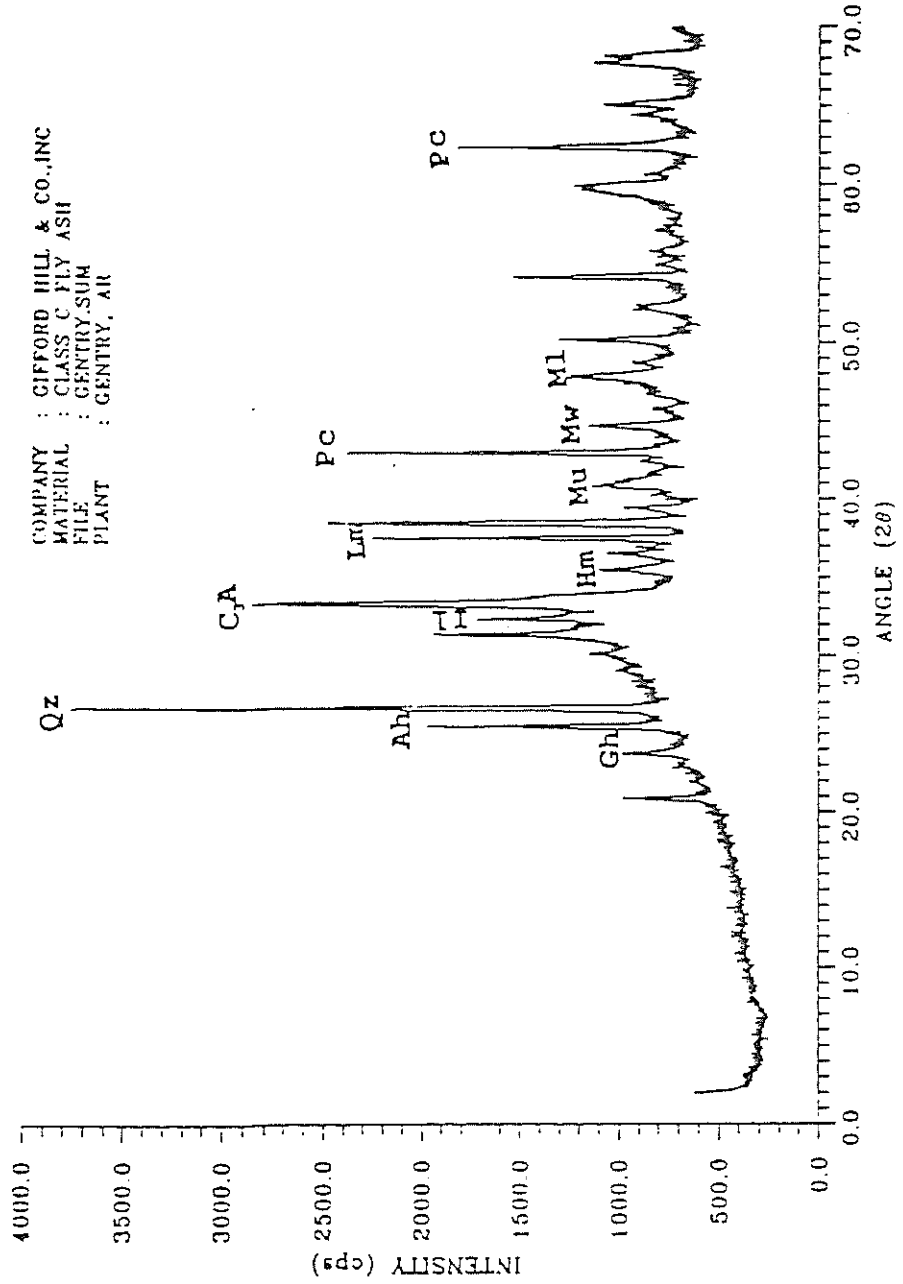

FIGURE 27. Sum pattern of fly ash from Gentry plant.

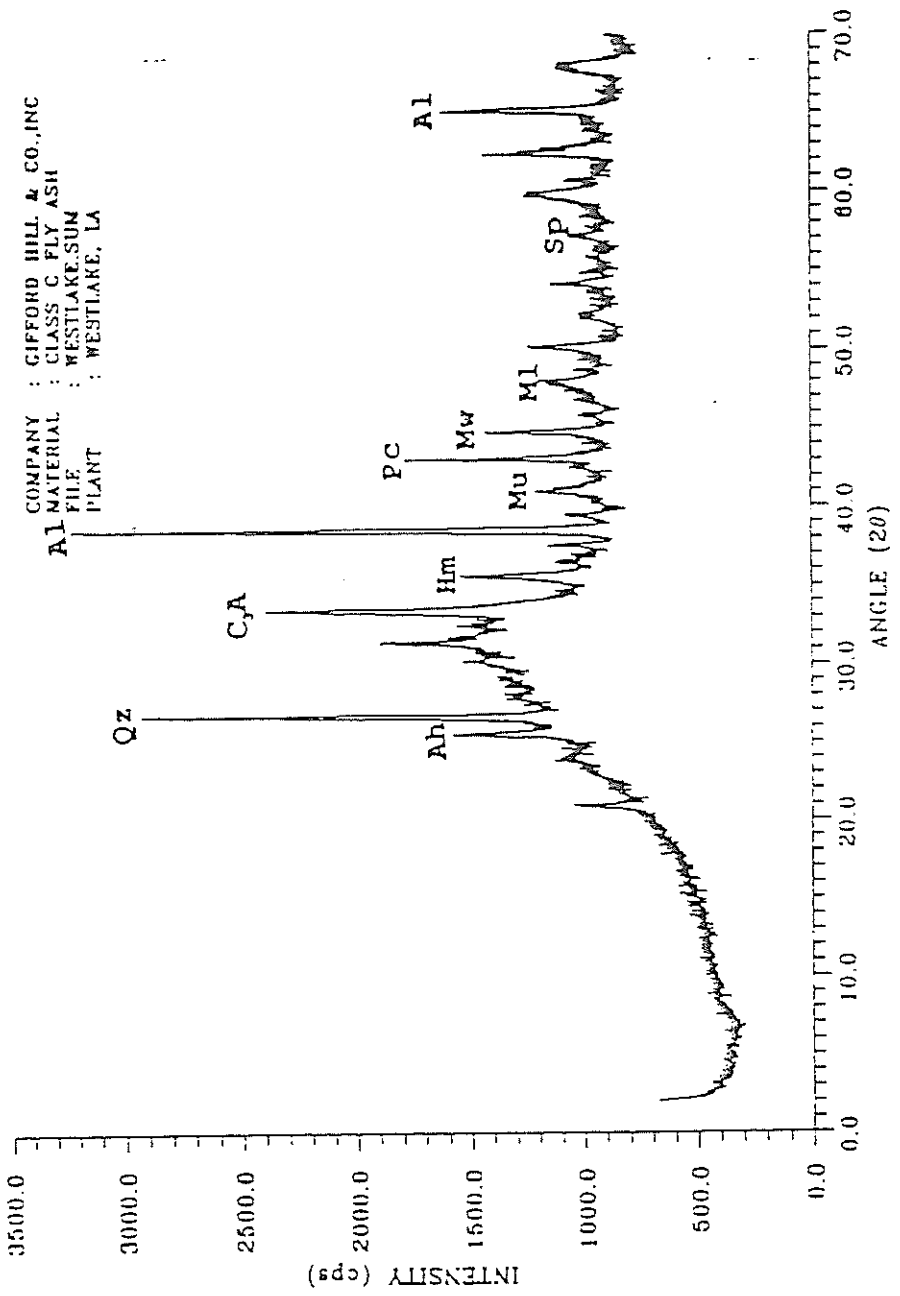

FIGURE 28. Sum pattern of fly ash from Westlake plant.

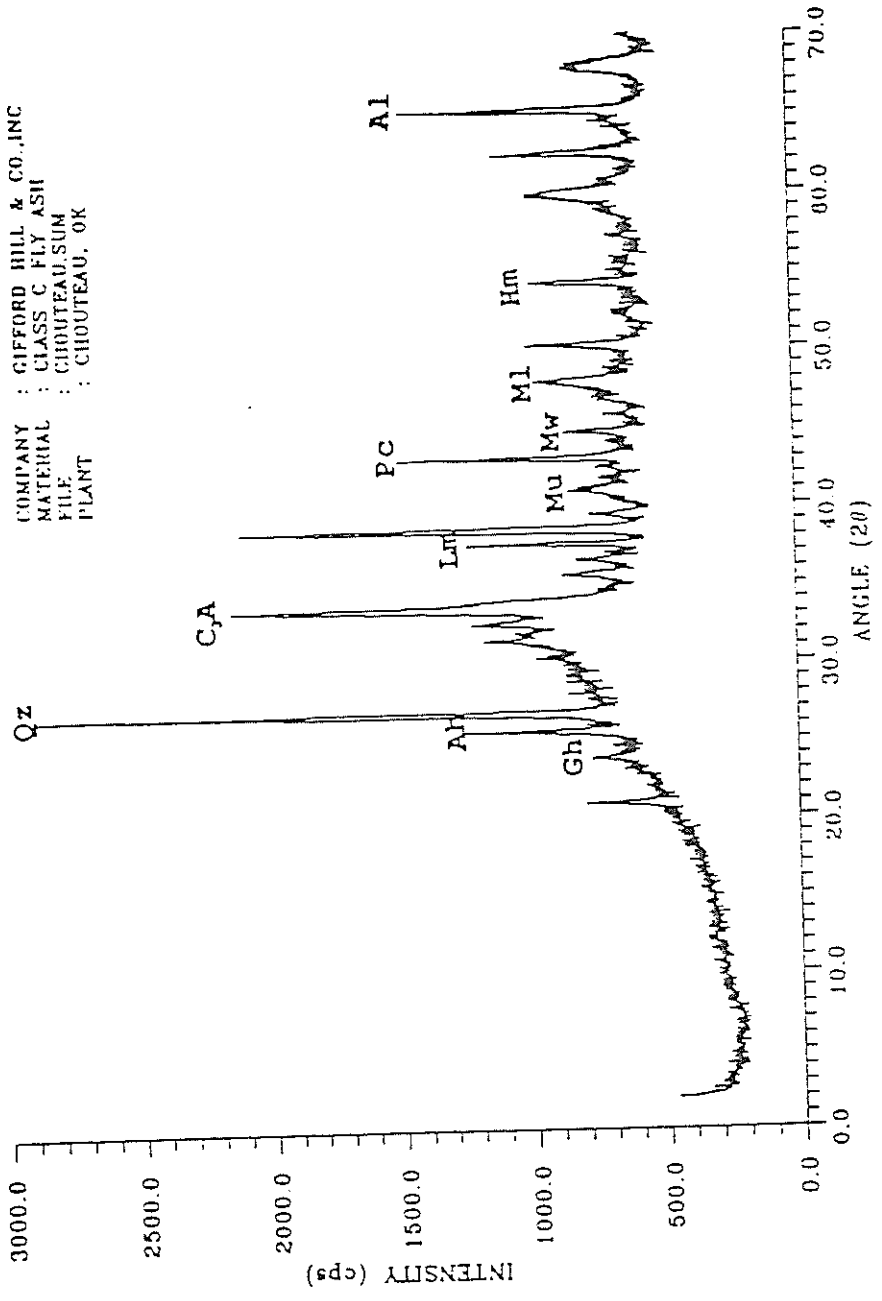

FIGURE 29. Sum pattern of fly ash frmo Chouteau plant.

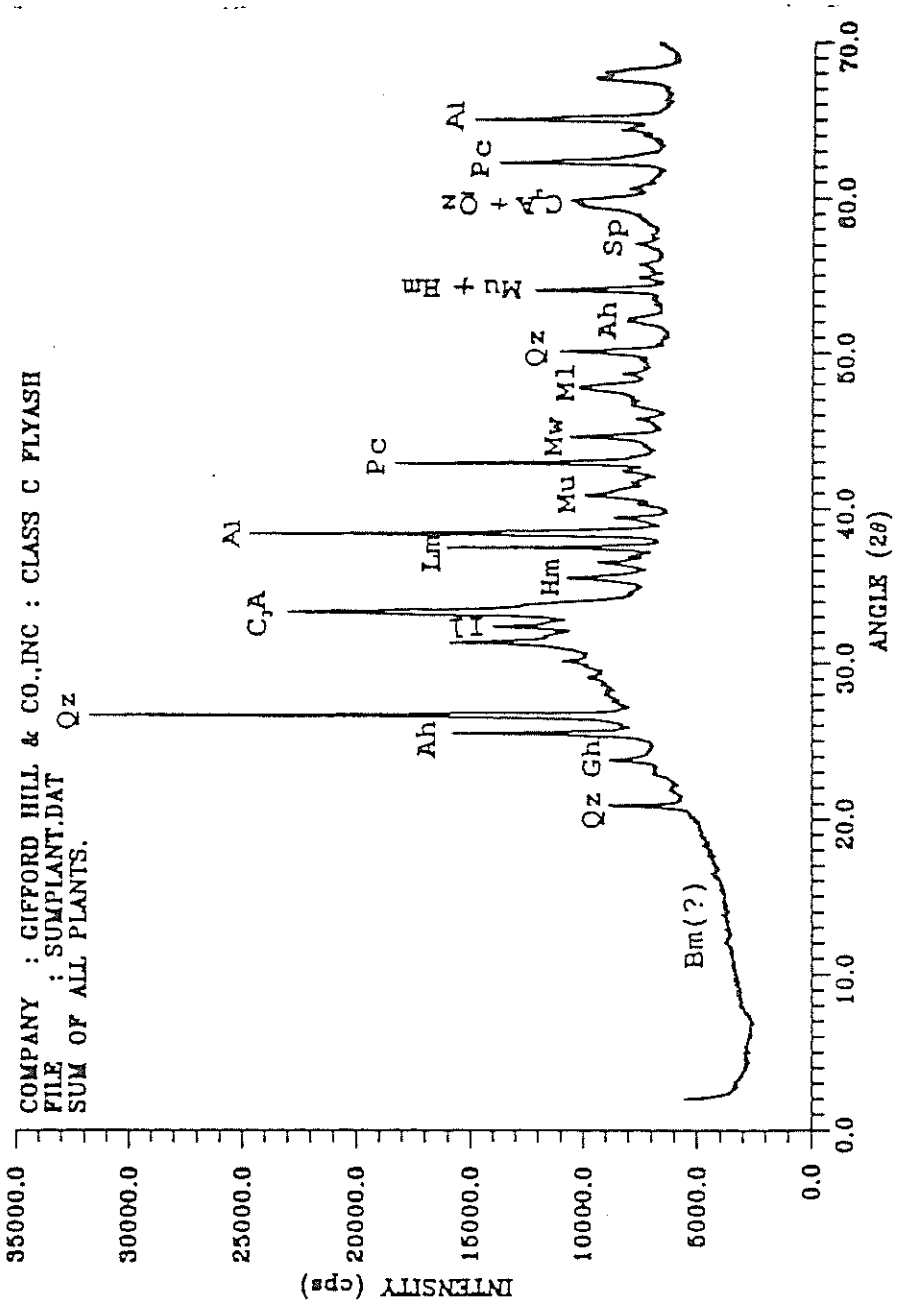

FIGURE 30. Master sum pattern of fly ash.

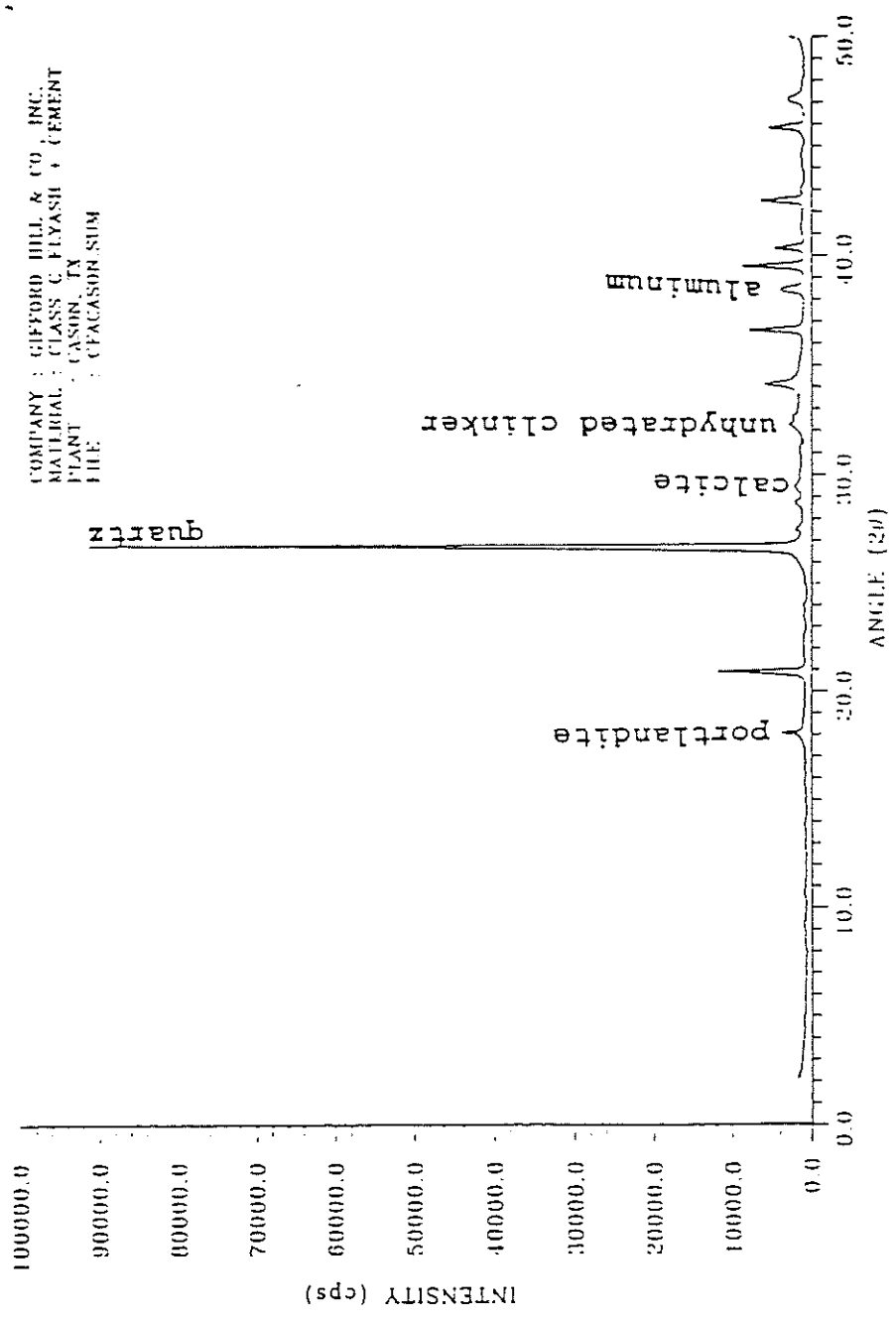

FIGURE 31. Sum pattern of concrete with ash from Cason.

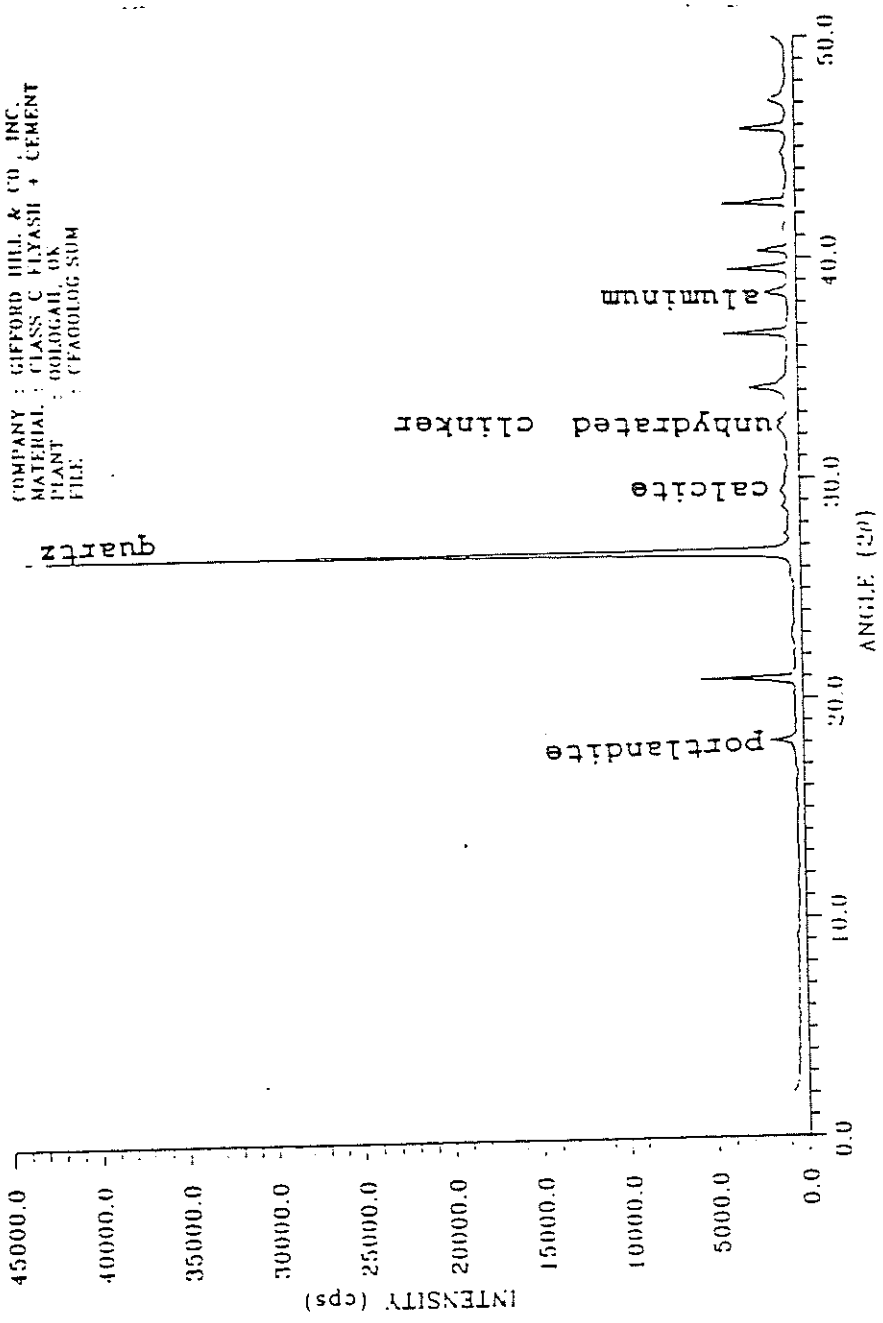

FIGURE 32. Sum pattern of concrete with ash from Oologah.

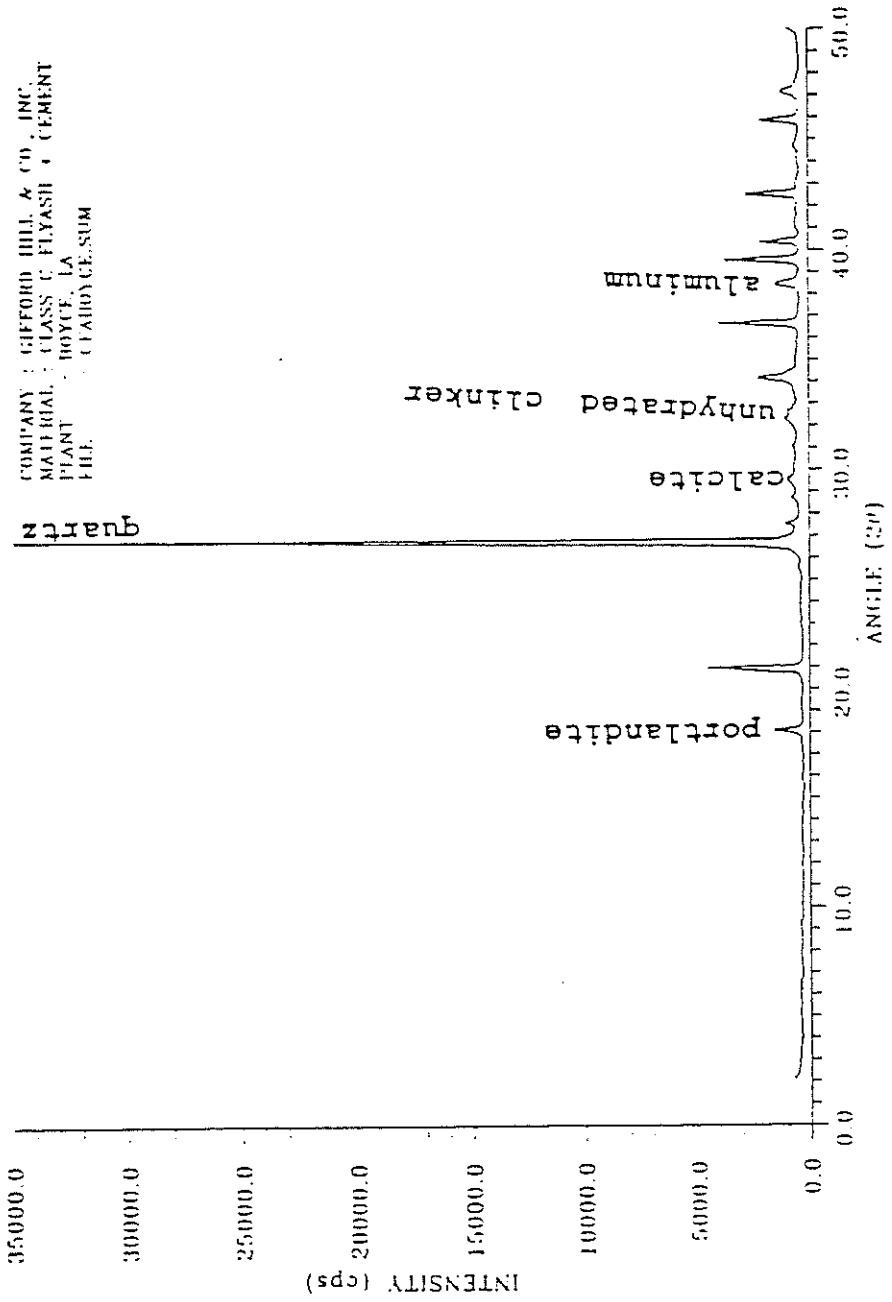

FIGURE 33. Sum pattern of concrete with ash from Boyce.

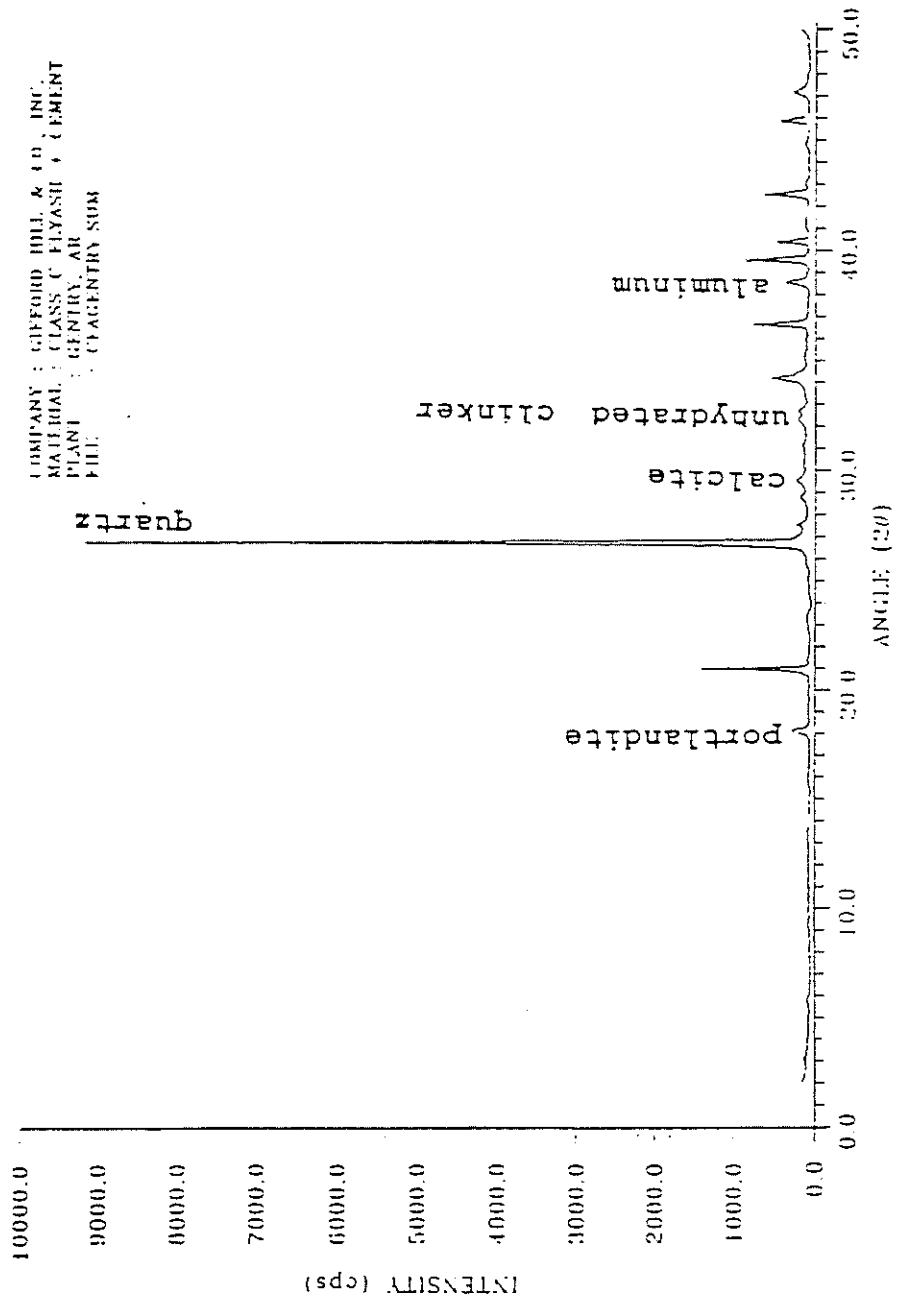

FIGURE 34. Sum pattern of concrete with ash from Gentry.

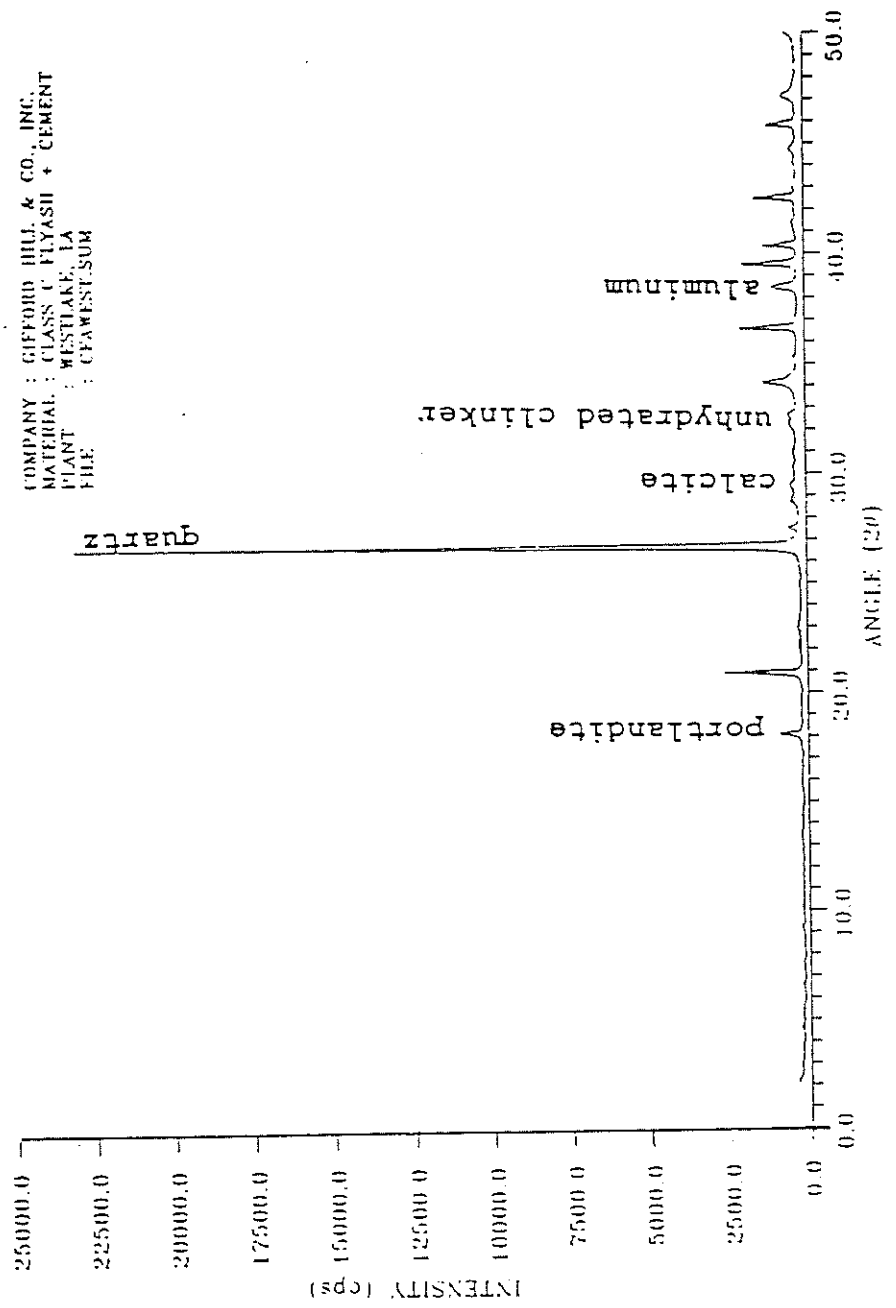

FIGURE 35. Sum pattern of concrete with ash from Westlake.

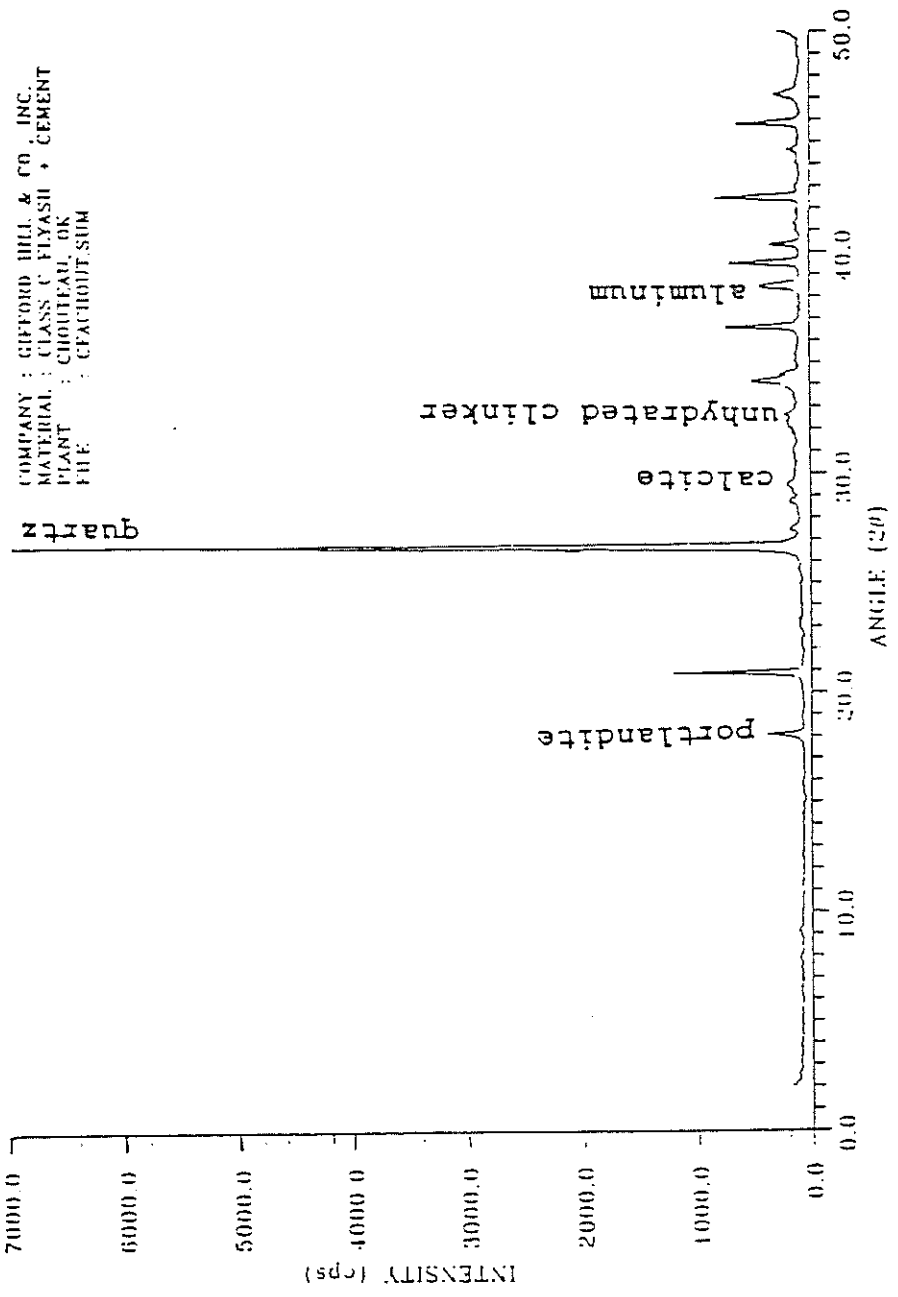

FIGURE 36. Sum pattern of concrete with ash from Chouteau.

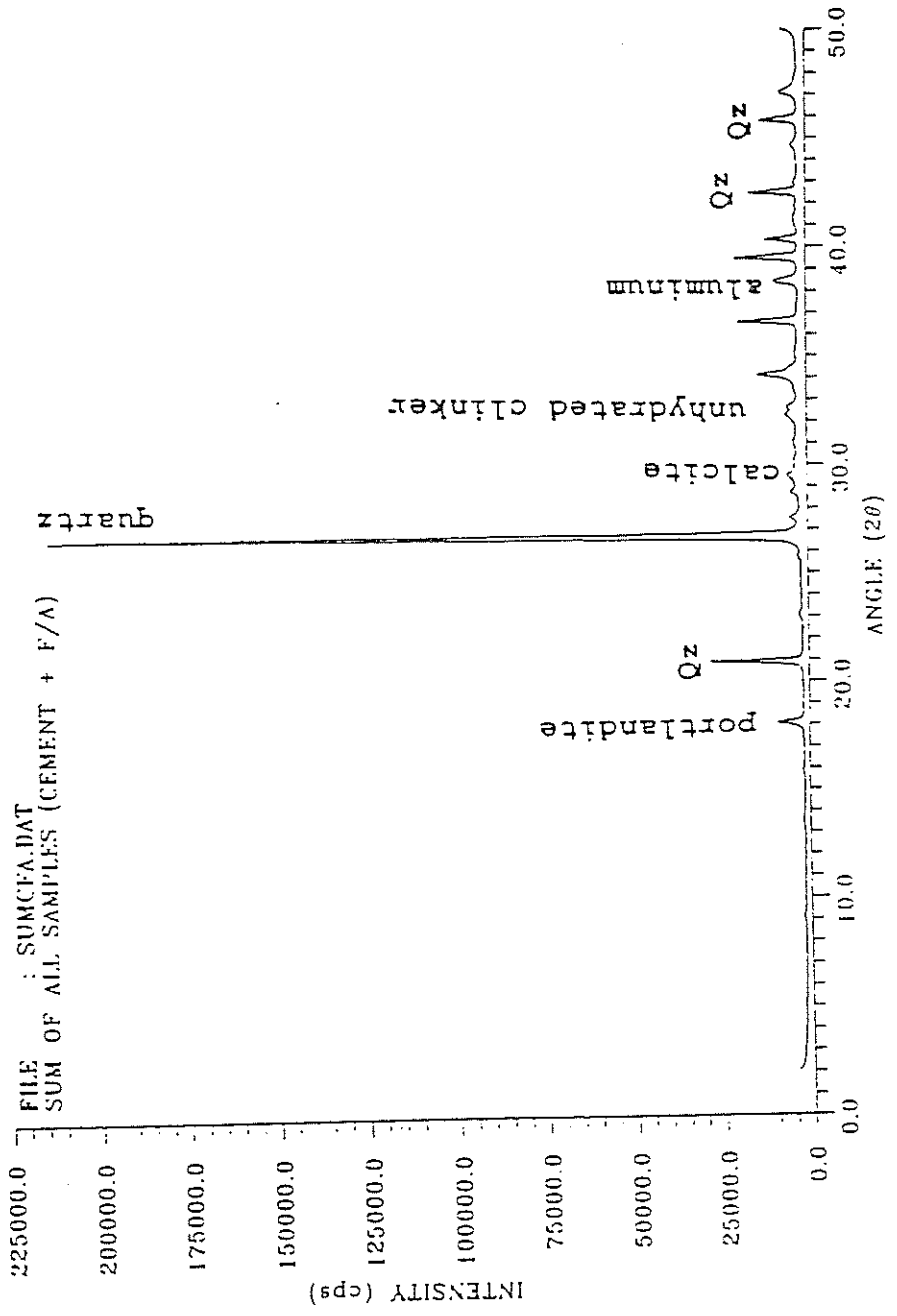

FIGURE 37. Master sum pattern for concrete with fly ash.

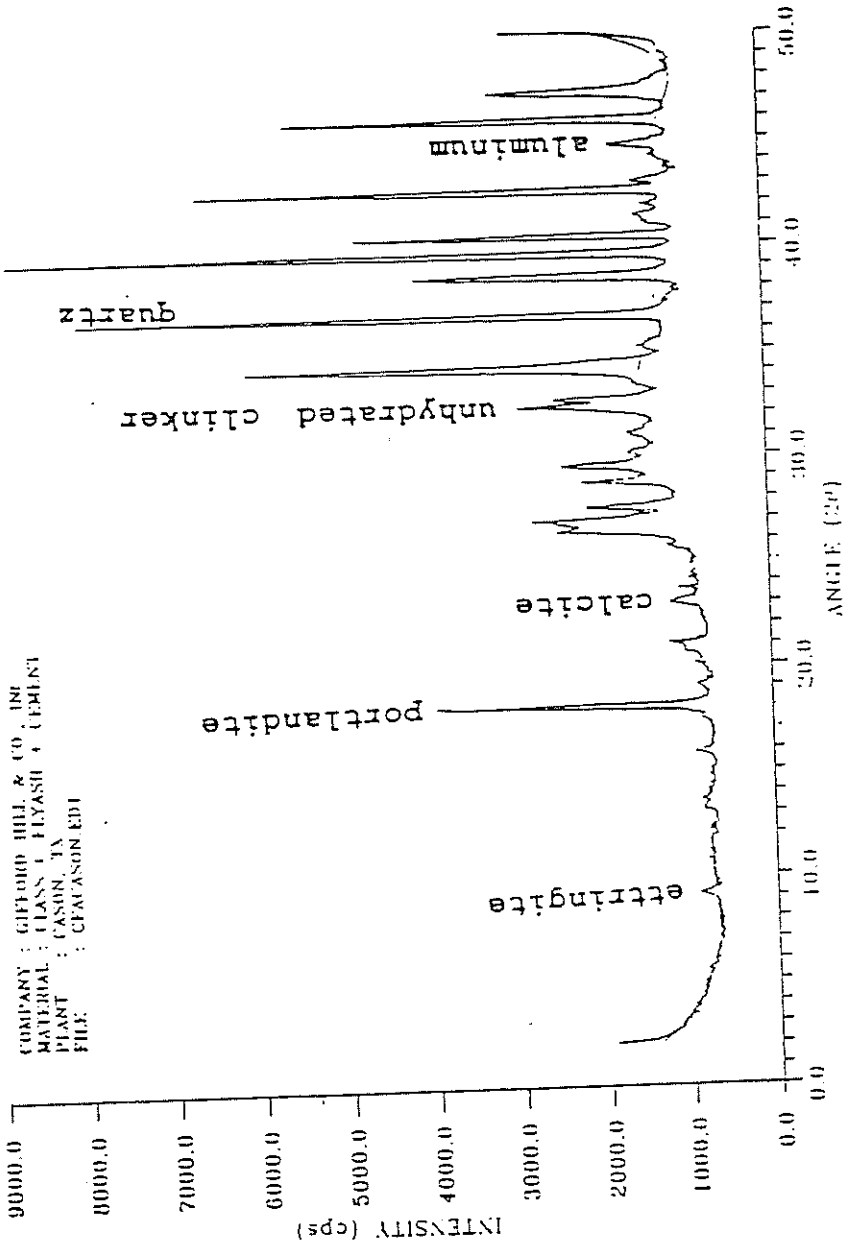

FIGURE 38. Sum pattern of concrete with ash from Cason with edited quartz peak at 0.334 nm.

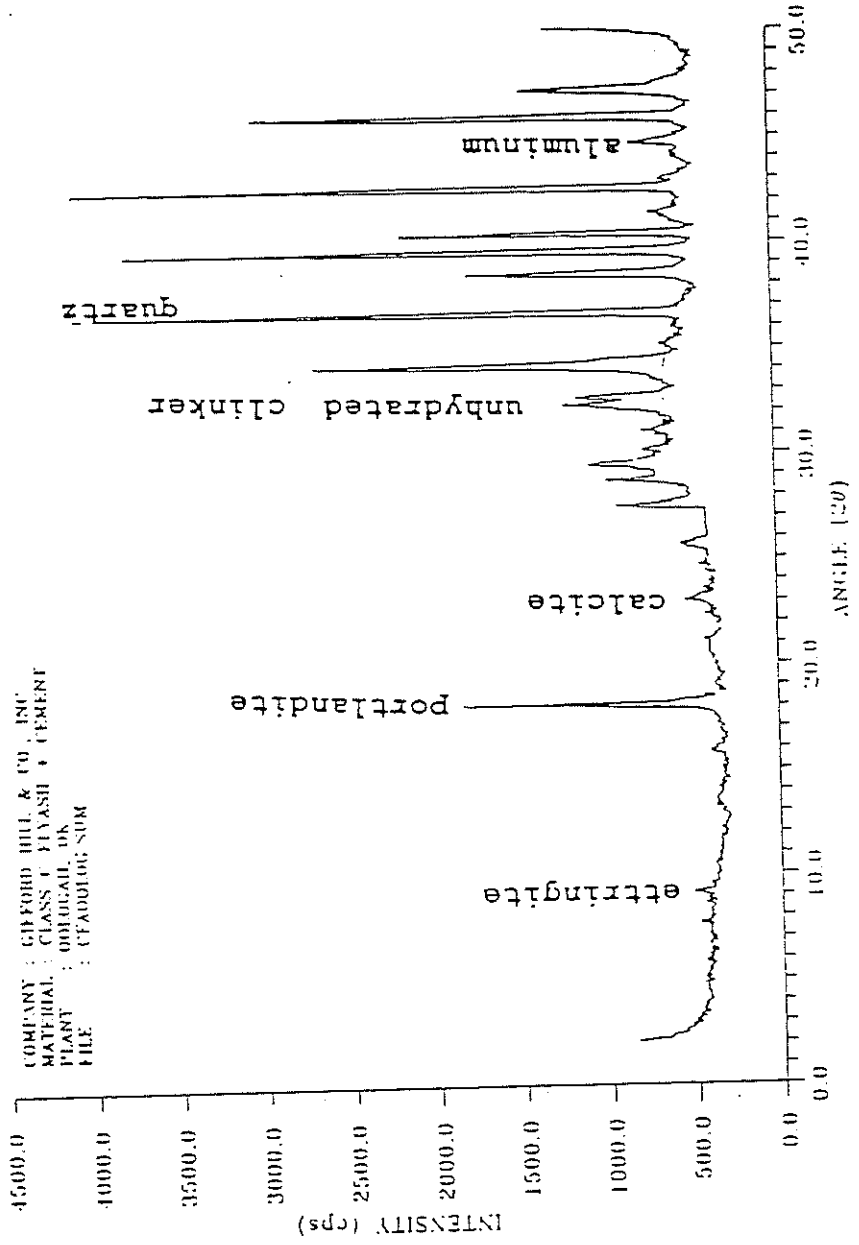

FIGURE 39. Sum pattern of concrete with ash from Oologah with edited quartz peak at 0.334 nm.

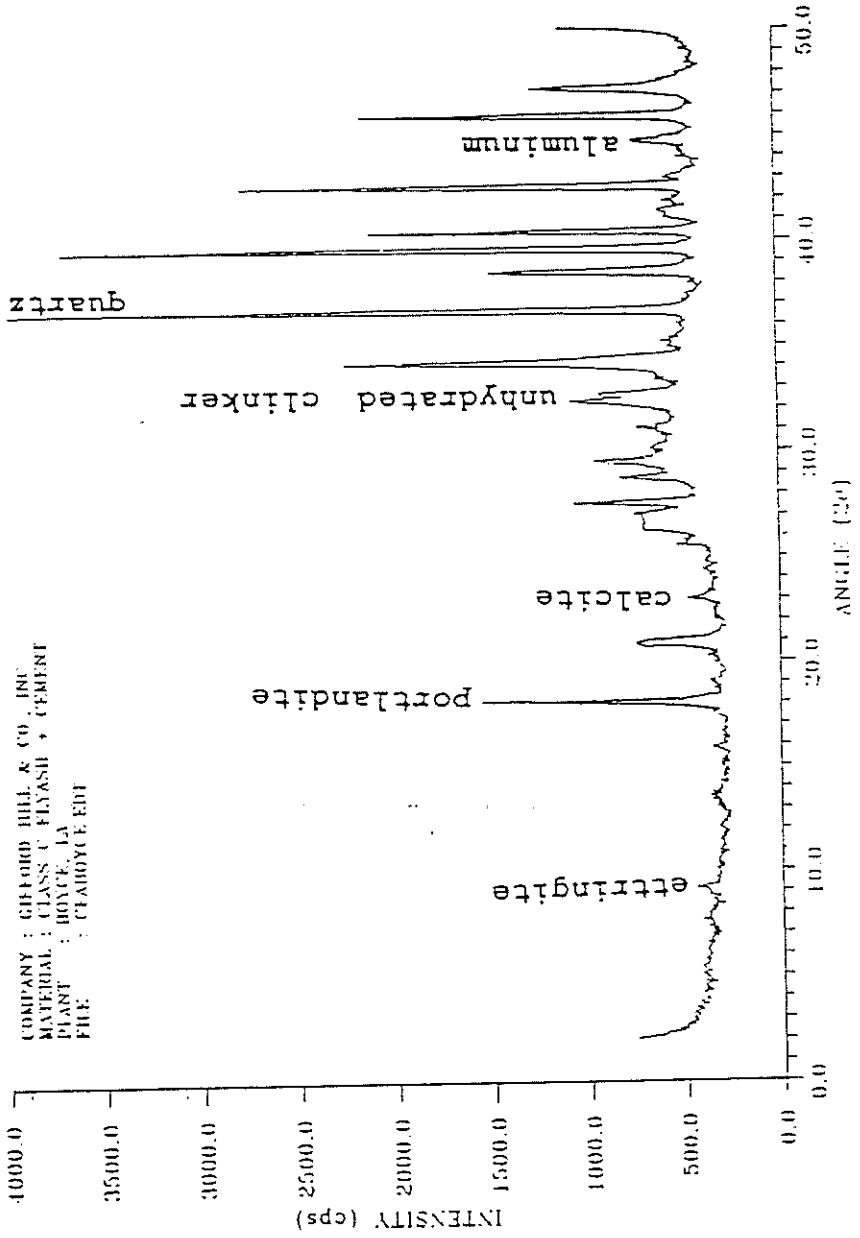

FIGURE 40. Sum pattern of concrete with ash from Boyce with edited quartz peak at 0.334 nm.

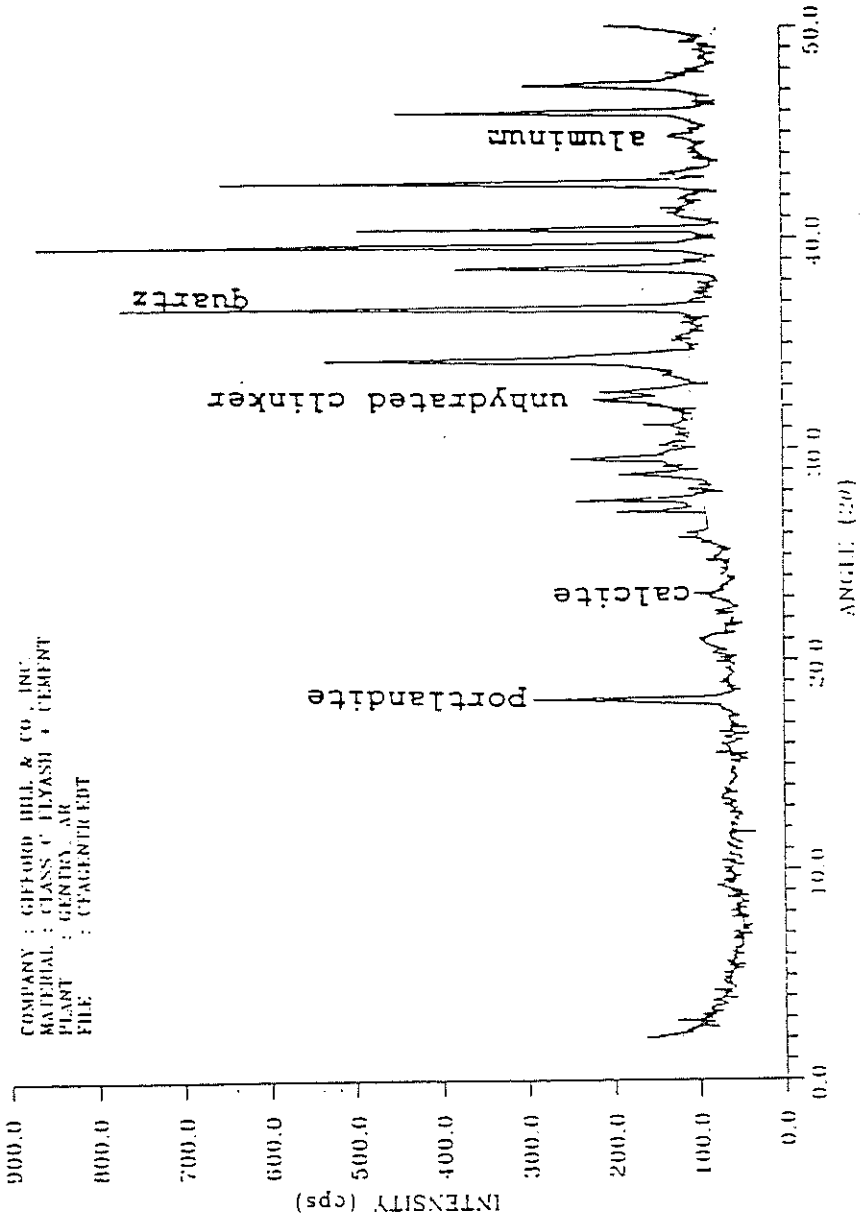

FIGURE 41. Sum pattern of concrete with ash from Gentry with edited quartz peak at 0.334 nm.

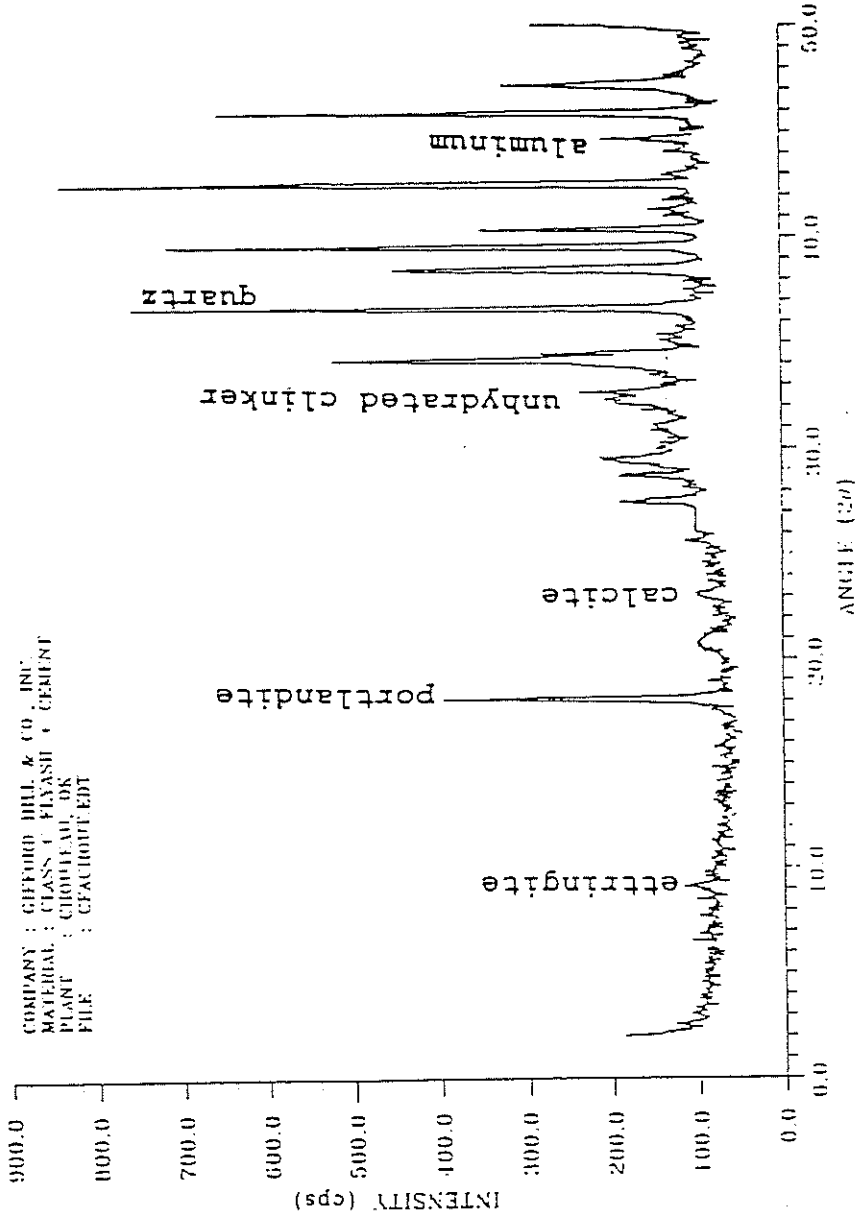

FIGURE 43. Sum pattern of concrete with ash from Chouteau with edited quartz peak at 0.334 nm.

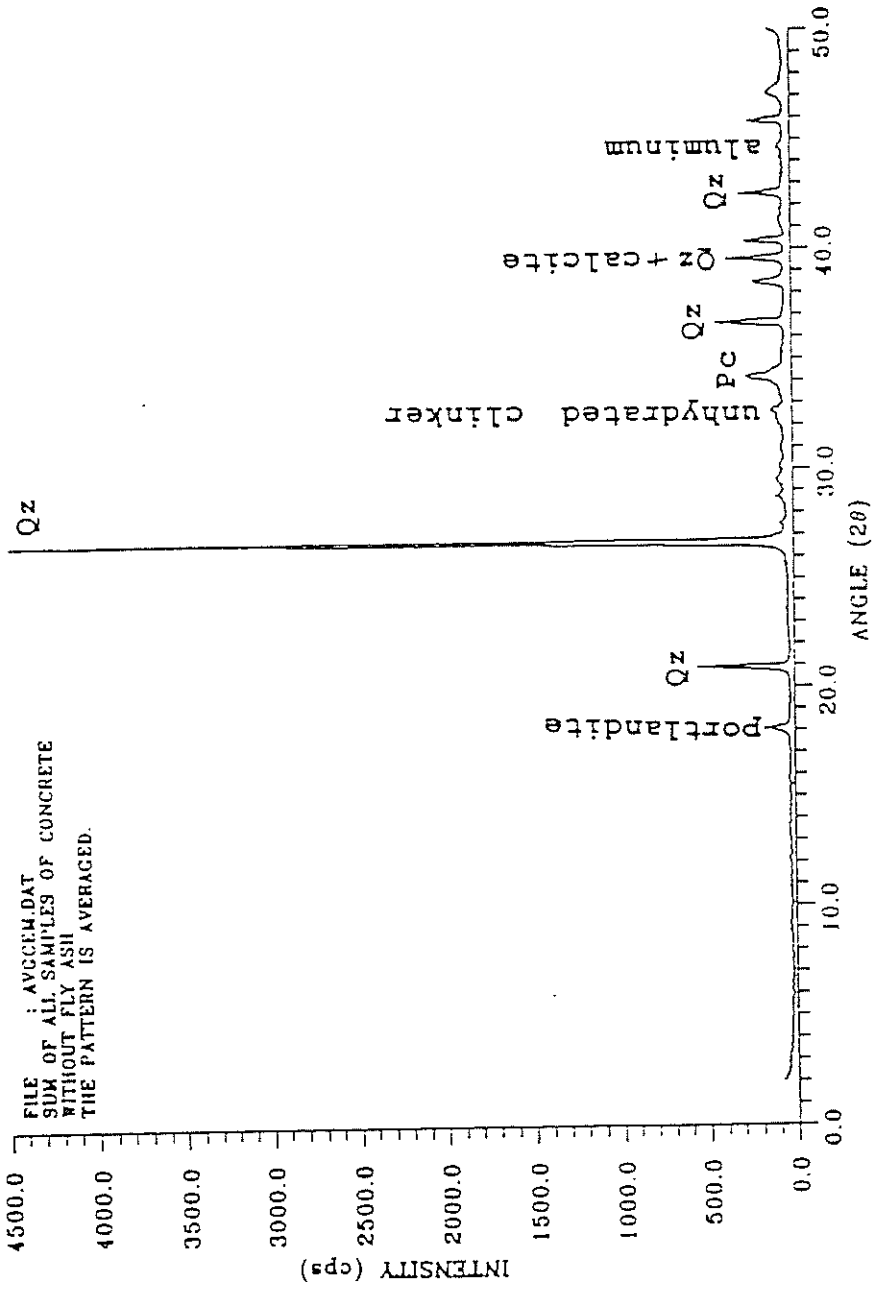

FIGURE 44. XRD pattern for concrete without fly ash.

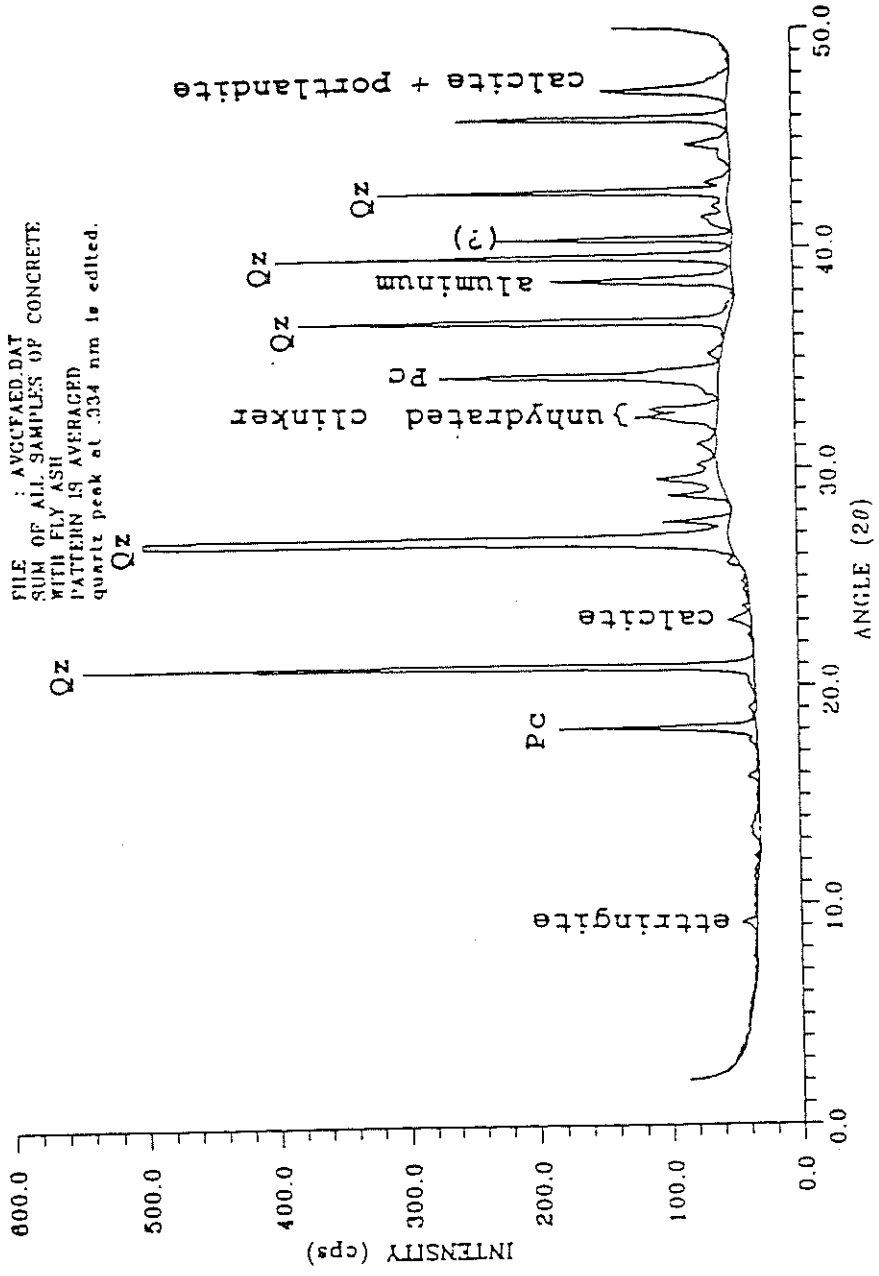

FIGURE 45. Averaged XRD pattern of concrete with ash.

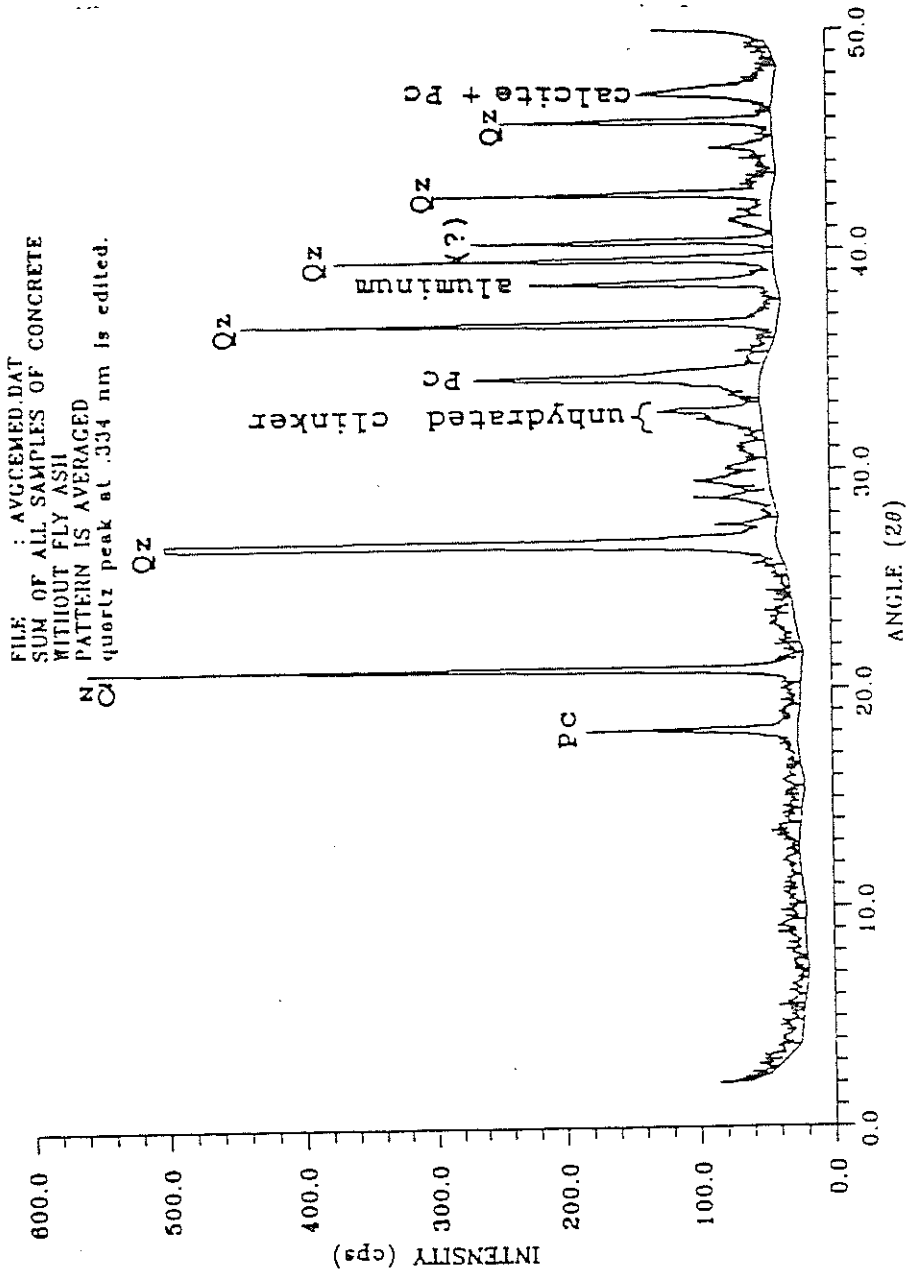

FIGURE 46. Averaged XRD pattern of concrete without ash.